THESIS FOR THE DEGREE OF MASTER IN MATERIALS SCIENCE

Thermal Damage Evaluation during Internal Cylindrical Grinding

Mario Perez Coto

Department of Industrial and Materials Science

CHALMERS UNIVERSITY OF TECHNOLOGY

Göteborg, Sweden 2018

Thermal Damage Evaluation during Internal Cylindrical Grinding

MARIO PEREZ COTO

Department of Industrial and Materials Science

Chalmers University of Technology

Abstract

Grinding is a widely used finishing process to attain tight tolerances and surface integrity. However, it produces high local temperatures that can alter the properties of the material, altering the microstructure of the component. As grinding is done in an already hardened material, these changes caused by overtempering or rehardening will affect the final properties of the component, reducing the lifetime of the bearing. Several analytical models used to predict this behaviour already exist but are mostly based on simple geometries.

To expand the knowledge to more complex geometries, grinding experiments using similar conditions as production were performed. However, those conditions limited the ways the temperature could be directly evaluated, requiring indirect methods to obtain it, in this case the hardness profile. Three different analytical models for the decomposition of the tempered martensite were assessed, to obtain a relationship between the hardness profile and the apparent temperature. Moreover, two FE models, one focusing on the macro geometries of the workpiece and wheel and a micromodel focusing on the grinding area, were built to simulate the behaviour seen in the analytical models and the obtained results.

A good fit between one of the analytical models and the hardness profile was obtained. This analytical model was derived from Malkin's studies of the phase transformations during grinding, with consideration of the tempering effect of several consecutive grinding passes. As only the outmost layers of the component were removed during grinding while the affected area was substantially bigger, the effect of several passes had a considerable importance in the hardness drop in the outmost layers of the material. Both FE models obtained temperatures similar to those expected using analytical methods, with the macromodel having some flaws that could be attributed to the difficulties of modelling a sufficiently small mesh.

Keywords: *Cylindrical grinding, Grinding Burns, Temper Burns, White Layers, Phase Transformations, Shallow grinding, Microhardness, Material Characteristics*

Table of Contents

1. Introduction 1
   1.1. Company 1
   1.2. Objective of the thesis and research questions 2
   1.3. Research approach and limitations 2
2. Grinding 4
   2.1. Geometry of contact 4
   2.2. Forces and chip formation 5
   2.3. Grinding wheel 7
   2.4. Grinding process 9
      2.4.1. Grinding system 9
   2.5. Basic parameters 10
   2.6. Thermal aspects 11
      2.6.1. Chip and fluid energy 12
      2.6.2. Work-wheel fraction 13
   2.7. Temperature approximations 14
      2.7.1. Heat input method 14
      2.7.2. Dimensionless method 16
      2.7.3. Numerical solution method 16
      2.7.4. Creation of burns 18
      2.7.5. Temperature evaluation during grinding 19
3. Material properties 20
   3.1. Phases and phase transformations 20
      3.1.1. Significant phases 22
      3.1.2. Grinding burns 23
   3.2. Analytical models 25
      3.2.1. Larson Miller parameter 25
      3.2.2. JMAK equation 26
      3.2.3. Differential approach to tempering 28
   3.3. Hardness 30
      3.3.1. Testing procedures 32
      3.3.2. Sample preparation 32
4. Methods and experimentation 33
   4.1. Grinding operation 34
   4.2. Metallography 36

4.2.1. Larson-Miller 36
4.2.2. Grinding and hardness testing 37
4.2.3. Etching and electrochemical etching 40
5. Simulations 41
5.1. Numerical models 41
5.2. Analytical models 42
6. Results 44
6.1. Damage evaluation 44
6.1.1. Larson Miller approach 45
6.1.2. JMAK evaluation 47
6.1.3. Differential approach 48
6.1.4. Critical temperature evaluation 52
6.2. Model evaluation 54
6.3. Best characterization parameter 56
7. Conclusions 59
8. Future research 61
9. References 62

Table of Figures

Figure 1 Research approach utilised in this study 2
Figure 2 Table stroke face grinding 4
Figure 3 Internal cylindrical grinding 5
Figure 4 Elastic and plastic deformation followed by chip formation (left) and the path created by the grain (right) (5) 6
Figure 5 Controlled-force internal grinding behavior showing no MRR until a critical force is reached (9) 6
Figure 6 Forces during plunge grinding (5) 7
Figure 7 Types of wheel damage during grinding (5) 8
Figure 8 Dressing operation (5) 8
Figure 9 Example of a principal grinding cycle 9
Figure 10 Maximum undeformed chip thickness for internal grinding (5) 11
Figure 11 Heat diagram for a single grain during grinding 11
Figure 12 Effect of the different coolants. Once a critical temperature is reached, they follow the dry (air) curve (5) 13
Figure 13 Temperature profile for a depth of cut 2.5µm, heat flux 579W/mm^2, workpiece speed 1.31 m/s and wheel speed 75.4 m/s 17
Figure 14 Temperature profile for a depth of cut 4.4µm, heat flux 292W/mm^2, workpiece speed 2.11 m/s and wheel speed 75.4 m/s 17
Figure 15 Derivative of the temperature for the first (left) and second (right) temperature profiles. 18
Figure 16 Fe-C Phase Diagram as obtained from ThermoCalc 21
Figure 17 TTT diagram for two common steels, P being Perlite; B, Bainite; and M, Martensite. 22
Figure 18 FCC to BCT transformation where the BCT is obtained from 2 FCC cells that are deformed. 23
Figure 19 Etched sample showing a white layer in the outmost part of the component followed by a dark layer before reaching the bulk of the component 24
Figure 20 JMAK curves at $\Phi = 1600000$ 27
Figure 21 JMAK curves for cementite at different gradients 27
Figure 22 Shape of the Vickers indent 31
Figure 23 Shape of the Knoop indent 31
Figure 24 Picture of the ring, showing the cut made for the prepared sample 33
Figure 25 Data obtained from the machine for case 1D (left) and smoothed using a robust loess method (right) 34
Figure 26 Comparison of the normal and the smoothed data for the tangential force of case 1D 35
Figure 27 Normal force increase with successive grinding of rings 35
Figure 28 Larson Miller curve for Vickers 37
Figure 29 Larson Miller curve for Knoop 37
Figure 30 Photo of the sample on the holder (top left), with a low magnification in the designated area (top left) and a higher magnification finally showing the affected area (bottom) 38
Figure 31 Zig-Zag distribution used in the hardness measurements, showing a Line 39
Figure 32 Cross-section of the sample, with the problematic interface in red 39
Figure 33 Etched example showing a small white layer (martensite) and a darker area (overtempering) obtained in ring 16H 40
Figure 34 Hardness measurement obtained after electrochemical etching 40
Figure 35 Contact area (light green) between the inner ring and the wheel surfaces (dark green) 41
Figure 36 2D Comsol model showcasing heat input occurring only when there is grain contact 42

Figure 37 Common 2D approach for FE analysis during grinding (34) 43
Figure 38 Temperature - Time dependence for LM6 (start of overtempering) 45
Figure 39 Hardness by Larson Miller changing the interaction time with a base value of 0.6ms..... 46
Figure 40 Larson Miller approach for Case 16E, BR=1.4 46
Figure 41 LM approach for case 2D(left), BR=1.1; and 6D(right), BR=1.5 47
Figure 42 Transformed fraction of the material (left) and its hardness equivalent (right) for case 4D47
Figure 43 JMAK hardness profile for case 1D, BR=0.8; and 4D, BR=1.5 48
Figure 44 Example of hardness profile using differential approach..... 48
Figure 45 Differential approach for case 1D (left), BR=0.8; and 2D (right), BR=1.1. 49
Figure 46 Differential approach for case 4D(right), BR=1.5; and 16E(left), BR=1.4 49
Figure 47 Temperature graphs for case 4D (left) and 16E (right) using the numerical solution and the triangular heat Input..... 50
Figure 48 Etched showpiece of sample 4D (left) and 16E (right)..... 50
Figure 49 Differential approach for case 9J(right), BR=0.9; and 10F(left), BR=0.9..... 51
Figure 50 Comparison of LM and differential model for case 3E(left), BP=1; and 6D (right), BP=1.5.. 52
Figure 51 HAZ for a 20HK drop in test 1 53
Figure 52 HAZ size comparison using a single pass and a multi pass for 20HK(left) and 5HK(right) drop for test 2..... 53
Figure 53 Cold front appears when the material enters into the grinding zone 55
Figure 54 Temperatures in the micromodel at the surface (blue), 10µm depth (green) and 10 µm depth assuming movement of the workpiece 55
Figure 55 Detail of the micromodel where the grain (white) at 1 nanosecond (left) and 1 microsecond (right) obtained through Comsol, where the color are isotherms above the boiling temperature of the coolant. 56
Figure 56 Thermal effect of grinding: HAZ (hatched) not completely removed in one pass leaves a residual in the following passes 57
Figure 57 Surface of the critical temperature with the depth of cut and workpiece speed 57
Figure 58 Size of the HAZ for a given constant surface temperature of 600°C 58

Acknowledgements

To all the team of MDC at SKF, especially my industrial supervisor Dr. Tomas Gustavsson, for teaching me all about grinding and helping me whenever he could, for all their help in teaching me how to properly use the machines, logging in and help with the experiments as well as their encouragement. Also, to the BEAST team in SKF for helping me with the program and the model.

To Dr. Peter Krajnik, my examiner, who guided me through the machining field and helped me when I had doubts.

To my friends in the Material Engineering masters in Chalmers. Being with you was a fantastic experience that has changed me and helped me grow as a person.

To Malkin, because your articles and books will be forever ingrained in my brain after reading them so much, and to the other authors I have read during this project, even if you have not been referenced, you have helped me understand the problem.

Abbreviations

BEAST – Bearing Simulation Tools

HAZ – Heat affected zone

LM – Larson Miller

TTT – Temperature Time Transformations

MRR – Material Removal Rate

UTS – Ultimate Tensile Strength

PCD – Polycrystalline Diamond

TTP – Time Temperature Parameter

HV – Hardness Vickers

HK – Hardness Knoop

HRC – Hardness Rockwell C

BR – Burning Ratio

FEM – Finite Element Modell

JMAK – Johnson-Mehl-Avrami-Kolmogorov

Nomenclature

d_s – wheel diameter
a_e – depth of cut
d_e – equivalent diameter
n_w – workpiece rotational speed
v_w – workpiece linear speed
U_d – overlap ratio
Q' – specific material removal rate
C_w – cutting point density
q – total heat flux
q_c – heat flux into the wheel
q_f – heat flux into the fluid
e_{chip} – specific energy per unit volume of the chip
c_w – specific heat of the workpiece
β_w – thermal property of the material heated by a moving source
R_{ws} – ratio between heat going to the workpiece and the wheel
L – Peclet number
θ – temperature increase
u – total specific energy
u_{sl} – specific energy for sliding
F_0 – process variable of grinding
z – depth
$\overline{\theta_{max}}$ – maximum dimensionless temperature
T_0 – scaling temperature
P_b – necessary power for thermal damage
M_s – temperature for the start of martensite transformation
H_1 – Hardness of soft phase
ξ – state variable for JMA analysis
H_0 – initial hardness of the material
U – activation energy of the transformation
R – gas constant
d_w – workpiece diameter
l_c – arc length / contact length
f_{ad} – dressing feed
n_c – wheel rotational speed
v_c – wheel linear speed
b_{Dd} – diamond tip width
h_m – undeformed chip thickness
r – shape factor of the chip
q_w – heat flux into the workpiece
q_{ch} – heat flux into the chip
b_d – width of the sample
ρ_w – density of the workpiece
k_w – conductivity of the workpiece
k_c – conductivity of the abrasive
r_0 – approximate grain contact radius
ε – ratio between heat going into the workpiece and total heat
α_w – workpiece thermal diffusivity
C_g – grinding constant
u_{cl} – specific energy for chip formation
u_{pl} – specific energy for ploughing
d – force exponent for a material
Z – dimensionless depth
τ – interaction time
P_b' – necessary power for thermal damage by unit of width
C_0 – material constant for LM
H_3 – hardness of hard phase
f – transformed fraction
ϕ – heating rate
ν – material variable for differential approach
T_0 – room temperature

1. Introduction

Machining requirements for components with tight tolerances and high surface integrity are significantly high, but as the necessity of those types of components rises, several solutions had been found to obtain them. Grinding can comply to those requirements while still maintaining a high production rate and in the specific case of precision machining, the ability to make very shallow cuts that depend on a high amount of small cutting edges (grains) of the wheel, creating low roughness. These advantages make it a widely used finishing process in the industry and even more when dealing with machining of hardened steels, which require higher forces.

As the final manufacturing process of a component made of hardened steels, except when dealing with highly loaded surfaces where a fine finishing process such as honing is used, it is crucial that the carefully generated microstructure and thus properties of the materials are kept unchanged. In the case of bearings, due to their high product life, the main failure mechanism that must be prevented is fatigue, more specifically rolling contact fatigue (1). As fatigue cracks grow from the surface (2), several measurements such as compressive stresses in the surface and high surface hardness are used to obtain a long fatigue life. High surface hardness also helps prevent wear. In the case of hardened steels, as the name indicates, high hardness is obtained which can be focused on the surface, with surface hardening processes such as case hardening, or the whole component, also called through hardened. The workpieces used were through hardened and the hardness was obtained by a heat treatment which creates a tempered martensite microstructure all through the component. This phase has a high strength while still maintaining some ductility which helps endure possible overloads without splintering.

However, the main drawback of grinding is that it generates larger amounts of heat per removed volume than turning and milling, resulting in a significant increase in the localized temperature (3). This temperature increase can lead to several issues in the surface of the component such as softening by overtempering, the creation of a hard but brittle area or even oxidation and tensile residual stresses. All these defects will sharply decrease the fatigue life. The first two alterations directly affect the material microstructure, and the first one is an early sign of process failure where the component must be scrapped due to not complying with the quality standards of the company. Thus, the understanding of the reasons behind the thermal damage and how it is linked to the process settings is important.

To prevent scrap during production, it is necessary for the product to be within the required specifications and there is a need for tools to understand when a defect may occur and can prevent this from happening. That, together with future needs of better material utilization, and tighter tolerance requirements on material properties due to the desire for lower weight optimize friction for improved energy efficiency, act as push factors to look for high process robustness at a high production rate and the requirement for better thermal control during the process.

1.1. Company

SKF was founded in 1907 and as one of the top worldwide manufacturers and supplier of bearings (4) has a long history of using grinding and has a huge amount of knowledge both on production and design, making them one of the best in finishing techniques. SKF continues to perform research on grinding and other finishing methods, looking for new methods to prevent scrap during production and increase their product lifetime. Within SKF, the Manufacturing Development Centre (MDC) in Gothenburg is the company's central research and development facility for manufacturing process development.

1.2. Objective of the thesis and research questions

The main objective of this thesis is to utilize material knowledge to be able to predict what type of thermal damage would occur during grinding, by comparing the obtained hardness-depth profiles with several possible damage models. As most of the previous experimentation and analytical models of grinding are based on trials and settings focused on surface grinding, the following project will utilize this knowledge and apply it to internal diameter cylindrical grinding and see if the use of the assumptions is correct or if changes must be made.

As this thesis is the first one in an ongoing project to better understand the nature of the thermal damage and eliminate this thermal damage in the process, the main objective is the creation of a solid knowledge base that could be expanded to fit the different grinding operations done in SKF. Different methods shown in the literature will be evaluated to create that knowledge, and the most suitable process control parameters will be selected. This led to the following questions:

1. If previous thermal analytical models for surface grinding can be applied to other set-ups and if the temperature can be evaluated indirectly using them.
2. How the temperature during grinding affects the final properties of the material and which model is closest to reality.
3. How process parameters affect the thermal damage in the component.
4. If a Finite Element Model (FEM) can be created to simulate the results correctly.

1.3. Research approach and limitations

The following approach was used to study the thermal damage caused during grinding:

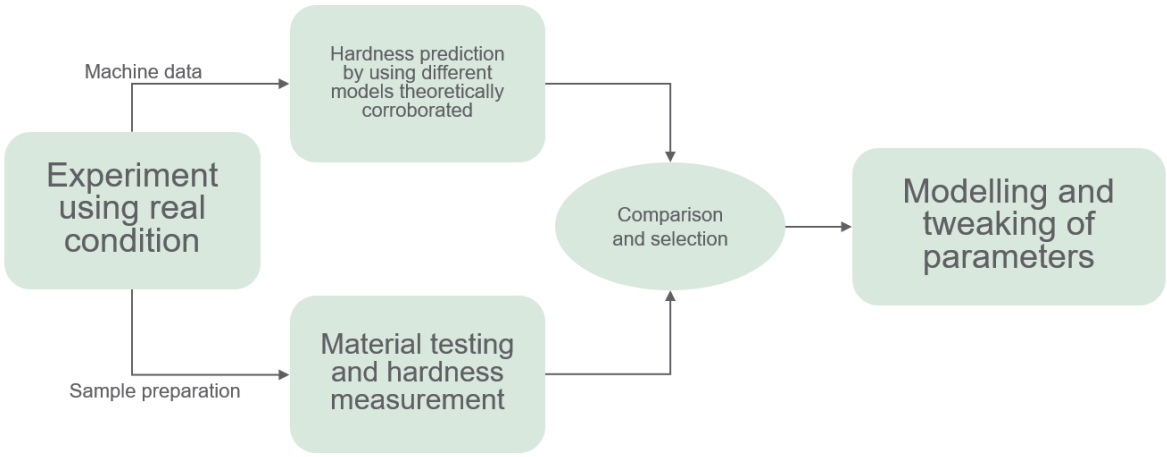

Figure 1 Research approach utilised in this study

The experiments were done under production conditions to portray the realities of production better; this meant using standard grinding production parameters, equipment and workpieces/samples. From the experiments, two types of information were obtained:

- The grinding process parameters and the process data, mainly grinding forces, will be utilized to calculate the temperature profile using different available thermal models. Then, a hardness-depth profile will be created using different damage models.
- The ground sample will be tested to see the type of damage found during grinding. The testing was done by etching and hardness-depth profiles.

The obtained hardness-depth profiles from the samples were compared with the analytically obtained from the damage model, selecting which method best portrayed reality. With the obtained data and temperature model a FE model will be created, focusing on the maximum temperature and the temperature profile in the first layers of the material.

Several limitations were present in this study due to time constraints and other issues. Several important parameters such as material properties and the heat fraction into the workpiece were taken from previous experimentation (5) (6). Testing was not done to all the ground samples, but those that have surpassed a force level during grinding, with other randomly selected sample being tested to corroborate the information. The analytical models utilised average values for the grinding force during the last passes, even if the values were highly dynamic stochastic in nature, creating a variance in the hardness-depth results from the samples when compared to the analytical models.

2. Grinding

Grinding as a material removal process has followed humankind since nearly its origins when it was first used to sharpen our tools and making complex geometries by utilizing a harder material than the processed one. It was not until the industrial revolution were its use became more needed, as more complex geometries and tighter tolerances were required to operate the machines of the time. In the late 19th century, synthetic abrasives were developed, the main abrasive used in wheels currently. Grinding continues to be one of the most commonly used finishing processes and is even more important in the case of hardened steels.

To correctly understand the grinding process, it is important to compare it to other machining processes, being quite similar with one crucial difference: the existence of multiple geometrically undefined cutting points with high negative rake angles. Due to the multiple cutting point mechanism, local variations will occur in the forces the material experiences, but a general macro view of the process exists that can describe the behaviour between the cutting tool and the workpiece

2.1. Geometry of contact

An important aspect in all machining processes is the cutting interface as it will explain the contact situation between the cutting tool and the machined component. As most machining processes, there are several available grinding operations that can be evaluated, but the simplest one, surface grinding operation can be described as follows: with a wheel of diameter d_s rotating with a peripheral speed v_s taking a depth of cut of a_e from the workpiece as the workpiece moves at a speed of v_w.

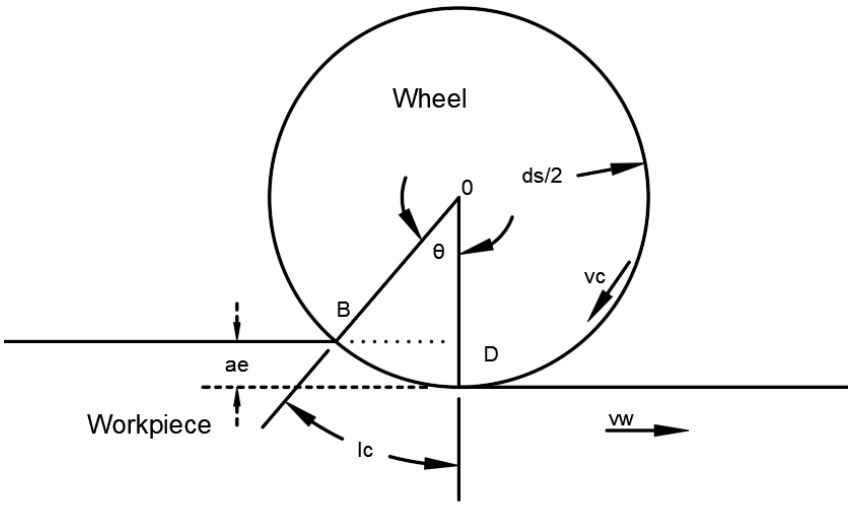

Figure 2 Table stroke face grinding

As the wheel penetrates the workpiece, there is an apparent arc of contact where the grinding action happens. The arc length is l_c, and if we assume that there is no motion between the wheel and the workpiece and no deformation, the arc length can be calculated as follows (7):

$$l_c = (a_e \cdot d_s)^{\frac{1}{2}} \quad (1)$$

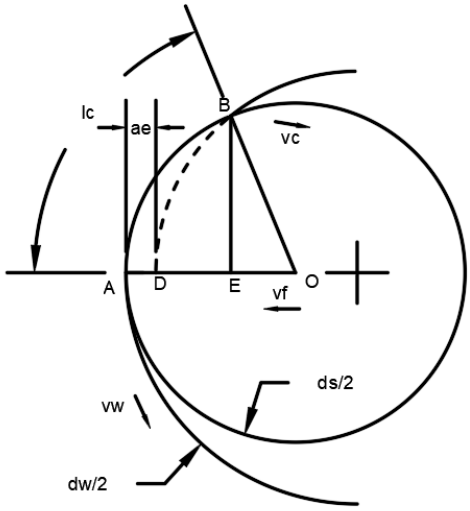

Figure 3 Internal cylindrical grinding

In any case of internal diameter cylindrical grinding, the geometry of contact is more complex as the approximate value of l_c continues to be AB. However, the triangle is not based on the depth of cut (AD) but rather on the distance AE due to the curvature of the workpiece. This gives a similar equation (7):

$$l_c = (a_e \cdot d_e)^{\frac{1}{2}} \tag{2}$$

Where d_e is the equivalent diameter that can be defined as follows:

$$d_e = \frac{d_s}{1 - \frac{d_s}{d_w}} \rightarrow d_e = \frac{d_w \cdot d_s}{d_w - d_s} \tag{3}$$

In most analytical approaches, the use of the equivalent diameter is used, to create equivalences between different types of grinding operations.

2.2. Forces and chip formation

Once the cutting situation is known, it is possible to start looking at how the material is removed, that is the formation of the chip. As the grains touch the workpiece, they will create a localized stress that can be imagined as:

$$\sigma_{grain} = \frac{F_{N,grain}}{A_{grain}} \tag{4}$$

This stress will determine whether chip formation occurs, or if the material is simply deformed as the localized stress is smaller than the Ultimate Tensile Strength (UTS). Due to the small contact area, only a small force would be required for each grain to penetrate the material (8). During the grinding process, a build-up of the force can be found out, as the grains start deforming the workpiece elastically and creating a “push” of the material called ploughing before the force reaches the critical force necessary to create a chip at a critical grain penetration.

Deflection in the machine is also important, as it can be quite large compared to the required accuracy. This deflection is affected by the stiffness of the machine system.

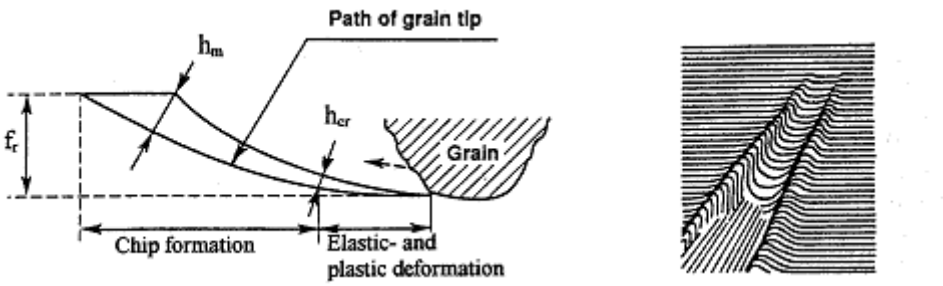

Figure 4 Elastic and plastic deformation followed by chip formation (left) and the path created by the grain (right) (5)

In the force diagram, there is no Material Removal Rate (MRR) until a certain value, after which ploughing would occur and finally after the critical force is reached a linear relationship appears between them, as the force is enough to create chips. In Figure 5, this can be seen with the A segment showing the penetration of the grains, B the ploughing and finally C the cutting.

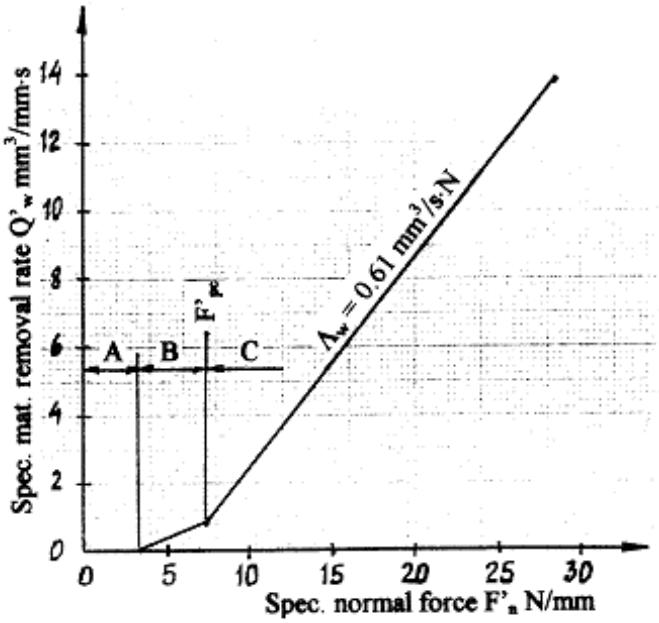

Figure 5 Controlled-force internal grinding behaviour showing no MRR until a critical force is reached (9)

The obtained chip is often called swarf (3) and is very similar to those obtained from larger-scale metal-cutting methods, with mostly curved chips but irregular in size and shape due to the variability in cutting. Due to the high speed at which they are made, it results in a nearly adiabatic deformation as well as sometimes melting and solidification of the metal due to the high local temperatures and reaction with the oxygen in the atmosphere causing spherical particles.

On the force side, the grinding force during plunge grinding can be divided into two main components:

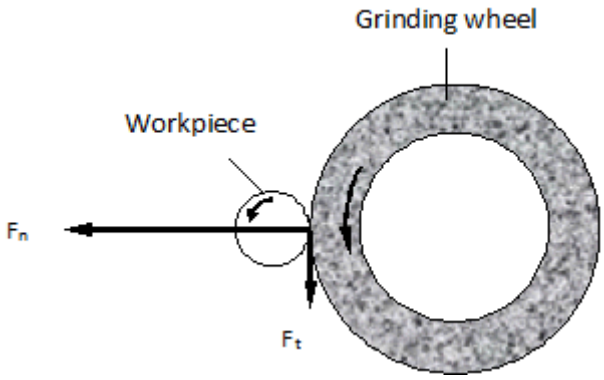

Figure 6 Forces during plunge grinding (5)

- Normal grinding force: F_N. This force is pushing against the workpiece, allowing the grits to enter the material. As the grinding wheel becomes duller, with larger wear flats on the grits, the force required for the grits to go to the desired depth increases.
- Tangential grinding force: F_t. This force is generating the heat during the operation and can be thought as the frictional force of the normal grinding force. As the grain gets duller, the contact area will increase, making it necessary to have a higher total F_N to obtain the same depth of cut. This increase of the normal force would increase the frictional loses even if the friction coefficient decreases due to the less rough interface between the bodies. The grinding power can be obtained by:

$$P = F_t \cdot v_c \tag{5}$$

$$F_t = \mu \cdot F_N \tag{6}$$

The normal force is much higher in grinding than the tangential force, with μ values often being lower than 0.2 with a newly dressed wheel, decreasing as the wear flats increase.

It is important to understand how the force is obtained from the machine. As previously explained, grinding is the combined effort of multiple geometrically undefined cutting points which will be individually removing the material like milling or turning. The forces measured are then the total sum of all those individual operations. Due to this, the value of the measured forces can and will change quickly with every measurement, as the grits properties are not perfectly uniform even just after dressing; and the contact situation between the workpiece and wheel will change with each pass, as the condition of the grits is affected by the cutting. As a macro view of the cutting situation is being used, the total sum of the forces exerted by the machine will be used to define grinding. However, this will act as the average of all the local forces, with places that will experience higher or lower local forces.

Another critical thing to notice with force is its connection with the hardness. As grinding is usually the final operation done in the component, the material is already hardened and will be heavily linked to the final hardness of the component. A harder material will require higher normal force for the grits to penetrate the material, increasing the wear of the wheel. It is also important to realize that the wheel must contain harder particles than the material it is supposed to remove, which is why carbides, an extremely hard phase, dramatically decreases the lifetime of the wheels.

2.3. Grinding wheel

The grinding wheel allows us to remove the material and because of that, it is essential to understand its behaviour and how its properties may be changed. Two processes are used to change the

properties of the wheel: truing, creating the wanted macro geometry of the wheel and eliminating any possible deviations in the shape; and dressing, preparing the wheel grains for cutting.

In the case of vitrified aluminium oxide wheels, both procedures can be done together in one go using a diamond dresser (10). This is the most common way of doing it and is often referred to as "conditioning". This procedure must be done regularly to perform a good grinding operation, but repetitive dressing and truing will reduce the lifetime of the wheel; hence a delicate balance between wheel wear and dressing must be found to improve the profitability of the process.

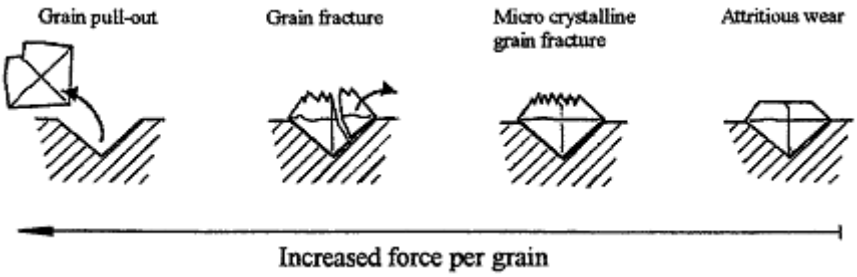

Figure 7 Types of wheel damage during grinding (5)

Dressing is necessary since, during grinding, the wheel will wear due to loss of grits, dulling and fracture of grits (10). The dressing process consists of using a harder abrasive, often diamond, as a dressing tool to create the wanted shape and topography of the wheel. In this case, this will mean "turning" the wheel with a single point 0.4x0.4 polycrystalline diamond (PCD) in a transversal dressing technique as shown in Figure 8. From a macroscopic point of view, this will create a truncated thread with a dressing lead:

$$f_{ad} = \frac{v_{fad}\left[\frac{\mu m}{s}\right]}{n_s[rpm]} = \frac{v_{fad} \cdot 60}{n_s}\left[\frac{\mu m}{rev}\right] \tag{7}$$

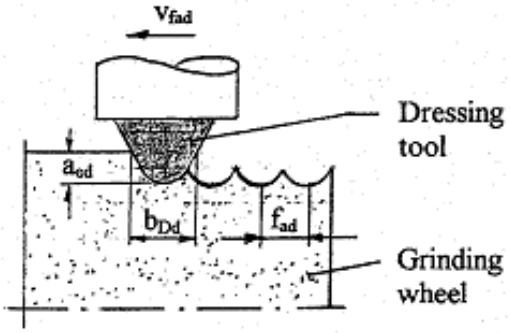

Figure 8 Dressing operation (5)

This thread is truncated according to the overlap U_d from the tip width b_{Dd} being larger than the dress lead. The larger U_d will generate a smoother wheel and can be calculated as:

$$U_d = \frac{b_{Dd}}{f_{ad}} \tag{8}$$

In general, the overlap ratio U_d is between 2 and 8 (11). This parameter will help characterize the wheel topography. This topography will evolve during production, so proper dressing is of paramount importance for the workpiece surface roughness and any thermal damage that might happen. The topography of the wheel is related to the efficiency of generating the desired workpiece surface roughness, with a smoother surface being easier to obtain with a finely dressed wheel. However, this

type of wheel will have a larger active area, meaning the normal and tangential forces will increase consequently. The balance between the surface roughness and the process forces is greatly affected by the grinding wheel specifications and the dressing conditions.

2.4. Grinding process

As the mechanics of grinding are known, it is important to understand how the grinding operation is implemented in a machine. For this, the grinding cycle usually consists of different parts, of which three main grinding steps can be obtained: rough grinding, fine grinding, and spark-out (5).

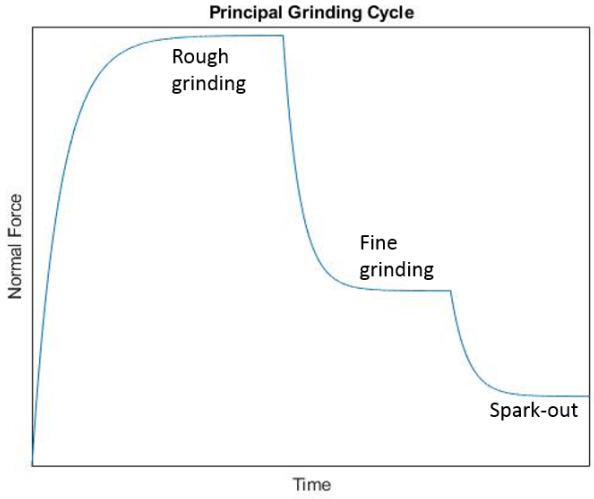

Figure 9 Example of a principal grinding cycle

The aim of the rough grinding process is to remove as much material as possible without damaging the material or overloading the machine. The roundness and tolerances are not as important if it is possible to improve them in the subsequent steps. This means that this phase of grinding is often where the highest temperatures can be expected and where the focus on the thermal analysis will be done in this work.

During fine grinding, the ring roundness, roughness and degree of damage are improved. This is done by decreasing the depth of cut compared to rough grinding, making for better tolerances and lower forces which generate less heat. Finally, during spark-out, the final ring quality is obtained, significantly improving the robustness of the process.

The process then goes from a higher MRR with more focus into the fast removal of material and as it gets closer to the end surface, slower and more meticulous grinding occurs to obtain the quality requirements.

2.4.1. Grinding system

The process parameters have been divided into four main categories to describe a basic model of grinding. These categories are the three main physical parts of the grinding operation: workpiece, wheel, and machine, as well as the process variables. All the parameters will interact with each other affecting the final quality of the product.

Table 1 Parameters in the production process

Workpiece	Wheel	Machine variables	Process Variables
• Hardness • Chemical Composition • Thermal Properties • etc.	• Abrasive • Dressing • Bonding Component • Structure • Hardness Grade	• Stiffness • Maximum Power • Lubrication	• Cutting Speed • Workpiece speed • Depth of cut

Previous research has been done to try to understand how these parameters interact with each other and how they can be used to correctly compare different grinding situations to obtain more information about the possible results of the production process.

2.5. Basic parameters

Due to the high amount of process variables existing in grinding, and the effect they have on the material due to the forces, rubbing, ploughing and wheel wear, several different numbers have been used to characterize the process in a simpler way (12).

Important parameters are the specific material removal rate Q' that measures how fast the material is removed per unit of width. This can also be calculated as the depth of cut times the workpiece speed, more aggressive processes will be faster and deeper, leading to higher values of Q':

$$Q' = a_e \cdot v_w \left[\frac{mm^3}{s}\frac{1}{mm}\right] \tag{9}$$

This parameter is widely used when comparing different grinding operations as it characterizes the production rate of the processes and can be used to study if the changes to the process are beneficial or not. However, this does not take into consideration the effect of the wheel. A larger wheel speed means that each grain is traveling the l_c in a shorter time. As the workpiece infeed is the same, at a constant MRR, the grain penetration decreases, and the work done by that individual grain decreases.

A better way to describe the stress on the abrasive grains in the wheel and hence the wheel wear is the undeformed chip thickness (7). If grinding is compared to other machining processes, this undeformed chip thickness can be thought of as the grain depth of cut. It is possible to visualise an approximation of the cutting path as a circular arc that will be created by the grains while cutting. To calculate this undeformed thickness, two-wheel dependent parameters must be accounted for: r, the shape factor of the chip; and C_w, the cutting point density:

$$h_m = \sqrt{\frac{4}{C_w \cdot r}\left(\frac{v_w}{v_c}\right)\sqrt{\frac{a_e}{d_e}}} \tag{10}$$

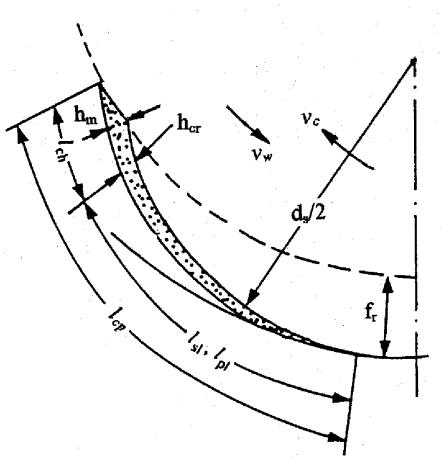

Figure 10 Maximum undeformed chip thickness for internal grinding (5)

h_m hence requires some values outside of the knowledge of the operator and that may change during the production process, i.e., C_w and r. Thus, the idea of only using the parameters that the operator can choose was born while the other values would remain constant, the aggressiveness number (12). For a fixed set-up, the relative change in the aggressiveness and h_m would be the same when the operator changes the process parameters.

$$Aggr = 10^6 \cdot \frac{v_w}{v_c} \cdot \sqrt{\frac{a_e}{d_e}} \tag{11}$$

This number applies to all type of operations as long as the geometry is known and can be used to evaluate the damage to a workpiece by changing the operator inputs.

2.6. Thermal aspects

An important aspect in grinding is how the heat that is generated during grinding behaves and is transferred. During grinding, the heat energy is closely linked to the generated power, and four different heat dissipation paths have been found: into the workpiece and the wheel, chips and the grinding fluid (13). It can thus be said that the total heat flux is:

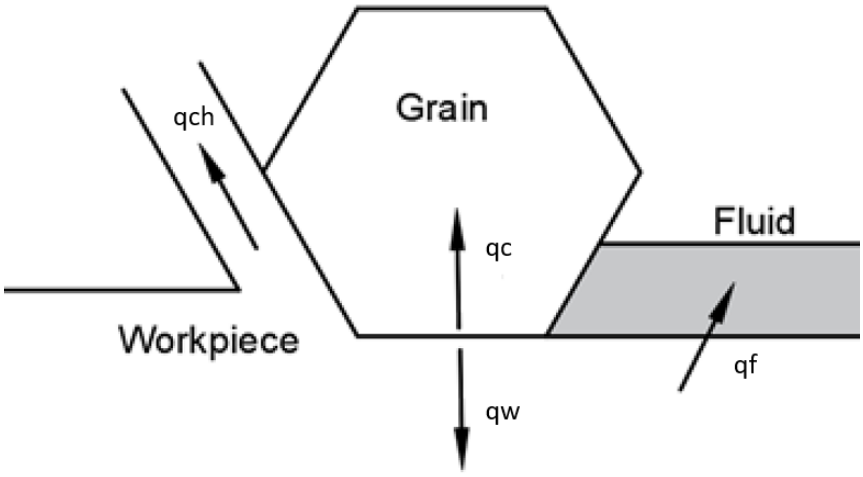

Figure 11 Heat diagram for a single grain during grinding

$$q = q_w + q_c + q_{ch} + q_f \tag{12}$$

Where the total heat flux can be described as the grinding power exerted by the machine in the small contact area:

$$q = \frac{P}{A} = \frac{P}{b_d \cdot l_c} \tag{13}$$

In some cases, such as in dry shallow-cuts, it can be assumed that all the heat goes into the workpiece, but it often tends to an overestimation of the temperatures that would melt the surface. All except the q_{ch} are generated in the contact area and shared between the workpiece and the wheel, with the heat to the fluid going initially into the workpiece to be later removed by convection with the fluid.

As the contact time is quite small, the grinding energy will be seen as small but intensive peaks of energy and temperature as the grains cut through the workpiece.

2.6.1. Chip and fluid energy

The energy transmitted to the chips can be easily estimated. This energy is related to the energy required to increase the temperature of the chips, being the highest limit, the energy required to melt them (14), as the chips do not tend to melt.

$$e_{chip} = \rho_w \cdot c_w \cdot \Delta T_{chip} \tag{14}$$

If we take into consideration the material removal rate and the contact area it is possible to obtain:

$$q_{ch} = a_e \cdot v_w \cdot \rho_w \cdot c_w \cdot \frac{\Delta T_{ch}}{l_c} \tag{15}$$

The kinetic energy could also be considered important, but for a high wheel speed of 100m/s it would only be 0.4J/mm, much smaller than the other terms and can be ignored. The total energy that leaves the system has been found to be approximately 6.2 J/mm^3 (15).

The energy that goes to the fluid can be calculated by the convection factor which will depend on the type of fluid used. There are two main fluid types: neat oil and water-based fluids. The latter one giving less lubrication, but more heat removal is the one used in this work, with a convection factor of around 80000 W/m^{2}K (8). During the grinding operation, the peak temperatures in the contact area will significantly exceed the boiling temperature of the fluid, creating a gaseous film that will greatly reduce convection in that area. However, as the material moves away from the heat source in the grinding area, the fluid would be able to cool both the wheel and the workpiece, obtaining a nearly similar starting temperature as before, as seen when using a thermal camera. This would mean that the residual heat, the heat gained between cycles, is sufficiently small to assume that the thermal conditions in the grinding zone will be the same between passes.

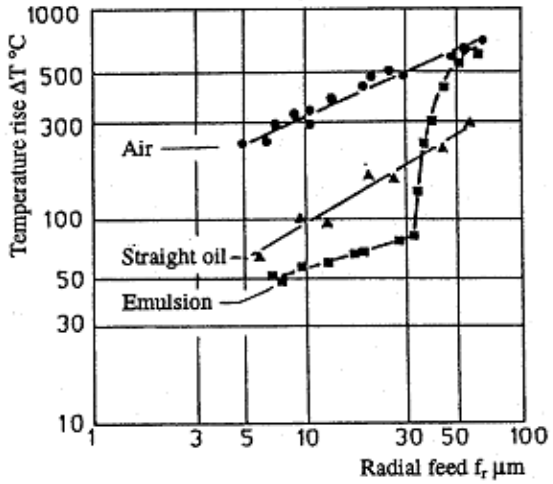

Figure 12 Effect of the different coolants. Once a critical temperature is reached, they follow the dry (air) curve (5)

2.6.2. Work-wheel fraction

An important thing to consider when evaluating the thermal damage is how much of the heat generated at the contact area goes into the workpiece compared to the wheel. An important first assumption is that both contact boundaries will be at the same temperature. Then, the thermal properties of the workpiece and the abrasive can be compared. For that, the thermal property of the material that is heated by a moving heat source can be evaluated as β_w (8):

$$\beta_w = \sqrt{k_w \cdot \rho_w \cdot c_w} \tag{16}$$

Moreover, the steady-state ratio can be found by:

$$R_{ws} = \left(1 + \frac{k_c}{\beta_w \cdot \sqrt{r_0 \cdot v_c}}\right)^{-1} \tag{17}$$

This implies a difference between an aluminium oxide and a CBN wheel. Alumina abrasives have lower thermal conductivity which leads to higher ratios compared to those of CBN wheel. Due to this, when grinding with CBN wheels, more heat will be going into the wheel and less into the workpiece, obtaining lower temperature in the workpiece. As the objective of this work was obtaining thermal damage, which requires higher temperatures, aluminium oxide wheel will be used in this work as a bigger fraction of the generated heat will go into the workpiece.

This concept can be further expanded if all sources of heat are considered:

$$\varepsilon = \frac{q_w}{q} = R_{ws}\left(1 - \frac{q_{ch}}{q}\right) - \frac{q_f}{q} \rightarrow q_w = \varepsilon \cdot q \tag{18}$$

This value will be much smaller than the work wheel ratio in circumstances where the heat evacuated by either the fluid or the chip is high. However, as explained before, the values of them can be assumed to be small enough not to consider them. In previous experimental research, alumina wheels have been seen to have ratios between 60-90% (15) while CBN wheels have lower ratios of 20-50% (16) due to their higher thermal conductivity. In previous examinations of the process with the given alumina wheel, it was obtained a ratio of 85%, and thus, this value was the one used during this research.

2.7. Temperature approximations

Several analytical models have been developed to understand how the heat generated in the grinding zone will affect the temperature of the material, as grinding could be considered a high-speed heating operation (17) where part of the material that has been heated is removed. To simplify the model where both the bodies are moving, the wheel is considered a moving heat source, and, due to grinding normally occurring in extremely thin layers and at high speed, the heat flux is assumed to only go in the radially (18). This assumption holds as long as the Peclet number is higher than 5 (3).

$$L = \frac{v_w \cdot l_c}{4\alpha} \tag{19}$$

Where α is the thermal diffusivity of the material that can be expressed as:

$$\alpha_w = \frac{k_w}{\rho_w \cdot c_w} \tag{20}$$

Two factors are taken into consideration when making these approximations:

- The cooling applied by the grinding fluid in the grinding zone is inefficient, as explained previously, only providing bulk cooling of the workpiece and acting as lubrication and washing out of chips (8).
- The temperature rise between consecutive passes, known as residual temperature, is small enough to be negligible compared to the maximum temperature rise (7). This has been corroborated through a micromodel using Comsol, where, as the affected area is small and there is a bulk cooling outside of the grinding area, the temperature quickly decreases once the heat rate provided by the grinding zone is removed.

Another important consideration is that these approximations were created considering surface grinding while the focus of this study is shallow internal grinding. However, as the affected depth will not exceed 100µm with a depth of cut of maximum 5µm while the internal radius of the workpiece will be 25mm, it can be abstracted as a straight workpiece being cut by a bigger wheel as described in Section 2.1 Geometry of contact. Therefore, as the heat will not be moving in the circumferential direction due to the high-speed grinding, the small interaction time and heat flow only in the radial direction, it can be said that these approximations can be used for this case.

Several temperature approximations models exist:

2.7.1. Heat input method

A one-dimensional analysis can be made by just assuming classic thermal equations (17) (18), where the heat that goes into the material for a short period of interaction will create an increase in temperature which is called θ:

$$\theta_{max} = q_w \cdot \frac{C_0}{\beta_w} \cdot \sqrt{\frac{l_c}{v_w}} \tag{21}$$

where C_0 is a grinding constant that depends on the Peclet number (8) but at the speeds and angles during production it can be assumed to be around 1 and where q_w is the energy by unit of area, commonly mm^2, going into the material in the grinding zone:

$$q_w = \varepsilon q = \frac{\varepsilon \cdot P}{l_c \cdot b_d} \tag{22}$$

If C_0 is a constant value 1 due to the grinding situation, the equation can be expanded to:

$$\theta_{max} = \frac{\varepsilon \cdot P}{b_d \cdot \beta_w} \cdot \sqrt[4]{\frac{1}{d_e \cdot Q' \cdot v_w}} \tag{23}$$

However, this value of C_0 is not a constant, but a value used to optimize the equation for several heat source shapes as well as vary depending on the slope of the surface. For instance, for a rectangular heat source in a straight component, the C_0 value is equal to 1.13 (17) such that:

$$\theta_{max} = \frac{1.13 \cdot q_w \cdot \alpha_w^{0.5} \cdot a_e^{0.25} \cdot d_e^{0.25}}{k_w \cdot v_w^{0.5}} \tag{24}$$

while for a triangular source, this value decreases to 1.06 (19). This heat shape has been proved to obtain a better fit with experimental results, as it considers that the heat is not evenly distributed in the grinding zone. The last equations can be combined with the total specific energy concept where the contribution is divided between chip formation, ploughing and sliding. There all the energy from ploughing (deformation of the component to remove) and sliding (generated in the interface between the wear flats and the workpiece) goes into the component, such that only a part of the chip energy, experimentally found to be around 45% is not conducted as heat to the workpiece (15):

$$u = u_{ch} + u_{sl} + u_{pl} \tag{25}$$

$$\varepsilon = \frac{u_{pl} + u_{sl} + 0.55u_{ch}}{u} = \frac{u - 0.45u_{ch}}{u} \tag{26}$$

$$\theta_{max} = \frac{1.13 \cdot \alpha_w^{0.5} \cdot a_e^{0.75} \cdot v_w^{0.5} \cdot (u - 0.45 \cdot u_{ch})}{k_w \cdot d_e^{0.25}} \tag{27}$$

Since u_{ch} is known to be approximately 13.8 J/mm^3 (7) for steels, and the loss from the system is known to be approximately 6.2J/mm^3. Another equation based on the research by Maris (20) can also be used where he assumes that 85% of the total grinding power will penetrate the workpiece:

$$\theta_{max} = 0.58 \cdot F_0 \cdot a_e^{d-0.24} \cdot v_w^{d-0.57} \cdot v_c^{1.1-d} \cdot d_e^{0.76-d} \cdot (\rho_w \cdot c_w)^{-0.47} \cdot k_w^{-0.5} \tag{28}$$

Where F_0 is a process equation that depends on grinding conditions such as dressing or lubrication and is found for every case, while d, the force exponent, is for the material in question 0.8.

Once the temperature in the surface is known the effect on the subsurface is important, as it is necessary to know the depth of the affected area. To obtain this information, it is essential to understand how the heat is transported in the depth / radial direction, z. As explained before, it is assumed that heat is mostly transferred in the depth direction, as the ring is moving at high speeds compared to the possible lateral diffusion. Several theories have been made in the infinite plate case. A simple way of obtaining this effect can be done employing an exponential behaviour, as Maris demonstrated (20), such that:

$$\theta_{depth} = \theta_{max} \cdot \exp\left(-0.45 \cdot \left(\rho_w \cdot c_w \cdot \frac{v_w}{k_w}\right)^{0.63} \cdot (a_e \cdot d_e)^{-0,18} \cdot z\right) \tag{29}$$

Which can be combined with the equation for the maximum temperature to understand the behaviour with respect to the depth. It is important to remember that in power-law functions it is much easier to insert all parameters in SI units. Otherwise, it would require a complex conversion factor.

2.7.2. Dimensionless method

Another common way of calculating the temperature below the grinding surface is the dimensionless method (21). In this method, a moving-band heat source is assumed allowing the calculation of the maximum dimensionless temperature at a dimensionless depth Z:

$$Z = \frac{v_w z}{2\alpha_w} \tag{30}$$

Which will depend on the material, workpiece speed, and depth z, obtaining a temperature:

$$\overline{\theta_{max}} = \left(\frac{\pi \cdot k_w \cdot v_w}{2 \cdot \alpha_w \cdot q_w}\right)\theta_{max} = 3.1L^{0.53} \cdot \exp(-0.69L^{-0.37}Z) \tag{31}$$

Where the surface temperature can be obtained by using Z=0. The value of this equation will show a small discrepancy as the constants in this method were made to fit over the ranges 0.5<L<10 and 0<Z<4. Other more accurate approximations have been obtained (20). Still, the equation shows that a steeper gradient, that means a shallower heat affected zone, is obtained if there is a higher speed v_w or a shorter contact length l_c, as the heat will have less time to act and propagate through the workpiece while the material goes through the grinding zone.

2.7.3. Numerical solution method

Another approach was used by Malkin (22) where, similarly to the heat input method, a semi-infinite workpiece is assumed to move past a stationary triangular heat source. The normal energy equation was reconsidered in a dimensionless form by normalizing T, x, and y by using the scaling variables:

$$T_0 = \frac{\varepsilon \cdot q}{\beta_w} \cdot \sqrt{\tau} = \frac{\varepsilon \cdot q}{\beta_w} \cdot \sqrt{\frac{l_c}{v_w}} \tag{32}$$

Which coincides with the maximum surface temperature by the heat input method assuming C=1.

$$x_0 = l_c = \sqrt{a_e \cdot d_e} \tag{33}$$

$$y_0 = \sqrt{\frac{k_w \cdot \tau}{\rho_w \cdot c_w}} = \sqrt{\alpha \cdot \frac{l_c}{v_w}} \tag{34}$$

Such that $\overline{\theta_m} = T/T_0$, Y=y/$y_0$ and X=x/x_0. The differential equation can then be reduced to:

$$C\frac{\delta\theta}{\delta X} = \frac{1}{2L}\frac{\delta}{\delta X}\left(K\frac{\delta\theta}{\delta X}\right) + \frac{\delta}{\delta Y}\left(K\frac{\delta\theta}{\delta Y}\right) \tag{35}$$

where K and C are the dimensionless temperature-dependent thermal conductivity and heat capacity. As the workpiece is assumed to be moving at a constant speed v_w, the dimensionless length would also represent the dimensionless time. Furthermore, as the Peclet number can be assumed to be high enough for the first part of the equation to be negligible, the focus can be put on the second part of the equation where for a triangular heat flux:

$$-K\frac{\delta\theta}{\delta Y}\Big|_{Y=0} = \begin{cases} 2(1-X) for\ 0 \le X < 1 \\ 0\ for\ X < 0; X > 1 \end{cases} \tag{36}$$

As the heat would only affect the component once it gets into the heat source area. This analysis of the metallurgical transformation required the effect of the temperature history in an asymptotic way, which was obtained through a numerical solution with a finite difference method. The maximum

temperature increase and its second derivative were approximated in the region 0<Y<10, by the functions:

$$a_0(Y) = \frac{1}{0.907 + 1.3 \cdot Y^{1.2}} \tag{37}$$

$$a_2(Y) = \frac{1}{0.317 + 0.3 \cdot Y + Y^5} \tag{38}$$

A comparison of all temperature methods is shown below

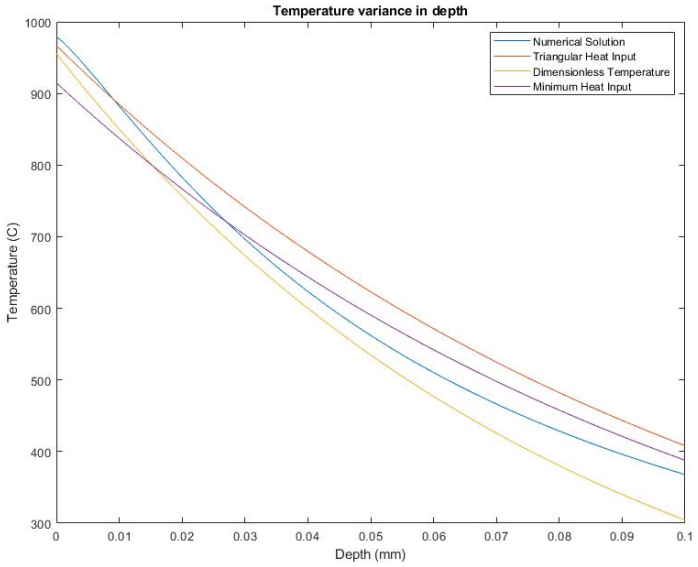

Figure 13 Temperature profile for a depth of cut 2.5µm, heat flux 579W/mm², workpiece speed 1.31 m/s and wheel speed 75.4 m/s

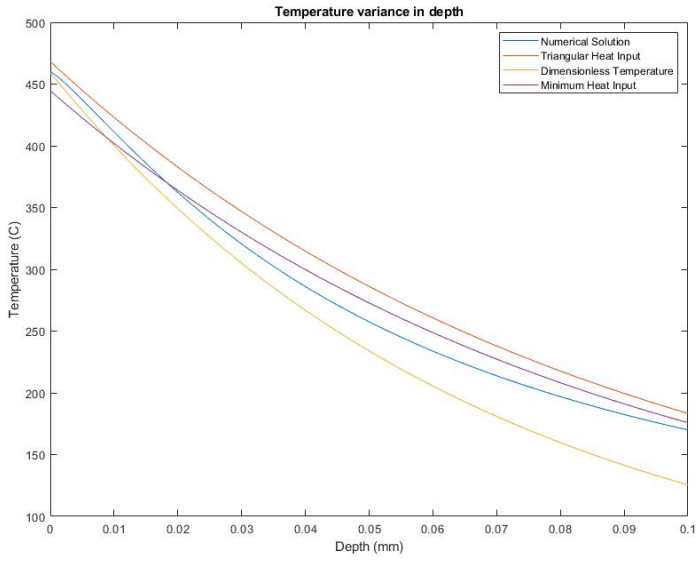

Figure 14 Temperature profile for a depth of cut 4.4µm, heat flux 292W/mm², workpiece speed 2.11 m/s and wheel speed 75.4 m/s

Both figures show the different temperature profiles following a similar curve behaviour, with the dimensionless method showing a more significant difference at higher depths. This difference could be due to this method being an approximation used for lower ranges of the Peclet numbers than those experienced during this process.

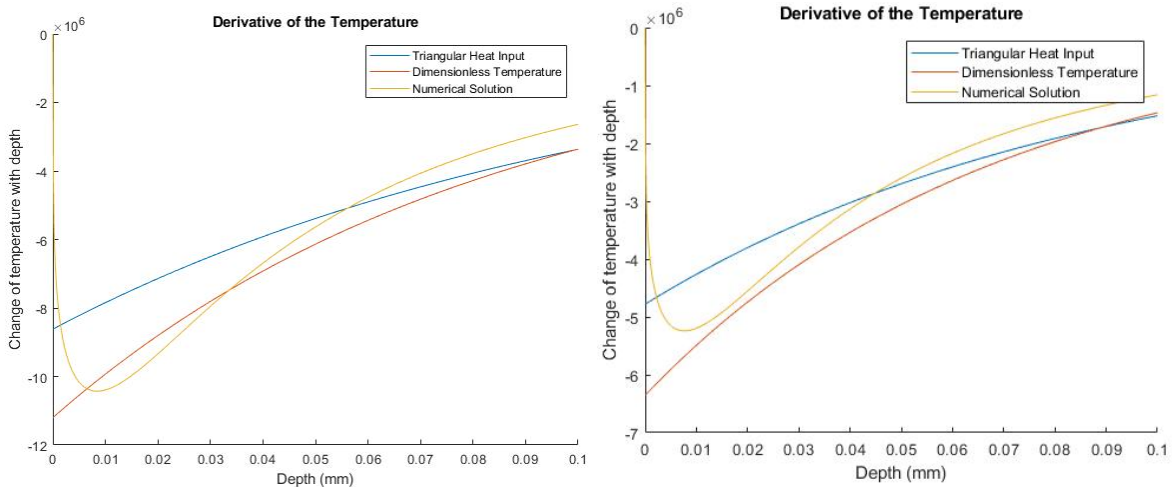

Figure 15 Derivative of the temperature for the first (left) and second (right) temperature profiles

From the derivative of the temperature a decrease of the slope can be seen, with it halving in value at around 50µm depth. This shows that most of the temperature increment will only affect the first layers of the material and that even at high temperatures, the expected affected depth will not be high.

All these approximation methods work as 2D approximations thanks to the high Peclet number. For a lower value, such as if the workpiece speed was much lower, then the assumption of heat only traveling in the depth direction would not be acceptable, and heat transfer in the grinding direction should be considered.

2.7.4. Creation of burns

One of the main issues during the project was obtaining stable burns in the subsurface. To make sure burns were obtained, an equation for the burning power was used. This equation would ensure that any ground ring whose power had gone above this threshold will show some degree of thermal damage. Malkin proposed the following equation (15):

$$P_b^{'} = 6.2 \cdot a_e \cdot v_w + 7.2 \cdot (d_e)^{0.25} \cdot (a_e)^{0.25} \cdot (v_w)^{0.5} \ \left[\frac{W}{mm}\right] \tag{39}$$

This equation can be expanded to calculate the necessary energy to have a certain temperature increase θ_m, and it can be seen is linked to Equation 27 by multiplying it by the volumetric removal rate:

$$P_b = 0.45 \cdot u_{ch} \cdot b_d \cdot v_w \cdot a_e + \frac{k_w \cdot \theta_{max}}{1.13 \cdot \alpha_w^{0.5}} \cdot d_e^{0.25} \cdot a_e^{0.25} \cdot v_w^{0.5} \cdot b_d [W] \tag{40}$$

This can be transformed into a force as the force controllers of the machine are more precise than the power controllers:

$$F_{t,burn} = \frac{P_b}{v_c} \tag{41}$$

As there existed previous knowledge and approximations of when the grinding burns would start $\theta_m = 400 \sim 500°C$ for tempering and over 800°C for burns, this equation was used before the tests to know the forces needed to obtain a grinding burn. Once a ring had exceeded that force, the grinding of that test was ended.

2.7.5. Temperature evaluation during grinding

Different experimental methodologies have previously validated the previously explained analytical methods. However, as this work will not be using any of those methods to evaluate the temperature directly, it is important to know the reasons behind that. Most of the experiments validating the previous methodology have been done in surface grinding and dry conditions (17), although more research is being done in grinding with coolants (23). However, in the temperature range interesting for this project, film boiling has occurred, and hence dry grinding is a correct approximation (8). This leads to three main ways of measuring the temperature:

- Thermocouples (17), being welded into the material at different depths, obtaining an accurate measurement of the temperature. For cylindrical grinding, the rotation of the workpiece would make the use of them very complicated, especially for small components such as in this study.
- Infrared (24), situated inside the machine, can film the grinding area and obtain the correct temperature. However, as the grinding will be done with lubrication, the fluid and the steam caused during grinding will make it difficult for the camera to obtain a correct reading, as well as causing damage to the camera. Also, it would be hard to evaluate for small rings in cylindrical grinding as the workpiece and the wheel will be blocking the view of the grinding zone. Due to this, it will not be used.
- IR interferometry. New research has been done on embedded IR (25) in the wheel which would be able to obtain accurate temperature values close to the grinding zone. However, it was not possible to utilise in this set-up as the grinding wheel was too small.

As the typical methods of analysing temperature have been considered difficult to obtain in this project's set up, other indirect methods were considered. As the reasons behind the properties degradation are known, it should be possible to obtain an accurate reading of temperature through the hardness. This will be done using the different heat transfer models' estimations explained before, together with the properties degradation models (26).

3. Material properties

An important part of any production process is obtaining a high-quality product that will satisfy the needs of the customer. In the case of bearings, that is heavily linked to the materials properties, as the customer expects a long-life of the product and an expected performance even after operating for a high number of cycles. The most common material used in the bearing industry for rolling bearings is AISI 52100, which was the same as the one used in this project. Its nominal composition is given in the following table:

Table 2 Chemical Composition of the material in weight percentage. (27)

C	Si	Mn	Cr	Fe
1.00	0.30	0.30	1.4	-

Due to the application for which the component was made, a high toughness while still maintaining some ductility are required to obtain a high fatigue life. In this material, that is mostly obtained by using a tempered martensitic microstructure, created by a carefully crafted heat treatment which will have a high hardness.

As the nature of the work is trying to analyse the defects created during real production conditions, rings coming from the production line were used instead of performing a separate heat treatment for the samples. This could account for small variations in the bulk microstructure which should not be affected during the grinding process. However, it is important to describe this process: austenitization followed by quenching to obtain a fully martensitic microstructure followed by a tempering process for 4h at 160C. This workpiece had a hardness of about 870HK.

As the temperature of the material will be analysed analytically, the material's thermal properties of it are also important, which in this case were:

Table 3 Workpiece Thermal Properties

Conductivity [W/mK]	Specific Heat [J/kg K]	Density [kg/m^3]	β [J/m^{2}s$^{0.5}$K]	α [m^2/s]
47.7	477	7840	13356	1.27e5

3.1. Phases and phase transformations

In steels, there are several possible microstructures obtainable, depending not only on the carbon percentage but also on other factors such as rate of cooling, as can be seen in this graph:

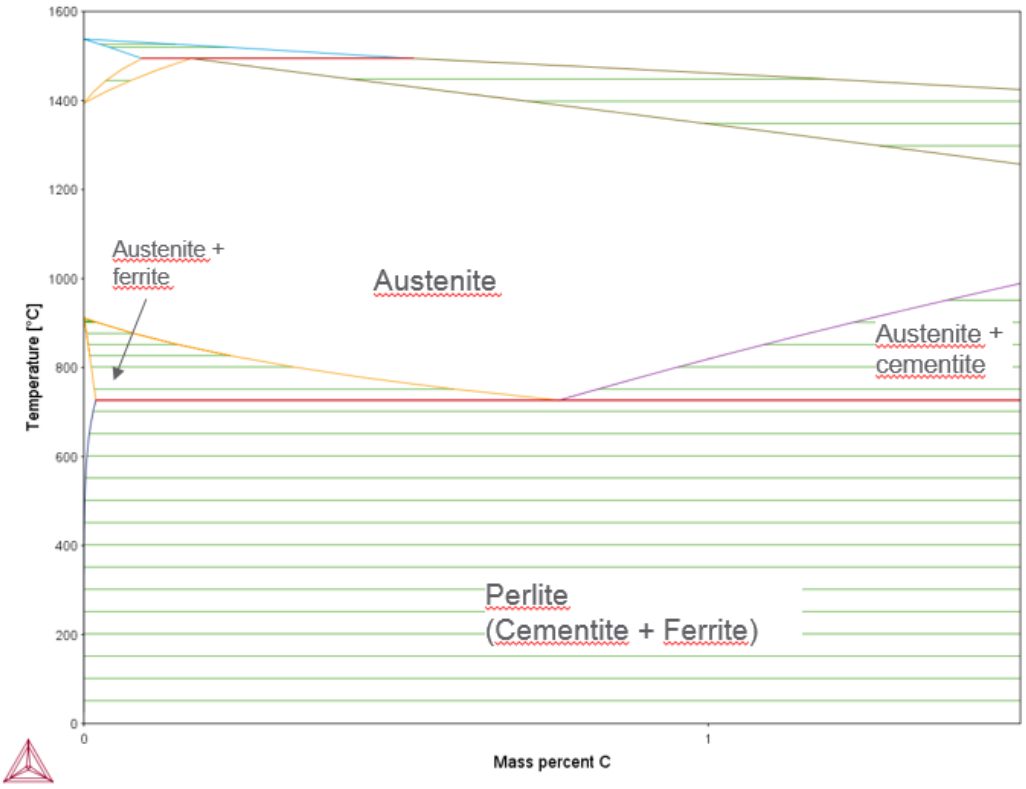

Figure 16 Fe-C Phase Diagram as obtained from ThermoCalc

In hardened steels, several possible phase transformations occur, but it is important to first characterize two different types of phase transformations (28):

- Diffusion phase transformations which occur via atoms moving through the material, this will change the structure of the cell and obtain a different phase. To initiate this process, a critical energy is required which is mostly obtained by the temperature. The atoms will then be able to move, requiring time for the stable microstructure to be obtained. An increase in the temperature over that critical value helps the kinematics of the transformation, making it go faster.
- Diffussionless phase transformations occur via a homogeneous change of the atoms which slightly move to create a new cell structure. These coordinated changes occur in an extremely fast way, and after the critical temperature, most of the material would have transformed. The most studied example of this is martensite.

In the given steel, there are several possible phase transformations:

- Pearlite and Martensite to Austenite. As the material goes above the austenitization temperature, Fe-γ, also known as austenite, becomes the stable microstructure. The microstructure of it is Face Centered Cubic (FCC) and allows for more carbon to be dissolved into it. However, in this type of steel, austenite will not be stable at room temperatures and the only interest is in whether this transformation would occur or not during the grinding process. As a diffusion transformation, higher temperatures than austenitization temperature are required to improve the kinematics of the transformation. In this case, as the heat rate is extremely high, it can be compared to laser heating, where experiments have seen requirements of temperatures above 800°C (29). This has also been corroborated with physical knowledge during grinding.

- Austenite to Martensite. As the material is quickly cooled down from the austenitization temperature, not enough time will be given to the austenite to transform into the stable pearlite phase. This transformation will create an untempered martensite microstructure and, depending on the amount of carbon in the material, some level of retained austenite. This untempered martensite provides a hard but brittle structure, that is not desirable for the final product, while the retained austenite is a soft material which could lead to some localized soft spots and could suffer further transformation during the lifetime of the component.
- Martensite Tempering. Due to martensite not being the stable phase at room temperature, once enough energy is provided, the carbon atoms in the microstructure will start to move, creating carbon-rich areas where cementite will be formed and carbon-poor areas where ferrite will appear.
- Austenite to Bainite or Pearlite. If the material is cooled slowly, the carbon atoms have time to move, and the microstructure can change to pearlite or bainite depending on the available time, as can be seen in the TTT diagrams. In the case of grinding, this will not happen due to the high cooling rate.

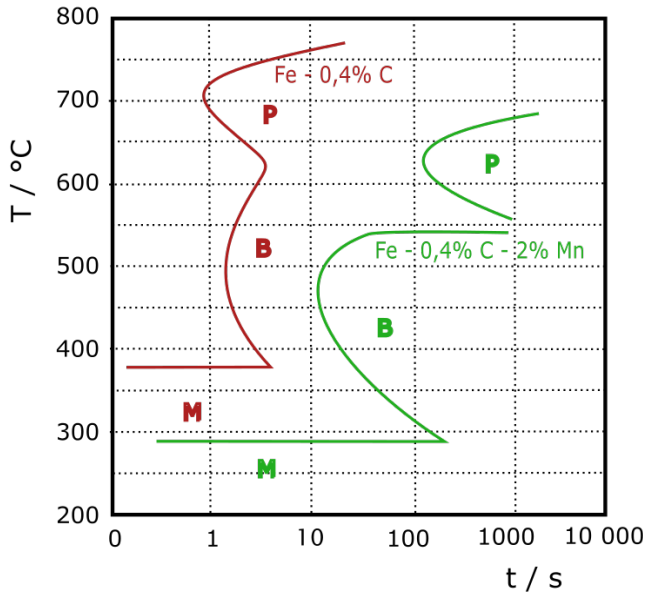

Figure 17 TTT diagram for two common steels, P being Perlite; B, Bainite; and M, Martensite.

3.1.1. Significant phases

Due to the material being hardened steel, the main phase is martensite, the phases of interest are the martensite and the phase it will be transforming to during the tempering process, cementite.

Martensite (α') is a common name given to those structures that have undergone a diffussionless transformation after reaching a certain low temperature during quenching called the martensitic transformation start temperature (M_s). This temperature has been widely studied and several empirical relationships exist to describe the effects of the alloying elements. The most widely used one was given by Andrews (30) in weight %:

$$M_s(C) = 539 - 423 \cdot C - 30.4 \cdot Mn - 17.7 \cdot Ni - 12.1 \cdot Cr - 7.5 \cdot Mo \qquad (42)$$

In this material, as the base would be austenite, the chemical composition between both will not change significantly, just having a small decrease in the carbon content due to the creation of retained austenite, carbon-rich austenite whose martensitic transformation temperature was lower than the quenched temperature.

The crystal structure changes from the face-centered cubic (FCC) structure of the austenite to the strained body-centered tetragonal (BCT) of the martensite, as can be seen in the following diagram (28). The phase change also causes an increase in volume, as the martensite has a lower density / packing parameter than the austenite.

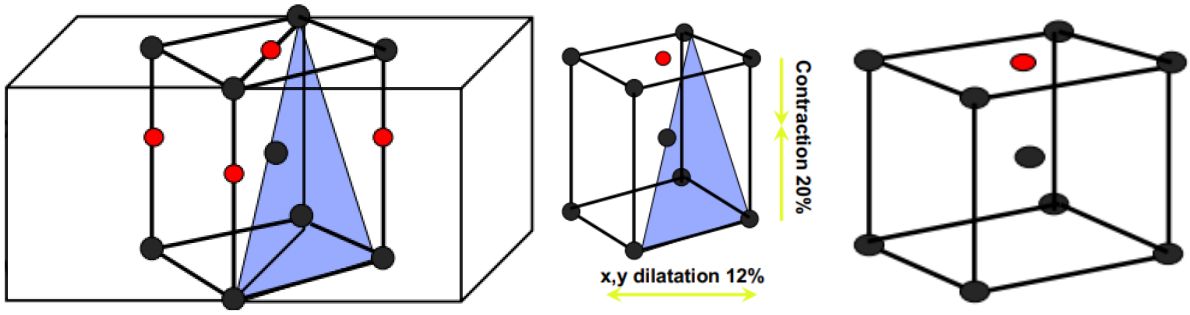

Figure 18 FCC to BCT transformation where the BCT is obtained from 2 FCC cells that are deformed.

Martensite itself is known to have a high hardness that increases with the carbon content. However, after a certain amount of carbon content, the hardness will decrease due to the existence of retained austenite, a much softer phase. This retained austenite also provides other problems, as it will continue to degrade into bainite during the lifetime of the product creating volume changes in the material which are undesired. The volume change is evaded by a posterior heat-treatment that releases the stresses caused during the transformation, creates transition carbides and changes the morphology of the martensite, taking away the more aggressive and dangerous needle shape, as well as stabilizing the retained austenite. This heat treatment softens the martensite but increases the critical elongation, making it more ductile.

Cementite is the intermetallic compound of iron and carbon Fe_3C. In combination with ferrite, it creates the pearlite structure, which will be stable at room temperature. As the ferrite is not able to contain a lot of carbon (only 0.008% at room temperature), the carbon movement in the martensite will create cementite, with the carbon deprived areas forming pearlite. It is an extremely hard but brittle component, but the overall hardness of the material will decrease, as less percentage of cementite will be present than martensite, due to the high C requirements for its formation (6.67%). This will mean that the softer pearlite would be more predominantly feature in the component.

3.1.2. Grinding burns

Due to the high requirements during the lifetime of the component, small variations of the properties need to be avoided as much as possible. As the material is machined in a hardened state and this process will be one of the last steps of production, it is crucial to avoid any possible alterations of it. However, during grinding, a high amount of energy is concentrated on a small area which could lead to temperatures high enough that they may damage the material or change its properties. Therefore, it is important to know which kind of damages can be caused during the grinding:

Temper burns (7), caused by overtempering, are a phenomenon caused by carbon diffusion and the transformation of the metastable martensite into the stable pearlite microstructure. The transformation causes a softening of the material due to the new phase being softer than martensite. This process is like leaving the material for too long in the furnace. An important aspect of this damage is that a small decrease of 20 HV, which is around 1 HRC, is expected to have a decrease in the total lifetime of the product of 50%. This type of damage is also called black layer, as it can be seen as a black layer on the outmost part of the material after etching.

Rehardening burn (7) refers to the formation of martensite in the outer layers of the material. These burns are expected to happen when the grinding zone reaches a critical temperature above the austenitization layer. As explained before, due to short heat intervals, a higher temperature than that is required, to drive the transformation in the short time. When grinding at a high workpiece speed, the heat will only slightly penetrate the surface of the material for a short amount of time. After the material leaves the hot spot caused by grinding, it will quickly cool down, creating an untempered martensitic microstructure if any material had transformed into austenite during heating. The untempered martensite will be harder and more brittle than the base material. The brittleness could lead to small parts of the surface to break during the use, creating hard particles that will be inside the component, leaving a pit as well as scratching the component, creating a crack which will help fatigue initiation. Rehardening burns are also called white layer, as it can be seen as a white layer on the outmost part of the material after etching.

As the mechanism behind both types of damages is quite similar, that is high temperatures inducing phase transformations; they can be easily grouped, calling them grinding burns. Moreover, as rehardening burns always require a higher initial temperature than temper burns, a rehardening burn is always accompanied by a temper burn below, which creates the total HAZ and may prove more problematic as the thin white layer would crack more easily due to the softer temper layer underneath.

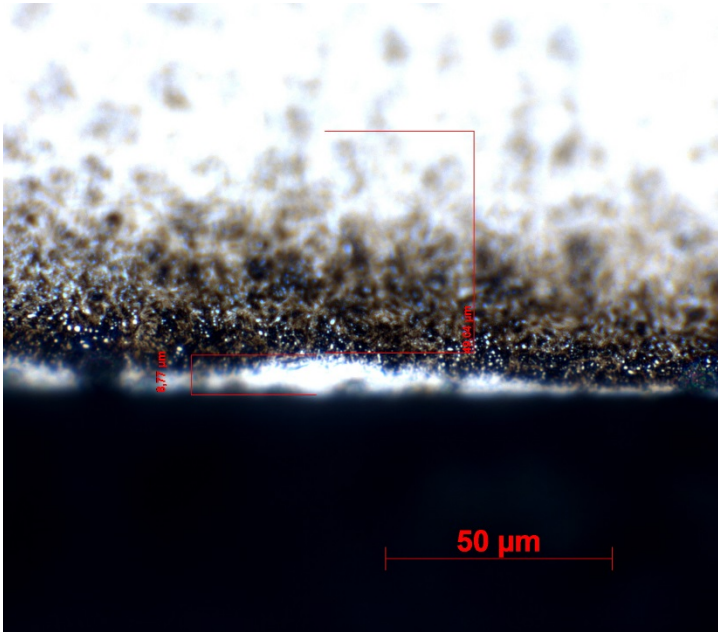

Figure 19 Etched sample showing a white layer in the outmost part of the component followed by a dark layer before reaching the bulk of the component

Oxidation burns are characterized by a discoloration of the workpiece, caused by a thin surface layer of oxidized metal and coolant without any metallurgical damage. They often cause a visible blueish mark that can be seen on the surface of the material and affects the adhesion to the wheel.

Residual stresses may be caused by the change in volume caused by different thermal expansions of the phases of the material from austenite to martensite. The volume changes can create tensile or compressive stresses in the surface. For high thermal loads, the result is predominantly tensile stresses which would create a faster crack propagation. For lower heat inputs, it is possible that the stresses during grinding create a plastic deformation in the surface which is not relaxed by the temperature, creating significant compressive residual stress, which would significantly enhance fatigue life. In the

case of tensile residual stresses, they may reach such a point where they go above the yield stress and cause a localized crack or crack easily on impact, as was found out during some of the samples.

Work hardening can also take place during grinding in certain conditions. As the grits may perform plastic deformation of the material and no recrystallization process is done due to the too short heating cycles. The stress during the work-hardening can also cause the creation of some stress-induced martensite due to the deformation of the retained austenite.

The main focus of this master thesis is in the damage of the material caused by the phase transformations; thus, the focus will be in the temper burns and rehardening burns, were three different methods of analysing the hardness has been used.

3.2. Analytical models

The transformations of a phase into another has been an important research focus in material science as it makes it possible to understand the change in the material properties. Due to the different variables involved in this process, several analytical models have been created:

3.2.1. Larson Miller parameter

As the transformation of martensite into more stable phases is a product of the diffusion of carbon inside the material, it is possible to use the Arrhenius equation (28) to see the temperature dependence of this process. Due to that dependence, it can be helpful to design a time-temperature parameter (TTP) that will allow for extrapolation and interpolation in case one of the parameters is changed. The Larson Miller (LM) parameter is the most widely used TTP in the creep rupture life (2), and it can also be used to predict the softening of materials as all components that have been subject to processes that cause the same LM parameter have the same mechanical properties. This LM parameter can be found through:

$$LM = \mathrm{T(K)} \cdot \frac{\left(\mathrm{C_0} + \log\left(t(h)\right)\right)}{10^3} \tag{43}$$

Due to previous experimentations on the material (5), it is known that the material parameter C_0 is 14 (5). As the temperature will be measured in Celsius and the time in seconds, the above formula can be rewritten as:

$$LM = \left(273 + \mathrm{T(C)}\right) \cdot \frac{\left(14 + \log\left(\frac{t(s)}{3600}\right)\right)}{10^3} \tag{44}$$

Once this parameter is known, testing of the material must be done to obtain the characteristic curve of the material in question, that is the softening of the material with a combination of time and temperature. Once that is known, it should be possible to estimate the softening occurring in the material if both temperature and time are known. It is important to notice that this parameter only works as the diffusion of carbon atoms from martensite into the component. Therefore, it is only able to correctly estimate the tempering of the component and not any possible rehardening that may occur at high temperatures.

Even then, the Larson-Miller equation has been reported not to be reliable in grinding (7) as it is based on the material experiencing a constant temperature for an extended long period. However, the simplicity of the equation, which only requires two variables temperature and time, would make it useful if the predicted damage was close to the obtained one.

As the temperature experienced during the grinding cycle is not uniform but rather an exponential increase as the material gets closer to the heat source, and the LM parameter assumes a constant temperature, it is important to choose the correct temperature approximation. The two main possibilities are either using the maximum temperature, as higher values of temperature are required to activate the transformation of the material or the average temperature over the heat source (7). Similarly, in the depth direction, as heat is assumed not to transverse in the circumferential direction, the direction of the grinding, due to a high Peclet number, it is assumed that whatever surface temperature that was chosen will affect the temperature with respect to depth in the same way. It is then important to see which of the temperature equations and maximum temperatures better fit the obtained results.

$$T_{max} = T_0 + \theta_{max} \quad and \quad T_{ave} = T_0 + \frac{2}{3}\theta_{max} \tag{45}$$

The second variable in the LM parameters is the time the material will be exposed to the heat. This time can be calculated as the interaction time. The time can be calculated easily as the contact length divided by the speed of the workpiece, which will explain one short cycle of grinding. However, as the workpiece is rotating, there will be more than one pass over happening during the entire grinding cycle. To simulate that, a higher interaction time could be assumed.

3.2.2. JMAK equation

The Johnson-Mehl-Avrami-Kolmogorov (JMAK) equation (31), describes the transformation of a solid from one state of matter to another at a constant temperature. For the transformation, the degree of transformation, f, can be expressed in terms of the physical property traced in the experiment:

$$f = \frac{H_3 - H}{H_3 - H_1} \rightarrow H = H_3 - f(H_3 - H_1) \tag{46}$$

Where the maximum hardness H_3, the minimum hardness H_1 and the hardness at that moment of time H are present. As the degree of transformation increases, the material hardness decreases due to the more prevalent percentage of the softer phases. The simple assumption of this fraction transformed being fully determined by the state variable ξ that, as the process will not be occurring in a continuous temperature (32), can be described by:

$$\xi = \int_0^{\infty} k\, dt \tag{47}$$

$$k = k_0 \cdot \exp\left(-\frac{E}{R \cdot T}\right) \tag{48}$$

As one can assume, in a non-isothermal case, this variable will depend on the thermal history of the material and can be in the case of a constant heating rate $\Phi = dT/dt$ rewritten as:

$$\xi = \frac{k_0}{\Phi} \int_{T_0}^{T} \exp\left(-\frac{E}{R \cdot T}\right)\, dT \tag{49}$$

Which can be approximated to:

$$\xi = \frac{T^2}{\Phi} \cdot \frac{R}{E} k \tag{50}$$

So, the fraction f can be calculated such that:

$$f = 1 - \exp(-\xi^n) \tag{51}$$

For the material properties, the following values were used, obtained in a previous project by SKF (6):

	Segregation	Transition Carbide	Retained austenite	Cementite 1	Cementite 2
E [J]	8.314e4	1.23e5	1.5e5	1.88e5	2.44e5
k0 [1/s]	2.11e10	3.18e13	6.51e11	1.97e15	9.68e17
n	0.502	0.378	1.04	0.465	0.395

Different transformations can be analysed with this method, but the focus will be on the transformation to the softer phase cementite as can be seen in their normal gradient where the transformation starts to occur in a similar place as expected in grinding.

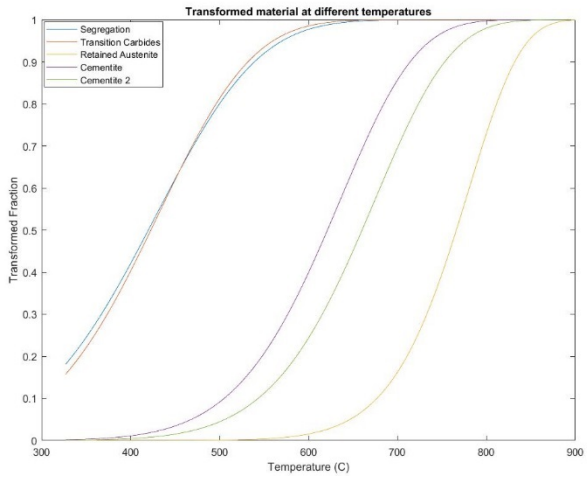

Figure 20 JMAK curves at $\Phi = 1600000$

It is important to notice that the curves will move as the temperature gradient decreases. The movement of the curves would mean that to create a more accurate representation of the transformation gradient, more than one general graph is needed:

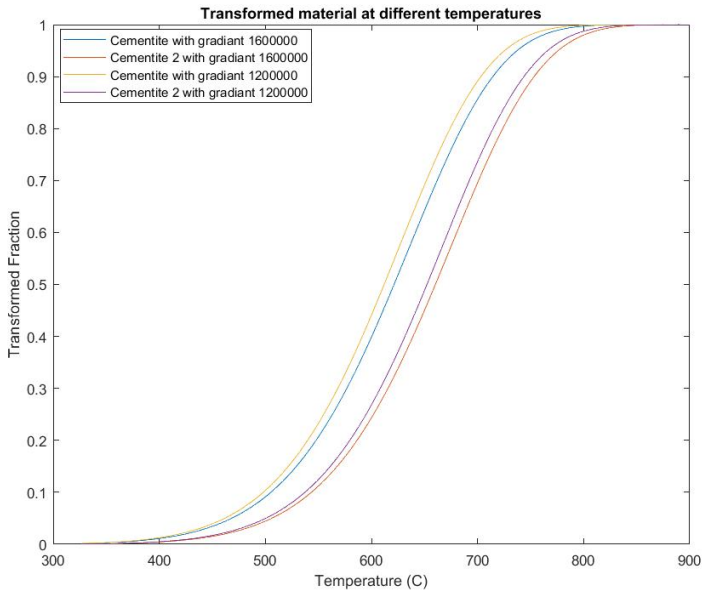

Figure 21 JMAK curves for cementite at different gradients

In this case, the gradient will be calculated in every point of depth by utilizing the temperature approximations and the interaction time to calculate the gradient at each depth, which would bring us to a graph where there is a dependence of fraction of phase transformation and depth.

As the hardness of the component can be easily related to the percentage of transformed material, if the hardness of both phases is known, the curve can be compared with the obtained results.

3.2.3. Differential approach to tempering

Another way of evaluating the tempering has been recommended, by integrating the rate of tempering over the grinding cycle (22). Like the JMAK equation, it would be possible to calculate the hardness through the transformed fraction f, with a material with a maximum hardness H_3 and minimum hardness H_1.

$$H = H_3 - (H_3 - H_1)f \tag{52}$$

Several models have been proposed; however, the experimental data tends to follow a third-order reaction such that:

$$\frac{df}{dt} = h(1-f)^3 \tag{53}$$

Where h is the reaction constant that follows the thermally activated Arrhenius equation:

$$h = \nu \cdot \exp\left(-\frac{U}{R(T_0+\theta)}\right) \tag{54}$$

And U is the activation energy of diffusion of the atom, which may vary depending on the transformation but should be a physical constant. In this case, the value should be 60 kJ/mol as it is the necessary activation energy for carbon in ferrite; R is the universal gas constant, and T_0 is the absolute room temperature while T is the temperature rise caused by grinding. If tempering were to occur at a constant temperature T and for a length of time t, it would be possible to integrate to obtain:

$$f = 1 - \frac{1}{\left(\frac{1}{(1-f_0)^2} + 2 \cdot h \cdot t\right)^{\frac{1}{2}}} \tag{55}$$

Where f_0 refers to the original tempering of the workpiece, where H_0 is the hardness of the material before grinding:

$$f_0 = \frac{H_3 - H_0}{H_3 - H_1} \tag{56}$$

However, during grinding the temperature experienced by the material is not constant but an increasing value as the points gets closer to the to the heating source / grinding area. Thus, to find the correct value, it is necessary to do an integral of h dt, which is called J. J should show the total value of h as, during the grinding cycle, it would change with time. As the location of the point can be related to the location of the heating source through the velocity of the workpiece, such that $d/dt = v_w\, d/dx$, it can be expressed:

$$J = \int_0^\infty h\, dt = \nu \cdot \int_0^\infty \exp\left(-\frac{U}{R(T_0+\theta)}\right) dt \tag{57}$$

To simplify the equation, several dimensionless numbers are recommended (22) such that:

$$p = \nu \cdot \tau \tag{58}$$

Where τ is the interaction time which can be found as a division of the contact length and the workpiece speed:

$$\tau = \frac{l_c}{v_w} \tag{59}$$

And, to move to a dimensionless temperature, whose change can be more easily mapped, a scaling temperature was recommended:

$$\lambda = \frac{U}{R \cdot T_0} \tag{60}$$

$$r = \frac{T_w}{T_0} \tag{61}$$

Such that:

$$J = p \int_{-\infty}^{\infty} \exp\left(-\frac{\lambda}{r + \bar{\theta}}\right) dX \tag{62}$$

Which if we expand the temperature to a simplified approach, based on the numerical solution method previously explained, it is possible to obtain:

$$J(Y) = p\left(\frac{2\pi}{\lambda \cdot a_2}\right)^{\frac{1}{2}} \cdot (r + a_0) \cdot \exp\left(-\frac{\lambda}{r + a_0}\right) \tag{63}$$

However, this equation would express the tempering occurring in one pass of the grinding process, whereas the ring in this study will be making multiple revolutions. It is necessary then to expand it so that it can showcase how the material is tempered while it is in a previous cycle, that is while its depth is y+k·a, where y is its final depth, and k is the number of cycles before the end. Adding this concept to the previous equations, only the J value would be affected such that:

$$f = 1 - \frac{1}{\left(\frac{1}{(1 - f_0)^2} + 2 \cdot \sum_{k=0}^{\infty} J(Y + k \cdot \gamma)\right)^{\frac{1}{2}}} \tag{64}$$

$$\gamma = \frac{a_e}{y_0} \tag{65}$$

Such that the sum of all the tempering damage that has occurred during a k+1 number of passes is considered. The infinite sum of the passes can be transformed into an integral over k. If the variable is changed to Y' = Y + kγ, the following equation for the integral is obtained, which can substitute J:

$$S(Y) = \frac{p}{\gamma}\left(\frac{2\pi}{\lambda}\right)^{\frac{1}{2}} \int_{Y}^{\infty} \frac{r + a_0}{\sqrt{a_2}} \cdot \exp\left(-\frac{\lambda}{r + a_0}\right) dY' \tag{66}$$

Where the exponential part will be a decreasing function of Y' having the highest value in the last pass, k=0, Y'=Y. It can be assumed then that for high values of λ, most of the damage is done during the last passes because it is where the exponent is the biggest. If the functions are expanded to depend on the temperature to a power series near to Y'=Y, it is possible to obtain:

$$S(Y) = \frac{p}{\gamma} \cdot \left(\frac{2\pi}{\lambda^3 a_2}\right)^{\frac{1}{2}} \cdot \frac{(r + a_0)^3}{a_0'} \cdot \exp\left(-\frac{\lambda}{r + a_0}\right) \tag{67}$$

Where a_0' is the derivative of a_0.

$$a_o' = \frac{-1.3 \cdot 1.2 \cdot Y^{0.2}}{(0.907 + 1.3 \cdot Y^{1.2})^2} \tag{68}$$

It is also possible to calculate the rehardening through this method. However, two main considerations must be taken: the rehardening will increase the hardness of the end material, and the transformation follows a first-order equation. Such that:

$$\frac{df}{dt} = -h(1 - f) \tag{69}$$

The reaction constant h will use the same equation as said before. However, the activation energy U will be 135 kJ/mol, the necessary energy for diffusion of carbon in austenite. The equation can then be solved:

$$f = 1 - \left(1 - f_{tempering}\right) \exp\left(\int_0^t h_{rehard}\, dt\right) \tag{70}$$

As the equation may reach values lower than 0 if the rehardening value is too high, the final transformed fraction will be:

$$f = \max\left[0, 1 - \left(1 - \psi_{tempering}\right) e^{J_{rehard}}\right] \tag{71}$$

Where the integral of h will be analogous to the previous one, which will show:

$$J(Y) = p_{rehard} \left(\frac{2\pi}{\lambda_{rehard} \cdot a_2}\right)^{\frac{1}{2}} \cdot (r + a_2) \cdot \exp\left(-\frac{\lambda_{rehard}}{r + a_0}\right) \tag{72}$$

For the rehardening model, the dimensionless numbers are different as the activation energy differs between tempering and rehardening. The rehardening model has been shown to work (22), but the focus of this master thesis was in preventing any damage to the material. As rehardening often requires higher temperatures than overtempering, it was not implemented in the models.

3.3. Hardness

As seen previously, one of the critical properties of the material for the product is the hardness, as it is linked with the fatigue life of the product. Hardness is a material characteristic that is defined as the resistance to indentation and can be determined by loading the sample with an indent and measuring the depth of it. As the material is loaded and plastically deformed, harder materials will see a smaller indentation compared to softer ones (2).

Due to the nature of hardness evaluation, in some metals such as steels, it is possible to relate hardness with yield limit. This is regularly used to evaluate materials without the necessity of big samples, as the indents only require a small volume of the component. As such, higher hardness points to a stronger material which would have a higher fatigue life for the same stress. Experimental testing at SKF has shown that a decrease of 1 Rockwell C(HRC) points towards a decrease in the lifetime by a factor of two. However, the use of extremely hard but brittle materials such as untempered martensite can also be a hindrance, as it can crack more easily in case of an overload. The crack could lead to the creation of a hard metal shard that would scratch and damage the inside of the bearings. Because of that, a requirement of hardness and ductility is put into the material. There are several methods of evaluating hardness, but the following were used due to the ability to measure in the microscale:

Vickers Hardness (HV) (33) uses a wide range of loads, from the macro to the micro scale. The indent is a diamond in the form of a square pyramid with an impression 3/8 of the ball diameter of Brinell.

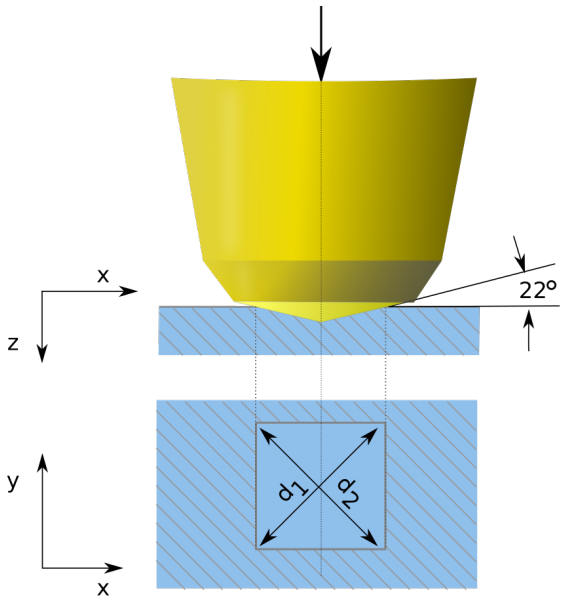

Figure 22 Shape of the Vickers indent

To obtain this shape, the indenter has an angle of 136° between opposite faces and an angle with the horizontal plane of 22°. The HV number is determined as the ratio between the force, and the area imprinted such that:

$$HV = \frac{F}{A} = \frac{F \cdot 2 \cdot \sin\left(\frac{136}{2}\right)}{d^2} = \frac{1.8544 \cdot F}{d^2} = (change\ to\ kgf) = 0.1891\,\frac{F}{d^2} \tag{73}$$

Knoop microhardness (HK) (33) is used particularly for very brittle materials or thin sheets, as it only requires a small indentation to be made for testing purposes. The pyramidal diamond point is pressed into a mirror polish surface with a known weight, with the hardness being evaluated by the following equation:

$$HK = \frac{F}{A_{PAC}} = \frac{F}{\frac{L^2 tg\left(\frac{\varphi}{2}\right)}{2tg\left(\frac{\theta}{2}\right)}} = 14.229\,\frac{F}{L^2} \tag{74}$$

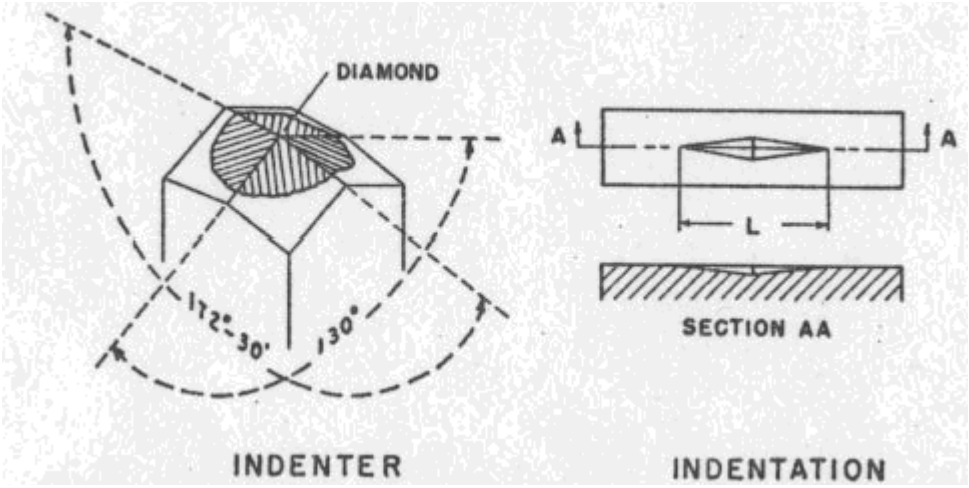

Figure 23 Shape of the Knoop indent

It is important to realize that the slender tip of this indentation will make it more difficult to precisely discern it and obtain an accurate result. However, it is also due to this design that much more local measurements in the minor diagonal direction are possible, as the volume used to measure the hardness will be much smaller. As the grinding damage will be mostly localized in the first µm of depth, this method was utilized. When utilizing HK, it is also important to correctly localize the interface between the holder and the sample, and the angle between them. This is due to the measurement being only dependent on the length of the main diagonal and that a small angle between them could lead to the diagonal not being parallel to the interface, not measuring the hardness at the desired depth.

3.3.1. Testing procedures

As hardness is evaluated by inducing plastic deformation in a material, it is essential to follow specific standards to make sure that the measurements taken are representative of the state of the material and do not present issues such as the effect of previous measurements or the effect of the polymer used as a holder. In this case, the recommendations are as follows (33):

- To avoid the effect of work hardening into the measurements, there should be some spacing between measurements and to the interface between the sample and the holder. According to ASTM standards, the spacing should be at least 2.5 times the main diagonal, counting from the centre of the indentation. As ISO standards pose a harsher spacing of 3 times, ASTM methodology was tested in a completely normalized steel to make sure it was viable. The obtained hardness was constant while using it pointing towards no work hardening occurring, making it viable. Testing was also done in more tempered versions of the material to obtain the maximum size of the imprint. The size of the imprint had a width smaller than 4µm. Due to that, it was considered that measuring at 10µm from the surface was possible.
- The machine should be stable and use the correct load and speed. The testing machine used was a QNess Q10A+ that has been validated. Calibration blocks for the different hardness were used to make sure the results were valid.
- Recommendations of the measuring parameters which in Knoop's case is the lengths of the major diagonal. It should be above 20µm to minimize the effect of measurement error of the machine. The obtained diagonals were larger than that size.

3.3.2. Sample preparation

Two main possibilities are available for hardness testing: cross-sectional or topmost analysis.

In a cross-sectional analysis, the sample will be cut and polished, and the testing will be done in that cross section. The depth of the measurement will be obtained with respect to the interface, and thin hardness indenters must be used, as the hardness will not only measure at the desired depth but the surroundings.

In a topmost analysis, the outer layers of the desired surface will be removed, and the hardness testing will be done in the new obtained surface. By removing material, there will be a bigger surface to test the hardness, making it so that there is no requirement for the shape of the indenter. Two methods were used in the laboratory: electrochemical etching and smooth polishing. Electrochemical etching consists on putting the desired surface in a NaCl solution and then applying a current which will polish the surface, with the obtained roughness depending on the solution, the voltage applied and the area of focus. A higher concentration of the solution, higher voltage or a smaller focus area will create a smoother surface. Smooth polishing consists of lapping on a diamond slurry to obtain the desired depth. Both procedures would require the use of a very precise depth gauge to calculate the correct depth obtained for each measurement.

4. Methods and experimentation

All samples used were inner rings of a “Deep Groove Ball Bearing” (DGBB) IR6210, as shown in Figure 24:

Figure 24 Picture of the ring, showing the cut made for the prepared sample

These rings are already part of a commercial product and are widely used. The machine used was a standard production internal grinding machine that for R&D purposes was equipped with a dynamometer from Kistler, to measure the grinding forces.

Based on the grinding theory, the highest risk for grinding burns are at high MRR or very low MRR (dwell or spark out). Herein the focus was the thermal behaviour at high MRR hence a rough test trial, and DOE was made. The steady state of the grinding forces during grinding was achieved by having large enough volume of material to remove, giving time for the defection build up. This was verified with the force signals.

The design process parameters were selected based on their availability to the machine operator as well as their importance as found in the literature. The focus on the availability to the machine operator makes it a more realistic approach during production, as the operator can easily change the parameters to meet surface demands or to stop the damage. A high and low value for each of them was chosen, with the study combining the settings for a total of 2^4 (sixteen), experiments. A more detailed table with all the different settings for each experiment can be seen in the Appendix.

Table 4 Setting Selection for the Experiment

	V_w (m/s)	V_c (m/s)	a_e (µm)	f_{ad}(µm/rev)
+	1.57	75	4.4	70
-	1.31	63	2.5	35

The above parameters are heavily interrelated in the grinding process, though some of them may be more influential in certain aspects. For instance, the workpiece speed is heavily related to the

interaction time as a higher value of it would lead to the material moving faster through the grinding area. This would lead to lower temperatures and a shorter time for the phase transformations.

The radial in-feed per workpiece revolution or depth of cut is not a direct input but has to be calculated from the radial feed rate and workpiece rotational speed. That will mean that this speed will be related to the workpiece speed and will not be able to be changed directly:

$$v_{fr} = a_e[\mu m] \cdot n_w[rpm] = \frac{a_e \cdot n_w}{60}\left[\frac{\mu m}{s}\right] \tag{75}$$

Similarly, the dressing parameter is related to the cutting speed, as described in Equation 7.

The machine used can be configured for many size ranges, but the current configuration used a 24-36k rpm spindle with a P_{s1} rating of 10kW. The belt driven workhead spindle used a gear ratio that enabled a range from 500-1100 rpm. The grinding wheel used was a Tyrolit AH120K6VC0LT3, with the initial rough trial being done with a Tyrolit AH120K6VC0L. The cooling was provided by a Castrol Syntilo 9954 with a concentration of 5.5%. The pressure used was 5.5 bar with a flow rate of 90 litres per minute.

4.1. Grinding operation

The process-monitoring data from the machine is obtained through LabView program, which acquires the signal from the force and power sensor. For the F_N and the F_T, a 3axis dynamometer 9255B from Kistler was used together with a Kistler5019 charge amplifier. A PS100 sensor from Montronix measured the power at the grinding spindle. The force from these sensors will be used to obtain the specific grinding energy. The information of the sensors will often not start at the zero position, which was fixed by taking off-sets before the wheel has detected touching the workpiece and the grinding operations were initiated. A Dittel 4100 acoustic emission device was used for the touch detection.

An important characterization consideration of the force is how it is measured in the machine. As explained before, forces in grinding are highly dynamics stochastic. Due to this, the value of the measured forces can and will quickly change with every measurement, as the grits properties, even just after dressing are not perfectly uniform, and the contact situation between the workpiece and wheel will quickly differ. However, as the main objective of this project is dealing with the macro situation of grinding, it is necessary to utilize an average value of the force. To do that, a low pass filter was used to obtain data such as this:

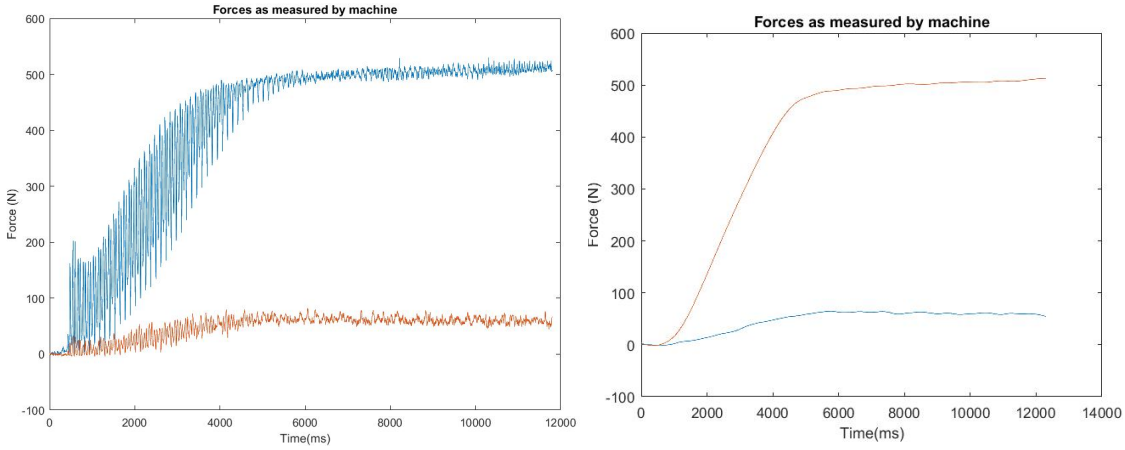

Figure 25 Data obtained from the machine for case 1D (left) and smoothed using a robust loess method (right)

It is also possible to use a local regression method to smooth the curves and obtain a better approximation of the average values. However, it is important to remember that the variation seen is not noise but rather the normal behaviour during grinding, the real noise can be observed in the initial part of the curves before the wheel touches the workpiece. As the interest is also in the last passes of the components, once it is stabilized, an average value of the last cycles was taken.

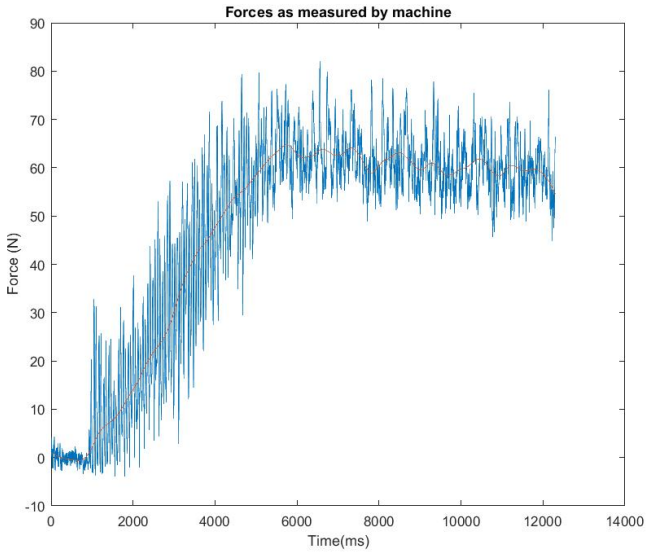

Figure 26 Comparison of the normal and the smoothed data for the tangential force of case 1D

The purpose of this study is to deepen the understanding of the thermal behaviour during production grinding. Hence, no parameters were extreme even though some combinations were outside recommendations. Nonetheless, it was proven hard to obtain grinding burns. A controlled way to create them was to allow larger wheel wear by increasing the number of workpieces ground between dress intervals. In this project that meant not redressing until the target tangential force was reached, paying attention to the normal force in order not to heavily damage the wheel. Not redressing will cause the wheel to become duller and have more wear flats which will increase the true contact area, resulting in a higher normal force. The grinding at the same machine settings will continue until the power and force sensors reach the desired values where damage is expected. To distinguish the ring ground with the same settings, an alphabetic order nomenclature (A, B, …) was used, its length depending on the total number of rings ground for each setting.

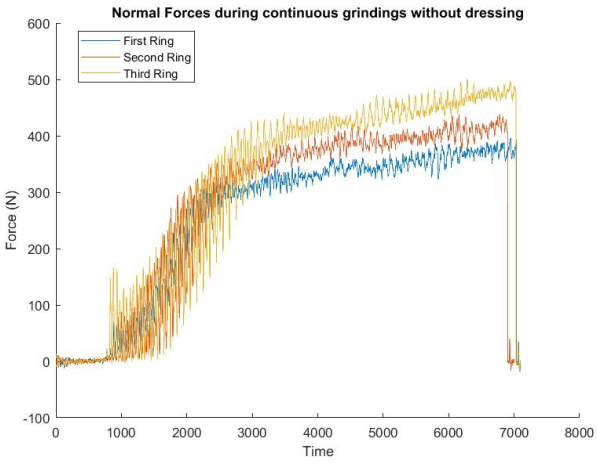

Figure 27 Normal force increase with successive grinding of rings

The process of continuously grinding rings without redressing, gave a gradual and controlled increase of the heat flux, while maintaining the same process settings, as the forces gradually increased with each ground ring. However, it also consisted on grinding a high number of ring, which would require too much time to analyse. As the interesting rings are those that have been thermally damaged, only the rings that have been exposed to high thermal loads / high tangential forces were evaluated, often only the last one of each setting. Other rings were selected at random to be treated with Nital to show any possible martensitic or over tempering transformation in the surface, as well as creating a hardness-depth profile. This way it was possible to confirm that no damaged occurred on rings that did not experience high temperatures as well as not finding signs for stress-induced martensite from the retained austenite.

4.2. Metallography

An essential part of every experiment is its repeatability and reproducibility. Repeatability will be addressed by performing the experiments more than once. As the Knoop hardness shows the local hardness of the material, each measurement should be looked at separately as certain factors such as proximity to carbides may create outliers that are not in accordance with the expected results. Reproducibility would be obtained by explaining the methodology as well as the set up for the experiments. The most critical part that must be studied during this work is the internal diameter as that is the surface that will be ground during experimentation, probably causing damage during the process.

As the ring has a small inner radius (25mm), it was proved hard to obtain many samples with their cut surfaces being parallel to mount and examine. This difficulty was mainly due to having to hold the smaller cut components as well as thickness requirements in the samples. The requirements for the samples led to a maximum of 4 segments per ground ring.

4.2.1. Larson-Miller

Ring sections of the same batch were kept in a furnace at different temperatures for a period of 4h with a 30-minute warm-up period to be later measured at HV1 and HK0.05. A total of three non-ground rings were used, cut into four sections each making a total of twelve sections. Five hardness measurements were done in each section to obtain an average result that better resembles reality.

A thermocouple was welded onto the samples to obtain more accurate measurements of the temperature. As the temperature of the test went above 500C, ceramic coating of the cables was necessary, as the glass fibre ones would be conductive and create false temperature results. Two ring segments were mounted into each sample to save time during the measurement. The following results were obtained:

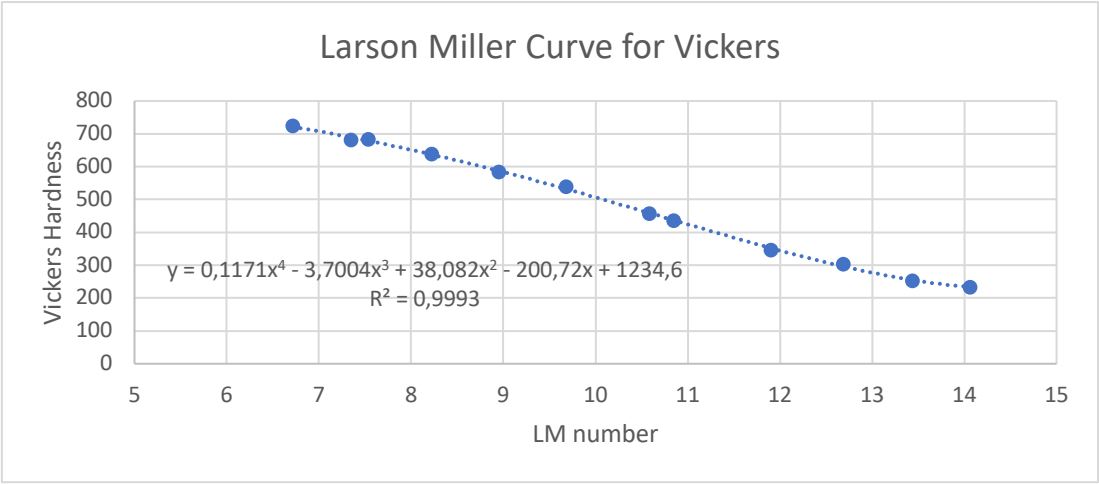

Figure 28 Larson Miller curve for Vickers

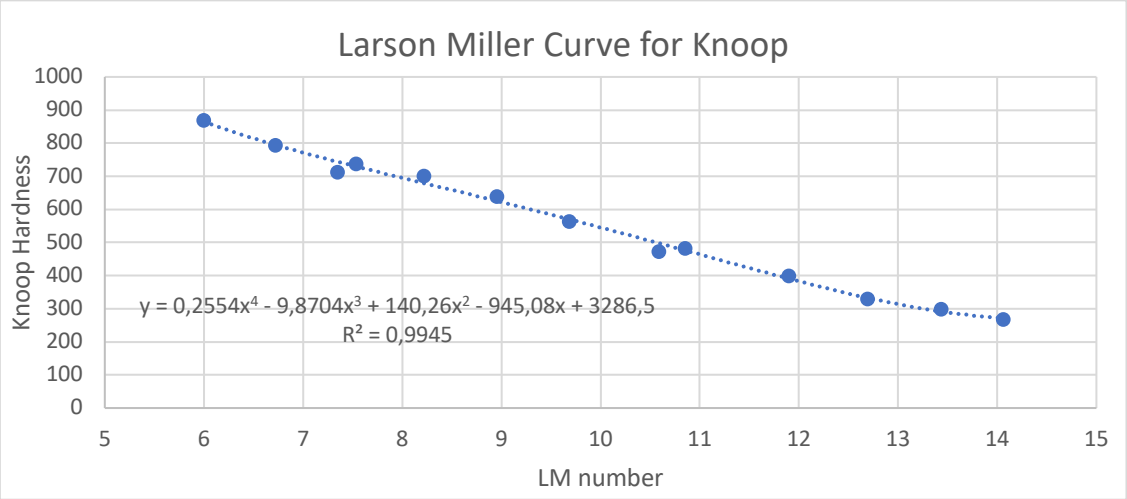

Figure 29 Larson Miller curve for Knoop

4.2.2. Grinding and hardness testing

To prepare the samples, the rings were cut similarly to those used for the Larson Miller Curve. Top-most analysis, slowly removing material to the desired depth by either grinding or etching, was tried, but difficulties in obtaining a correct depth reading due to the curved geometry of the inner diameter created too much uncertainty. Thus, a cross-sectional analysis was selected. The rings were mounted on a polymer holder and polished to obtain a mirror finish. In Figure 30 it is possible to see the mounted sample, with the point of interest being the inner diameter that was ground. It is possible to see that the damage is superficial and affects only the outmost parts of the workpiece.

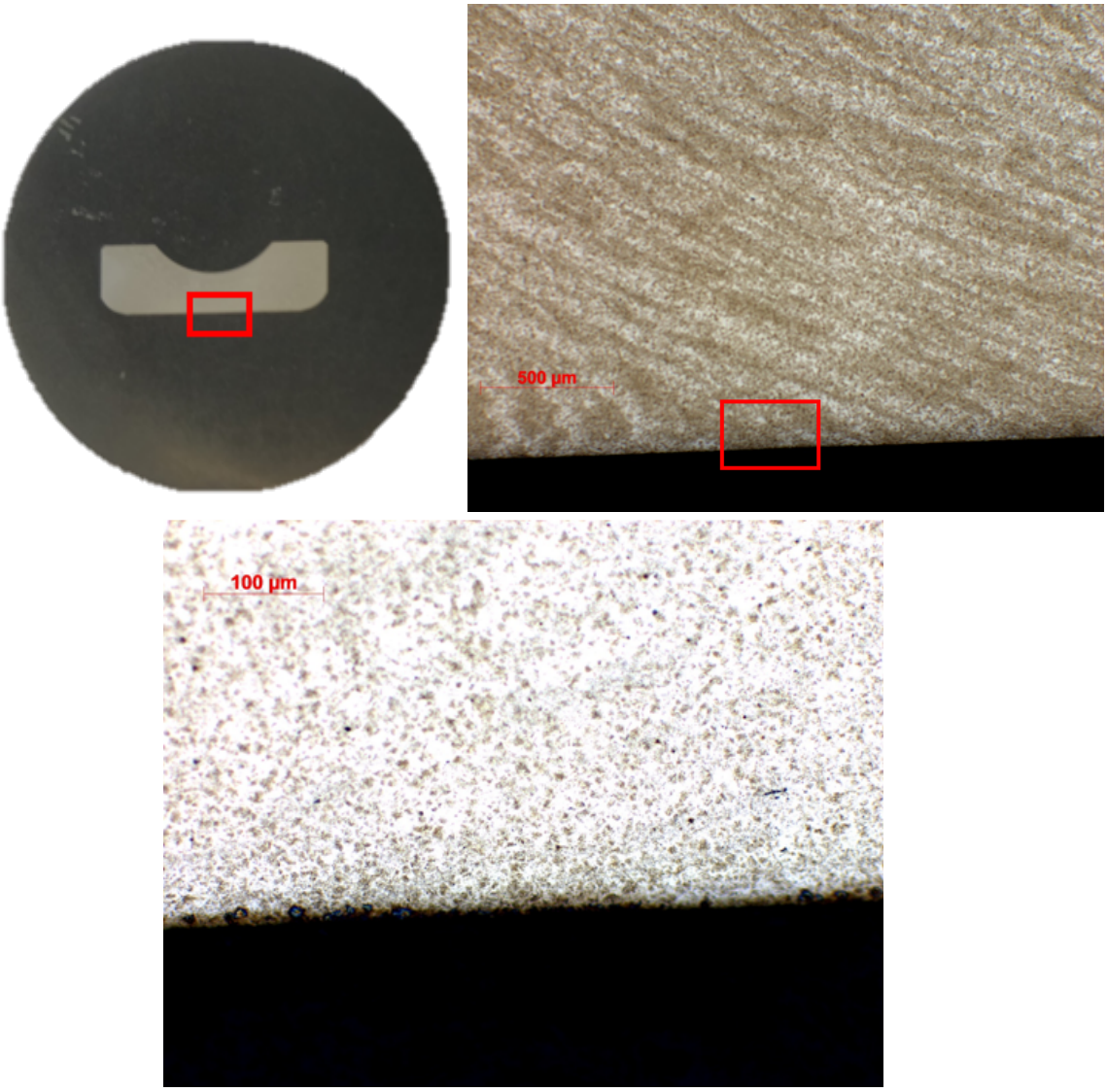

Figure 30 Photo of the sample on the holder (top left), with a low magnification in the designated area (top left) and a higher magnification, finally showing the affected area (bottom)

The samples were individually mounted as it was difficult to mount two or more samples parallel to each other. This parallel requirement was essential as Knoop measurements are directional and it is necessary to keep the indenter parallel to the surface between the mount and the sample. Five lines of Knoop measurements were made at 50g, each line beginning at 10µm and with a spacing between them of 15µm, up to 200µm depth. As they were distributed in zigzag, there was a spacing of 45 µm between the centre of consecutive measurements.

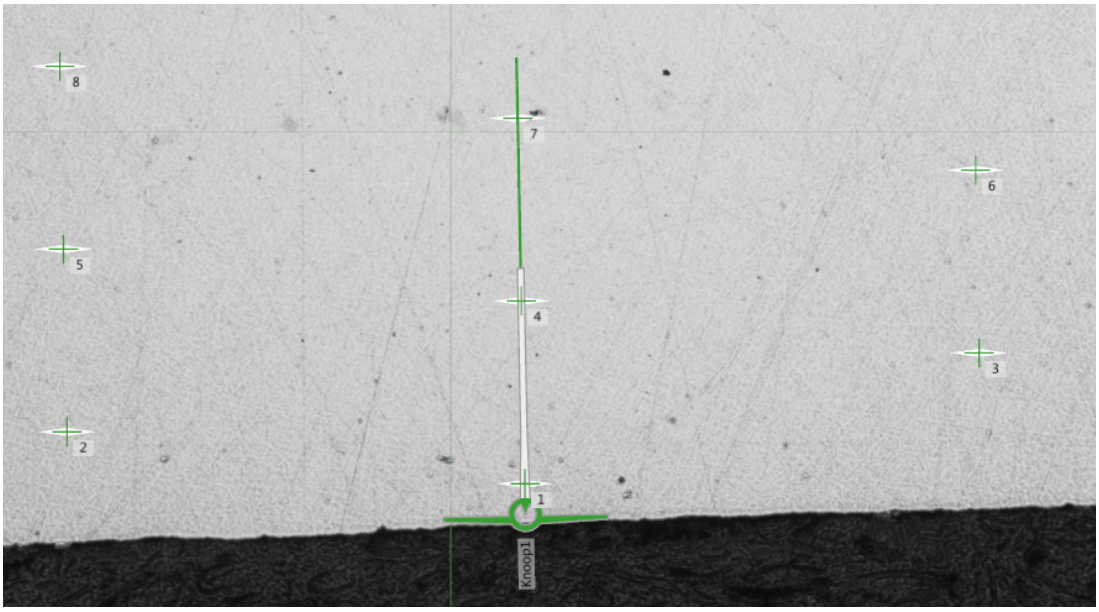

Figure 31 Zig-Zag distribution used in the hardness measurements, showing a Line

Two main standards for microhardness testing can be followed: ASTM or ISO. ASTM standards have more lenient requirements on the distance between indentations, with only 2.5x diagonal size, while ISO asks for 3x. To make sure it was possible to follow the ASTM standard, and that there was no effect of plastic deformation of previous indentations at that spread, tests were done on a ground piece in the outer diameter, where no thermal damage should have happened. The hardness obtained using these parameters maintained the same hardness, which was also the same as the one in the bulk of the component. During these measurements, the two diagonals were measured, obtaining a size of less than 4µm for the small diagonal and larger than 20µm for the main diagonal. The size of the hardness measurements in a much softer material together with ASTM standards shows that hardness can be evaluated at 10µm depth.

The error obtained during its validation was of ± 10 HK, which agrees with those measurements obtained in the bulk of the material, where no thermal degradation should have occurred. Several issues should be kept in mind while doing the hardness testing:

- Misalignments can occur between the sample and the holder due to the geometry of the sample. Whenever the cross section was not perfectly orthogonal to the polished plane, it became difficult to focus on the very edge. Any small deviation caused a shadow effect related to the bore radius, see red line in Figure 32.

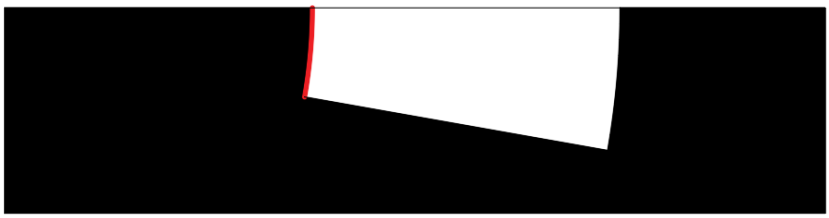

Figure 32 Cross-section of the sample, with the problematic interface in red

- High accuracy is required in the position of the indenter, as it must lay parallel to the interface. A small angle would lead to measurements in a different layer of the desired one. As the

temperature variation will also be high in the outer layers of the material, it is important to measure the hardness in the positions desired correctly.

- Local imperfections such as carbides or cracking of the material during the testing can also occur. That, together with measurements occurring too close to the surface may create outliers that can be easily identified during the checking of the testing and discarded if it is appropriate.

4.2.3. Etching and electrochemical etching

Etching of the workpieces was also done with Nital 1.5%, leaving the sample in the etchant for 4-5 seconds, obtaining a good contrast for both the martensite (white layer) and over tempered (grey / darker region) of the samples. If the sample did not show sufficient reaction, extra etching time was done, to obtain a clear view of both layers. The etching was also used in the ground surface of some non-analysed rings, to see if any possible external damage had occurred locally that was not picked up while using total power measurement of the machine. In some interesting cases, it was also used to view the cross-sectional cut using an optical microscope.

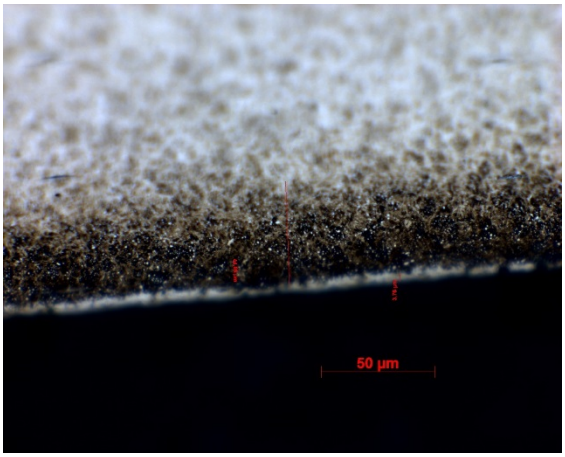

Figure 33 Etched example showing a small white layer (martensite) and a darker area (overtempering) obtained in ring 16H

Electrochemical etching was also tried, but the obtained surface was deemed too rough. Several tests were tried by decreasing the contact area and increasing the voltage, improving the quality of the surface, but still not up to the standards required for microhardness testing. The roughness, together with the amount of time required to correctly do this procedure due to the difficulty of putting the saline solution in contact with the component without spilling over and the use of depth gauges for every measurement, made us not follow up with it.

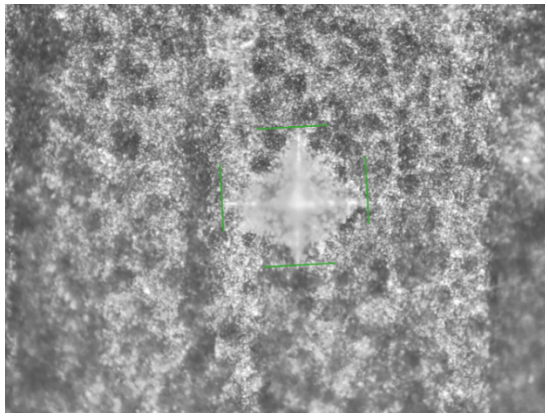

Figure 34 Hardness measurement obtained after electrochemical etching

5. Simulations

As previously discussed in this thesis, there are several analytical models available that can accurately predict the temperature experienced during grinding. However, most of them consider simpler grinding conditions and geometries such as surface grinding, while not so much has been published on more complex geometries such as ACBB raceways. These more complex geometries are where simulations are needed, to understand how the temperature gradient changes with respect to the heat flux and exposure times. With this knowledge, it would be possible to estimate the risk for thermal damage when setting up the grinding cycle, preventing grinding burns. They could also be used as a training tool for future operators of the machines, showing them what they should be paying attention to while setting-up machines.

5.1. Numerical models

An important aspect of these simulations is to represent the grinding process correctly. To do that, there will be several parameters that will be considered constant for all cases and other that can be changed to evaluate the different set-ups.

Because of that, the machine settings such as the workpiece and wheel speed, feed and coolant must be taken into consideration. As the heat generated during grinding will be distributed to both the wheel and the workpiece the thermal properties of both materials must be known. The temperature at different points and depths of the workpiece is critical to analyse the damage of it, so the thermal properties of it are needed, even if due to the small interaction times its properties can be assumed to be constant.

In the case of a 3D simulation, the geometries of the workpiece and the contact are already considered. More specifically to the used software: Bearing Simulation Tolls (BEAST), the heat input is done indirectly through the force instead of the heat input. As the power is the product of the tangential force and the wheel speed, it would be necessary to change the tangential speed to the values obtained in the tests. However, as this program does not simulate a grinding operation but rather a frictional state between the workpiece and the wheel, the tangential force is the frictional force. The normal force is not the force necessary for the grits to penetrate the material but rather the pressure created from the wheel to obtain the desired feed. That means that in this program, the normal force is not important except to calculate the tangential force.

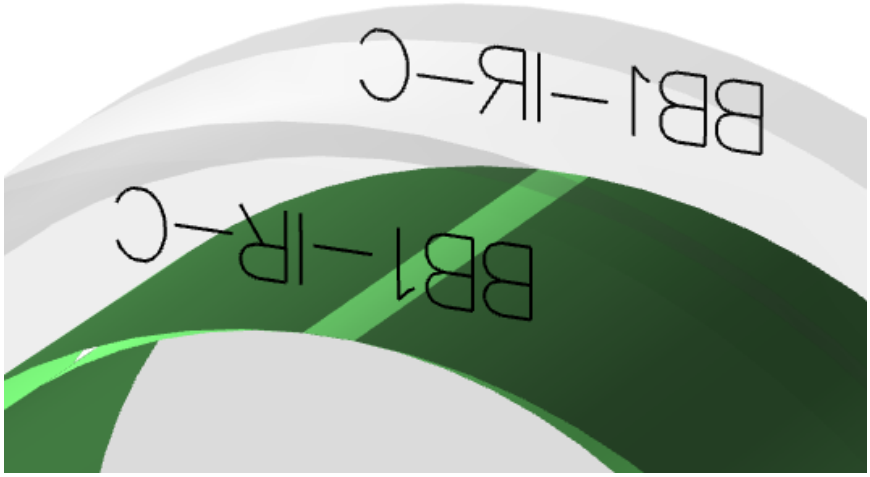

Figure 35 Contact area (light green) between the inner ring and the wheel surfaces (dark green)

In the case of a 2D simulation, it is necessary to take into consideration the geometry of the model. In this case, the depth should be there as an input parameter. As the heat is generated when the grains are in contact with the workpiece surface, the shape of the heat input is essential, as well as the total heat input in the material, which has been calculated experimentally. The shape of the heat input is assumed rectangular triangular.

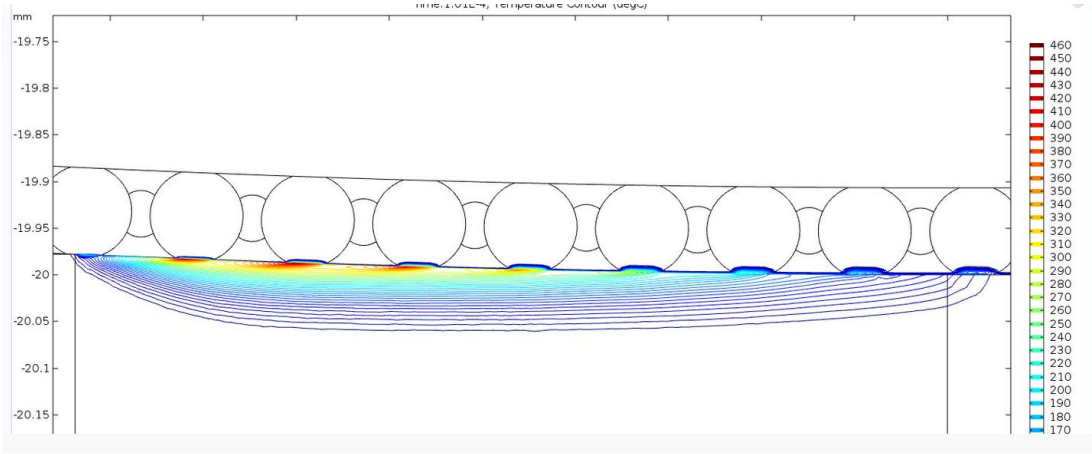

Figure 36 2D Comsol model showcasing heat input occurring only when there is grain contact

In both cases, an important aspect of the simulation is the mesh. As the main point of interest is on the ground surface, and even there only on the first 100µm where most of the material damage would occur, a super fine mesh should be obtained in the first µm, which can correctly follow the quick changes in the temperature experienced on the surface.

Another shared issue is time measurements. It can be easily calculated that the interaction time is often less than 1ms. This short interaction time forces us to use even shorter time intervals during the calculations, and that will, if more than one grinding pass is calculated, result in vast amounts of intervals being used. However, as the assumption of the workpiece returning to room temperature once it leaves the grinding area is made, every single pass would be the same, making it necessary only to calculate one pass.

5.2. Analytical models

There has been a continuous push for a simplified model that would help understand the temperature profile during grinding, starting with Jaeger (17), whose model for a moving heat source has been previously adopted for grinding. Jaeger considered the moving heat source as a square heating source that will be moving along the workpiece. This model was later improved, with different types of heat shapes being considered (34), the one obtaining a better convergence with the experimental results being a right triangular heat source, that can capture the difference of the heat distribution as it goes through the grinding zone.

On the nature of the cooling, most models consider the convective cooling is only occurring in the surface of the material, except where the moving heat source is located, to simulate the film boiling of the coolant near the heat source. Other new models for lower speeds, where heat may flow in the longitudinal direction can allow convective cooling in that direction. The lower part of the workpiece tends to be insulated, to correctly show that the bulk temperature of the component will not experience any increase of temperature as well as cooling occurring mostly in the surface thanks to the forced convection.

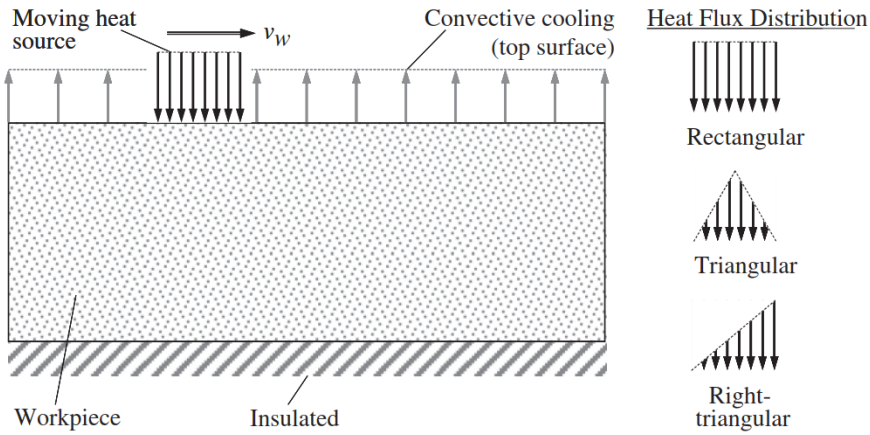

Figure 37 Common 2D approach for FE analysis during grinding (34)

It can be assumed that the heating source is not perfectly flat on the surface but rather on a slope caused by the shape of the wheel. However, this slope is not significant in internal diameter grinding as the contact arch can be assumed to be mostly flat but for other applications where a high depth of cut is used, the heat source can be set up at an angle. It can also be important to consider the pressure that occurs during grinding. As the wheel makes the abrasives penetrate the workpiece, forces will be created which might mechanically affect the residual stresses, an important aspect that could be studied in this way.

As grinding is a material removal process, it is also essential to take into consideration the removal of the material. The material removal is more important when considering that a considerable number of passes will happen, each removing the surface layers of the material while also affecting the workpiece.

Micromodels have not been as researched due to the difficulty on correctly mapping the wheel. However, several models trying to understand the behaviour of single grains, help in the understanding of chip forming and its phases and the importance of the elastic deformation caused by single grains (34).

6. Results

In this work, three main result evaluations were done:

(1) The damage evaluation of the rings, comparing the three analytical methods from previous research.
(2) Model creation and comparison with other models, where the more accurate temperature profile obtained thanks to the damage evaluation was used to tweak the BEAST model.
(3) Comparison of the characterization parameters, to have an overlook over the different grinding results when changing the parameters.

6.1. Damage evaluation

The obtained hardness profiles as seen in the Appendix were used to tweak and analyse the following methods to evaluate the damage by considering the degradation of the tempered martensite phase into softer phases. From the described settings in Table 4, sixteen different tests were done, grinding without redressing during each test until obtaining the desired heat flux as described in Section 4 Methods and experimentation. The rings were named in alphabetical order to differentiate between rings of the same trial /setting, such that the first case was named A. The results for the heat flux are:

Table 5 First and Last ring heat flux of the experimental setup, together with the number of rings ground for each setting

Test Number	Number of Rings ground	Initial workpiece heat flux [W/mm^2]	Initial BR	Final workpiece heat flux [W/mm^2]	Final BR
1	4 (D)	157	0.5	228	0.8
2	4 (D)	166	0.6	311	1.1
3	5 (E)	132	0.4	329	1
4	4 (D)	159	0.5	467	1.5
5	4 (D)	124	0.5	305	1.2
6	4 (D)	136	0.5	383	1.5
7	4 (D)	110	0.4	284	1
8	3 (C)	131	0.5	427	1.5
9	10 (J)	131	0.5	259	0.9
10	6 (F)	173	0.6	266	0.9
11	8 (H)	137	0.4	261	0.8
12	5 (E)	174	0.5	348	1.1
13	8 (H)	117	0.4	278	1.1
14	5 (E)	144	0.6	271	1
15	7 (G)	141	0.5	283	1
16	5 (E)	178	0.6	410	1.4

The burning ratio (BR), the ratio between the obtained heat flux and the burning heat flux as specified by Malkin (Equation 39) was calculated for both the first and last ground ring, as it is a common way to estimate if a ring is in danger of being thermally damaged during production.

$$BR = \frac{P_w}{P_b} \tag{76}$$

The settings for these tests are as follows:

Tests 1 to 8 used the higher wheel speed (v_c), which meant that lower forces were required to obtain a similar heat flux. Odd numbers used higher dressing parameter (f_{ad}) when compared to even tests, and tests 1-4 and 9-12 used the higher workpiece speed (v_w). Tests 1-2,5-6,9-10,13-14 utilize a higher depth of cut (a_e). A complete view of the settings can be seen in the Appendix.

f_{ad} plays an integral part in the initial heat flux, with an increase of it between all even and odd tests. It can also be seen that the burning ratio (BR), the ratio between the obtained heat flux and the burning heat flux as specified by Malkin, is lower than 1, mostly around 0.5 in the first trials while it increases massively on continuous rings, reaching values around the burning ratio.

6.1.1. Larson Miller approach

Both the HV (Figure 28) and HK (Figure 29) master tempering curves show a high value of R^2 for the fourth polynomial regression. In the observed region, the linear term dominated which was expected. The worse fit of the Knoop graph can be attributed to worse measurement accuracy when compared to HV due to the smaller imprint due to the weight and the focus on only one measurement: main diagonal length. A smaller imprint would mean that the individual data points might have a more substantial error and making it more important to use a correct regression model for HK as the statistical model will use more data points than just single readings.

During the evaluation of the Larson Miller curve, two main parameters can be analysed. Starting with the temperature, there is a choice between using the average or maximum temperature. The critical temperature necessary for the material to be damaged, that is the temperature for a LM parameter of 6, is calculated for different interaction times, can be calculated and seen in Figure 38. Critical values of 562.8C for an interaction time of 0.54ms and 549C for 0.71ms were obtained. If those temperatures were for the average increase, the maximum temperature could be calculated by:

$$T_{max,average} = (T_{LM6} - T_0) \cdot \frac{3}{2} + T_0 \tag{77}$$

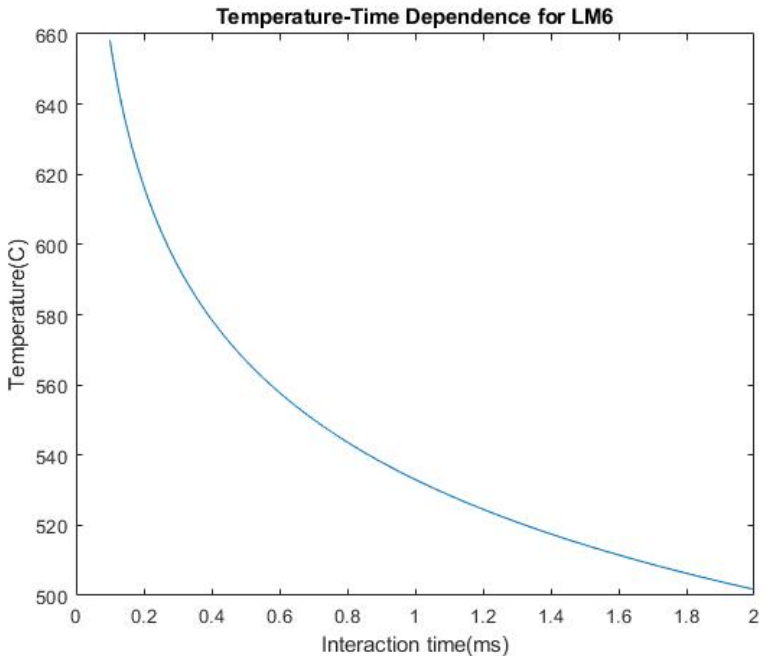

Figure 38 Temperature - Time dependence for LM6 (start of overtempering)

Obtaining the values 831.7C and 811C respectively, much higher than the temperature at which damage starts. These results show that the value that should be used is the maximum.

As the obtained values of critical temperature were still higher than the expected temperature, the other variable, the time, was evaluated. The time was first assumed to be only the interaction time depending on the geometrical contact length. However, due to Hertzian deformation, the true contact length will be different and might be up to three times the expected one (35). As the contact length is

directly related with the interaction time, it was interesting to see what the difference of the hardness would be considering both geometrical (1x) and Hertzian deformation (3x) contact lengths:

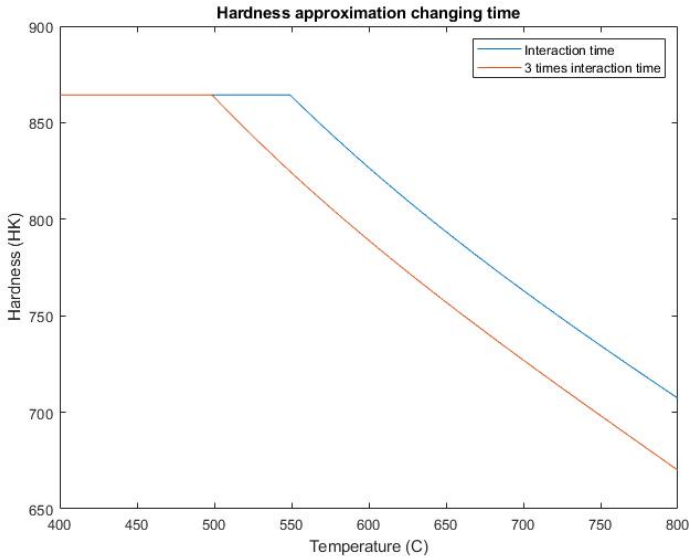

Figure 39 Hardness by Larson Miller changing the interaction time with a base value of 0.6ms

In this behaviour, it is possible to see that the starting point would change, but the slope would be approximately the same. Given the previous cases, the values for the critical temperature would go down to 510 and 498C, closer to the expected results. It can then be said that if the Larson Miller equation was to be used, higher interactions times are necessary. The obtained hardness profiles were plotted together with the LM curve:

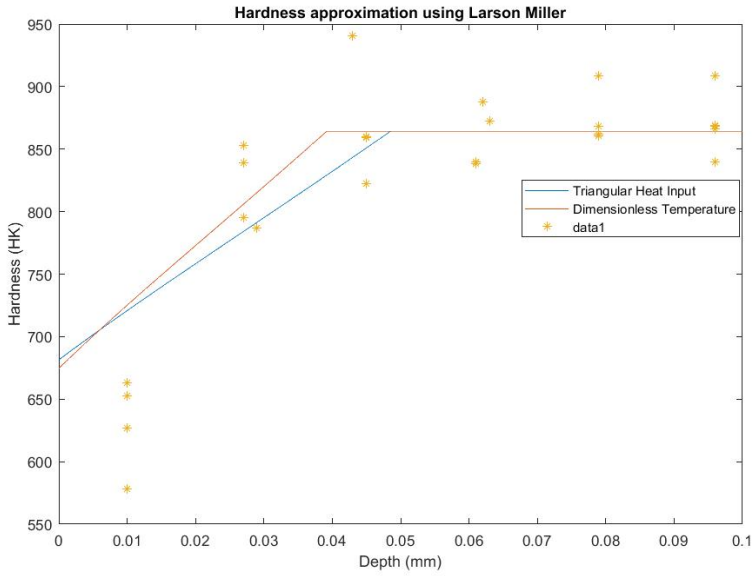

Figure 40 Larson Miller approach for Case 16E, BR=1.4

It is possible to see then that the shape of the curve does not have the same shape as the results, overestimating the damage in the beginning while underestimating in the latest parts. Out of the two methods used to obtain the temperature profile, the heat input method using a triangular heat input gave a more appropriate shape. That would mean that it should be possible to use this method as a rough calculation for the temperature at which damage would start. However, for the same

proportion of the interaction time of the process, it was not possible to correctly predict the start location in some cases:

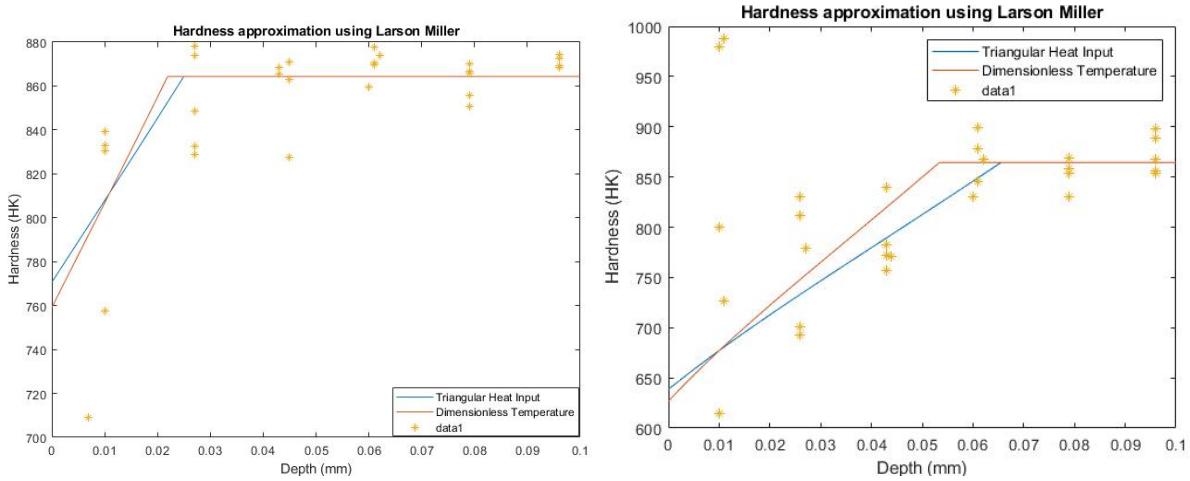

Figure 41 LM approach for case 2D(left), BR=1.1; and 6D(right), BR=1.5

6.1.2. JMAK evaluation

The transformed fraction f was calculated for the different cases, focusing on the cementite transformation. The fraction was changed into hardness as the values of both the hard and soft phase were known, obtaining curves such as:

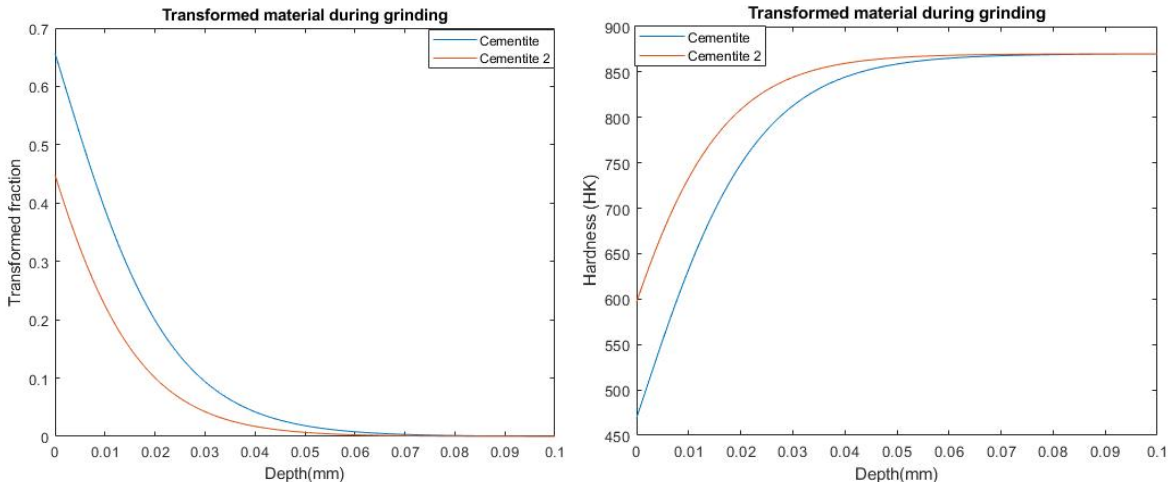

Figure 42 Transformed fraction of the material (left) and its hardness equivalent (right) for case 4D

If this were to be used with the obtained hardness results, the following curves could be shown:

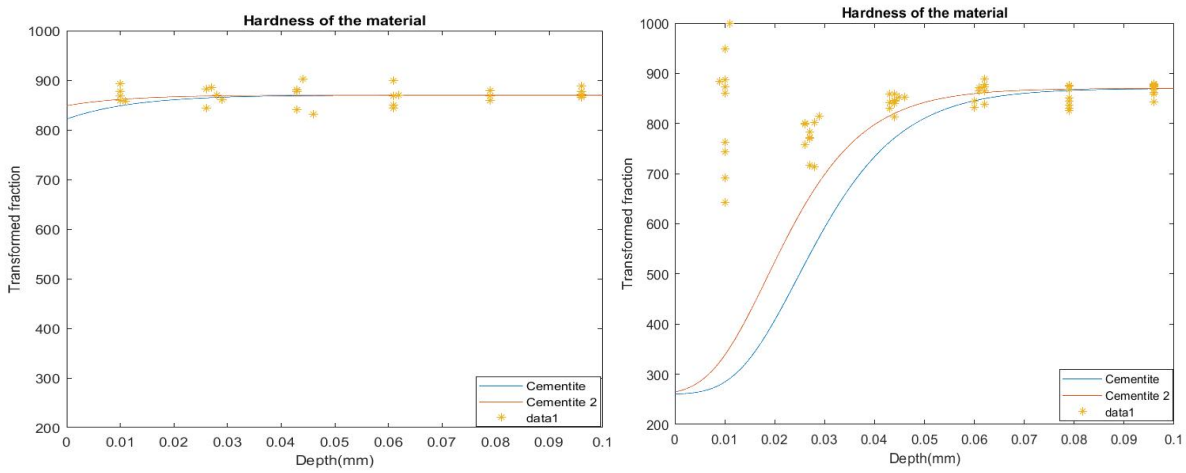

Figure 43 JMAK hardness profile for case 1D, BR=0.8; and 4D, BR=1.5

The obtained curves show a great resemblance near the bulk of the component than in the surface. The bulk of the component, located more to the right in the graphs, is where the temperature and thus the heating rate is smaller. At higher temperatures, when the JMAK equation reaches a linear behaviour, the curve will greatly overestimate the damage to the material. The overestimation could be due to the material properties creating a much faster transition between the first and the second phase of the material than it happens in this experimental situation. As it could be seen in Figure 20, the end phase of the transformation will occur much sooner than expected which is probably due to this model working on the assumption of a constant temperature growth.

6.1.3. Differential approach

The differential approach to phase transformation as expressed by Malkin (22) was used with its numerical method to calculate the temperature profile to analyse the hardness variation with depth. This method can be used to calculate not only the effect of the final pass but also the effect of the previous passes. This is important in our case, as the hardness drop near the surface is significantly higher as more passes have been done, as seen in Figure 44.

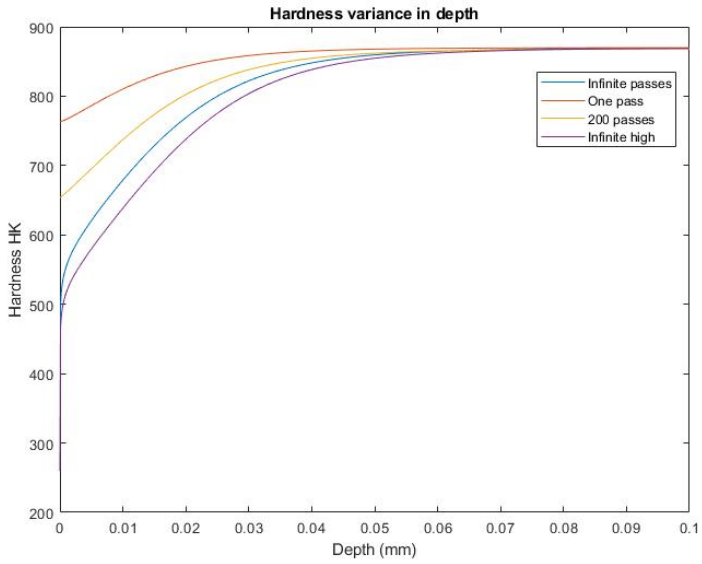

Figure 44 Example of hardness profile using the differential approach

The curves were fitted for all the 16 studied cases, as can be seen in the Appendix, obtaining a material constant of 9.5e6. With this value, the obtained hardness profiles were seen to closely follow the

"Infinite pass" curve, with variations due to the local nature of Knoop hardness and the highly dynamic stochastic of grinding forces. However, it is interesting to look in more detail at some of the results, as they show the validity and some of the flows of the method.

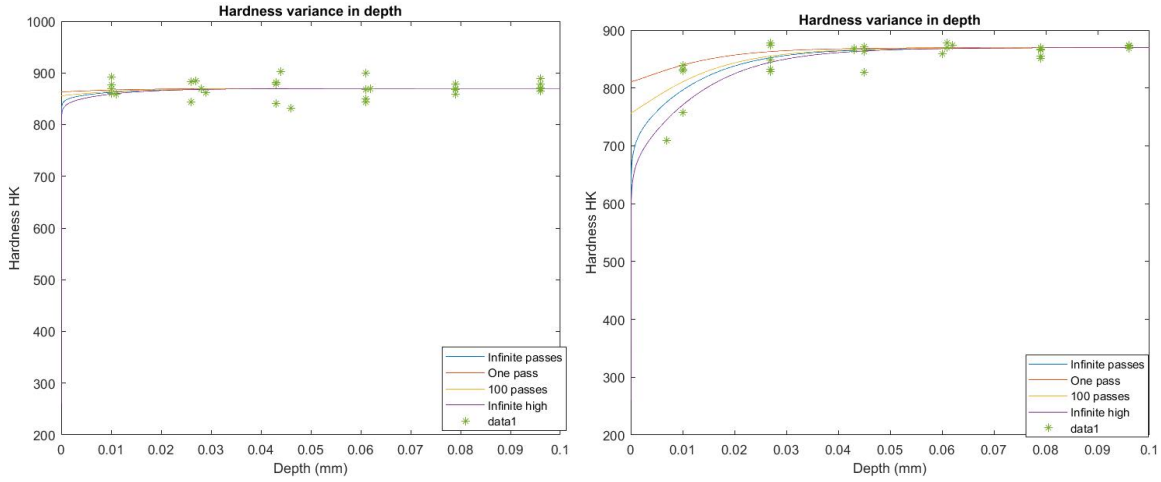

Figure 45 Differential approach for case 1D (left), BR=0.8; and 2D (right), BR=1.1.

The difference between case 1D and 2D lies in the forces experienced by the ring, with the 2D having higher force in part to a different dressing. In case 1D, no major softening can be seen in the component, with only a small softening in the outer layers of it. In this case, the difference between a single pass or a multiple pass approximation is not that significant, although, in case of utilizing a high number of passes, an error may occur lowering the average value of the hardness. This error can be solved by utilizing the infinite pass approximation which focuses mainly on the outer parts of the component, not adding more "damage" to the rest of it. This infinite pass approach has one minor issue: it will create a significant softening in the surface making it so that the analytical values at zero depth are not representative.

In case 2D, more energy has gone into the system, obtaining a higher value of softening. Here, the curves signalling the different number of passes start widening and that most of the points fall between or below the multiple passes line. The margin of error in the affected areas is more noticeable in the first layers of the material, as the combination of the error of measurement and the effect of the heat combine.

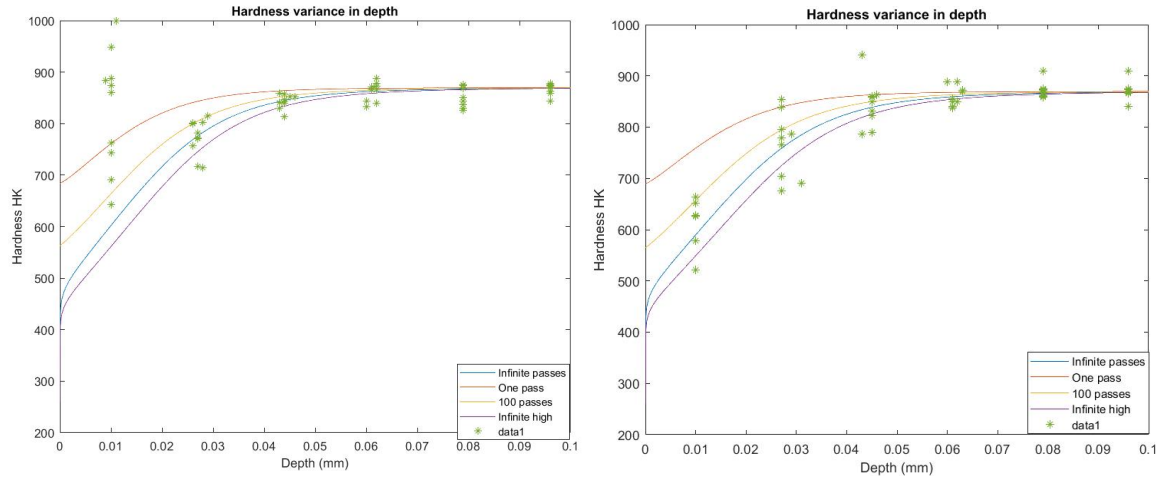

Figure 46 Differential approach for case 4D(right), BR=1.5; and 16E(left), BR=1.4

Between the cases 4D and 16E, it is interesting to notice that both of their curves are similar despite having different parameters and forces. However, in the case 4D, an increase in hardness is seen near the surface. This increase in hardness is due to the creation of a solid layer of martensite in case 4D, which affects the outer layers of the component and do not appear consistently in case 16E. Martensite appearing in one case over the other is due to the difference of temperature where, while case 4D reaches 855, case 16H barely reaches 810. In both cases, we can see that results go more towards the multiple passes route, as the effect of the repetitive tempering is more and more important the deeper the HAZ is.

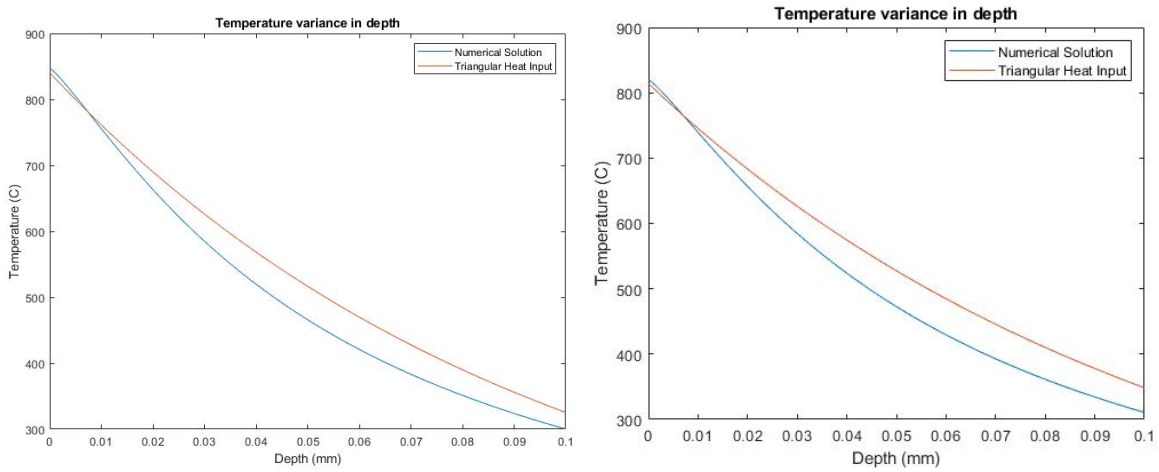

Figure 47 Temperature graphs for case 4D (left) and 16E (right) using the numerical solution and the triangular heat Input

Given these results, it was interesting to see the etched cross-sections of both cases to see the difference between them:

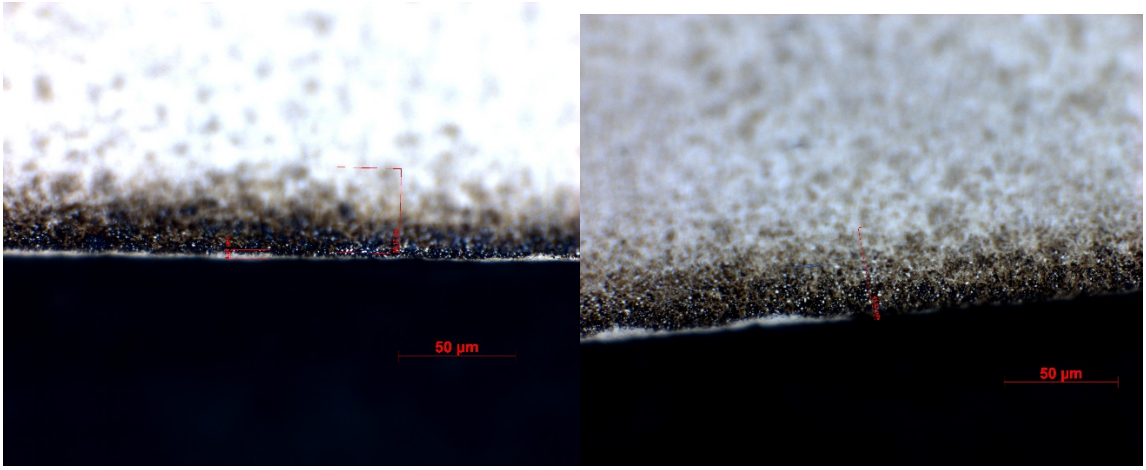

Figure 48 Etched showpiece of sample 4D (left) and 16E (right)

It is possible then to see that the ring 4D showed a more constant and more significant martensitic layer all over the surface while in the case of the ring 16E, a much less consistent layer appeared with most the surface not having it. This difference in the amount of martensite leads us to believe that in the 16E case the temperature is on the verge of the martensite formation while on the 4D it has already occurred. The final depth of the over tempered region is similar in both cases.

In general, the main difference with the previous models is the ability to consider the repetitive nature of grinding, showcasing that more attention must be paid once the Heat Affected Zone (HAZ) is bigger

than the depth of cut. If no attention is paid to it, there will be a more considerable underestimation of the drop in hardness as the material will be affected by several passes. However, the initial point where over tempering starts (that is the critical temperature) will remain constant, depending only on the process conditions, as can be seen with all curves stabilizing at around the same depth. This means that the material requires a minimum amount of temperature for the tempering to start, below which the grinding can be done without creating thermal damage.

There are still certain outliers that can be found in the material, and consideration of the widespread of the points must be taken, but most of them mainly affect the first set of points. This widespread is mainly due to the difficulty of measuring the hardness correctly so close to the surface where a small deviation by the machine or the initial position by the operator could cause a huge difference. Other issues such as carbide forming, or localized softening have been spotted, as well as cracking. Another important point for that type of error is the assumption of constant heat flux. As previously stated, grinding operations are the sum of the work of many individual grits which will cut in their local region. As each grit performs a cut, there will be a difference in the heat flux between regions of the wheel and point defects of the wheel may cause critical defects on the workpiece.

Otherwise, the infinite pass approach has been found to be the one that resembles reality the most, with the obtained data aligned with it with the scattering being due to the nature of the grinding. The alignment with the infinite pass approach is due to the HAZ generated for each pass being bigger than the removed material, meaning that in consecutive passes, the material will be affected by previous thermal loads before the last pass, which must be taken into consideration. As the material that is near the surface after the last pass will be the one that has been affected more significantly by previous passes, whose thermal loads might have been different, and the analytical model assumed a constant grinding force, they would show higher variance. A more advanced model which includes a quick transition to untempered martensite in the high-temperature cases could be build which would explain the increased hardness/underestimation of the hardness values.

The burning ratio (BR) is widely used to consider the grinding burn threshold. It can be seen in the cases 1, 9, 10 and 11 that the last rings had a BR below 1, which would trigger the burn alarm, which is often triggered at a 0.95 level. In the results, the tempering of one pass would be quite small, but if a multiple pass approach is considered, an important level of softening can be obtained in the outmost parts of the material:

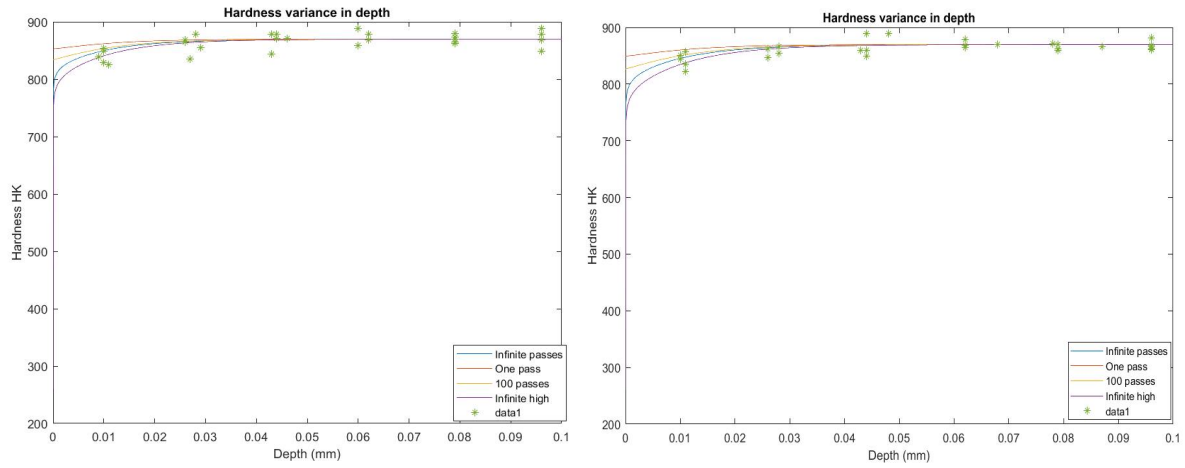

Figure 49 Differential approach for case 9J(right), BR=0.9; and 10F(left), BR=0.9

The multiple pass approach would mean that even if the burning power equation assumes that a relatively small amount of thermal damage can occur, as seen in the single pass approach, the previous

passes have damaged the material enough for the hardness drop to be significant even at 10µm depth, where the first measurements were done. This significant softening would mean that more conservative burning ratios should be chosen when working in these conditions, as the equation for burning power is focused on cases where the last pass generates most of the damage, which is not always the case for shallow grinding.

If the LM and the differential approach model were to be compared, it could be seen that the starting location for the LM method can occur either before or after the differential curve starts, pointing towards the mechanism of both not being directly related. However, the small difference in the starting position could be used to give a rough estimate of the critical temperature, if the interaction time is considered for the real geometrical contact length.

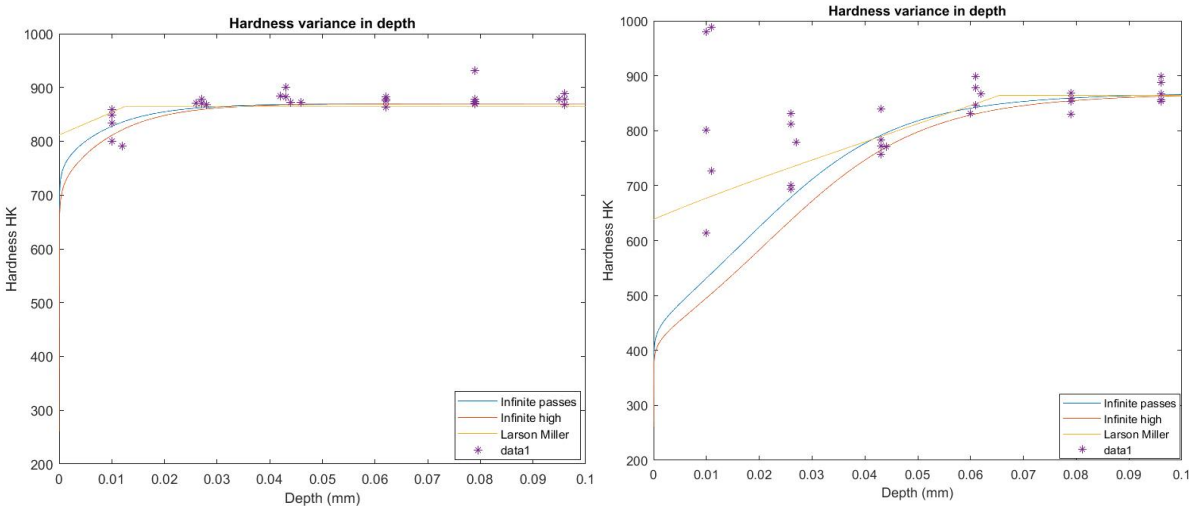

Figure 50 Comparison of LM and differential model for case 3E(left), BP=1; and 6D (right), BP=1.5

6.1.4. Critical temperature evaluation

From the start of this study, the idea of a critical temperature, below which the material would not be damaged, was an important concept, as it would greatly help with the reduction of the number of flaws while having a higher production rate. During this study, it was made clear that this temperature exists and is dependent on both the process settings and the original state of the material. The initial tempering state of the hardened steel directly affects this, with steels tempered for longer periods of time having higher critical temperatures.

The most significant change can be seen when changing the speed of the workpiece, going from 450°C to 520°C with the change from 1.31 to 2.09 m/s. However, it is important to realize that the HAZ has a much slower growth at the start, but once it passes the depth of cut, it grows linearly. This is more noticeable if the HAZ is considered for smaller hardness loses. As in the differential approach, the heat that goes into the workpiece is only used to calculate the temperature; it is possible to obtain the HAZ size with respect to the temperature:

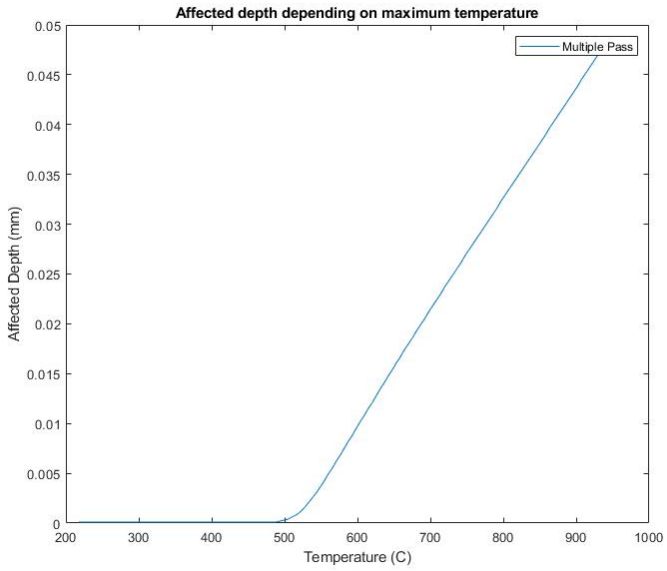

Figure 51 HAZ for a 20HK drop in test 1

An important aspect that is not usually considered and that dramatically affects the size of the HAZ was the repetitive process of grinding. If only one pass were considered, the total HAZ would be much smaller than the obtained one, and the critical temperature to obtain a certain size HAZ size would increase. The difference between a single and multi-pass approach is due to the small damage occurring over previous passes accumulating to create a sizeable effect, even if the last pass is a significant contribution of the damage. However, if a smaller softening is considered for the HAZ calculation, the distance between the multi-pass and single pass theory will decrease, pointing towards a common origin, which would be located near the tempering temperature, where the material will start to get damaged. There is also a difference in the slope, being steeper in the multi-pass model. This can be seen in the following graph, were the HAZ of the single pass model and the infinite model is shown:

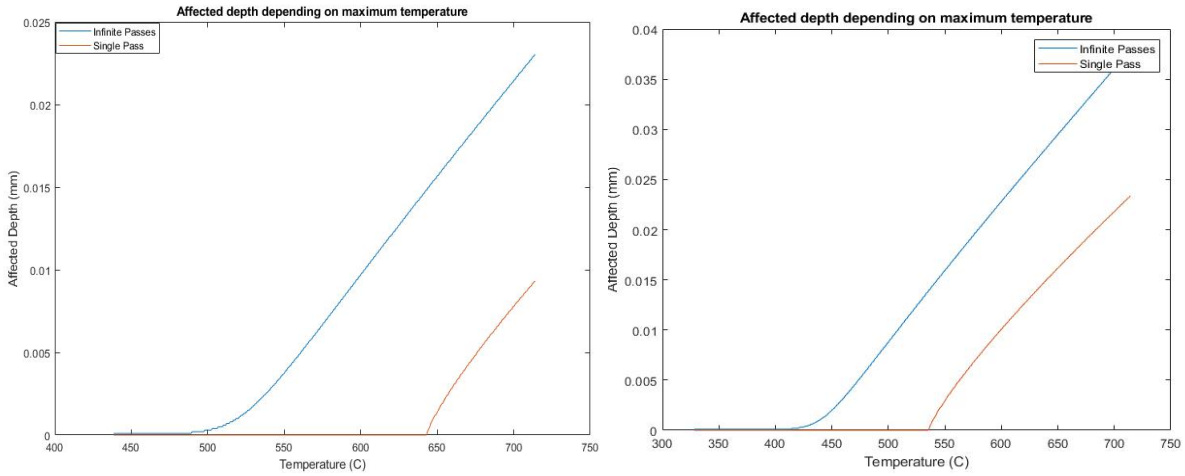

Figure 52 HAZ size comparison using a single pass and a multi-pass for 20HK(left) and 5HK(right) drop for test 2

Increasing the depth of cut will also converge both curves, as more of the most damaged material will be removed, hindering the effect of the previous pass. As both cases will converge, there exists a clear limit after which the multi-pass approach is not necessary, as most of the damage will be done in the

last pass. For the settings in this master thesis, this convergence occurred once the feed rate exceeded 10µm, as the effect of the last pass accounted for more than 80% of the total damage in the surface.

As the outmost layers of the material will be removed more carefully, taking away this damaged material without creating high temperatures that would create thermal damage, a certain degree of softening can be accepted during rough grinding. Also, due to the nature of the calculation, where the material will start experiencing tempering if enough energy is provided, which requires less than 200°C, the damage will start at low temperatures. However, previous tempering processes serve to stabilize the microstructure, making this damage be minuscule and not significant enough to be found while measuring hardness. Nonetheless, it would interfere with the calculation of hardness drop for small hardness drops such as 0HK.

Mathematical comparisons can be made with the Larson Miller Parameter. However, there is not a good relationship between both calculated temperatures, with the results of high interaction times only serving as a rough indication of approximate temperatures. This can be because of repetitive tempering not working with LM, as well as the tempering effect not being at a constant temperature.

The critical temperatures obtained can then be used to compare with those measured from sensors during production, helping prevent degradation of the material and allowing for better quality control.

6.2. Model evaluation

Two main points of interest were taken in the model evaluation: correct temperature increase and correct variation with respect to the depth. Interest should be taken into the residual temperature, as it could lead to much higher final temperatures as the base temperature increases over several cycles, which had been assumed not to happen.

On the BEAST (3D) macromodel, issues with the residual temperature occur. The issue happened due to the coolant being applied in the same way along the internal surface and it not boiling near the grinding source due to high temperatures. This leads to two main possibilities: either not considering the effect of the coolant, which will have an overall increase of the residual temperature while not affecting the increase of temperature every cycle or considering it and seeing a decrease of it. As the interest is only on one cycle, no cooling was used during the simulations.

Given the input data, the maximum temperature increase was in the range of the expected ones. However, due to the way the temperature is calculated in the program, several errors may occur. An interesting one that occurs is the creation of a “cold front” just before entering the heat source. The “cold front” was more noticeable if the ring was static, as it occurred in both sides of the heating spot.

Issues with the correct temperature with the depth variation occurred, obtaining higher temperatures than expected. Two main reasons were found behind that problem: the mesh not being fine enough, so that most measurements are taken from the same triangle, with small variations of temperature; and the before mentioned “cold front” which would create areas of low heat.

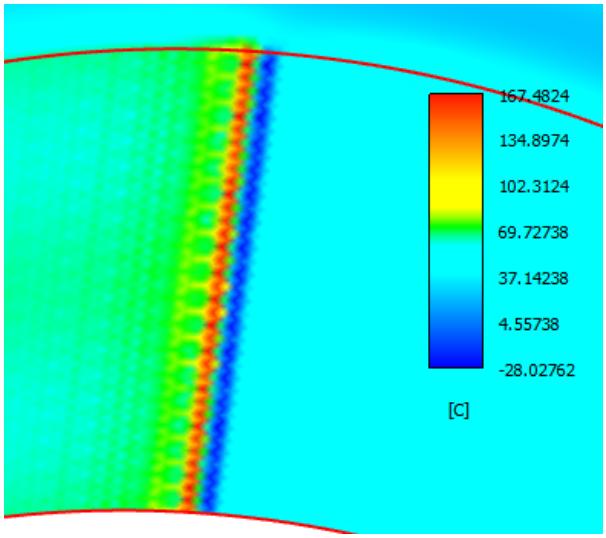

Figure 53 Cold front appears when the material enters the grinding zone

On the micromodel, an important aspect was how the grains were distributed and how long the wheel interacted with the workpiece. The interaction time is important as a long one was required to obtain the steady state conditions. The obtained results in the surface once the steady state was obtained were good, although due to the grains having a more concentrated heat flux, higher point temperatures were experienced near them. The isothermal lines are interesting in the uppermost part of the material, where the effect of each grain is significant as well as the heating caused by different grains during a single pass. This quickly stabilizes with depth, obtaining a somewhat flat isotherm. This model correctly portrays both parts of the temperature, although the heat lost due to the chip generation might be higher than the expected amount.

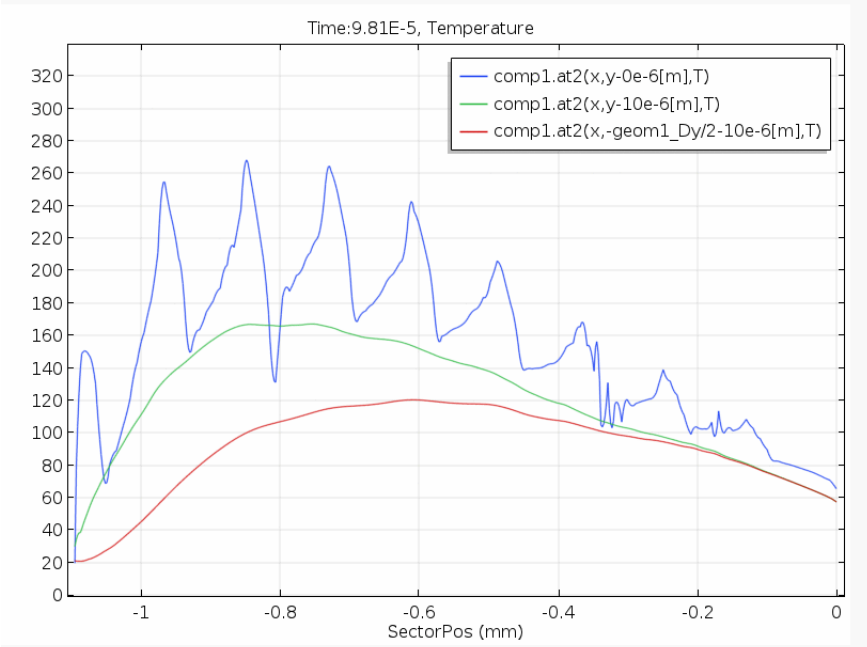

Figure 54 Temperatures in the micromodel at the surface (blue), 10µm depth (green) and 10 µm depth assuming movement of the workpiece

Due to the small interaction time during grinding, the micromodel was also used to verify the creation of the vapour layer that would allow us to simplify the model to dry grinding. The vapour layer is shown as the white grain emits the expected heat flux surrounded by the coolant. In 10 nanoseconds,

a small layer surrounding the grain was already above the vaporization temperature, and after 1microsecond, that layer surrounded the grain and had a thickness bigger than the depth of cut.

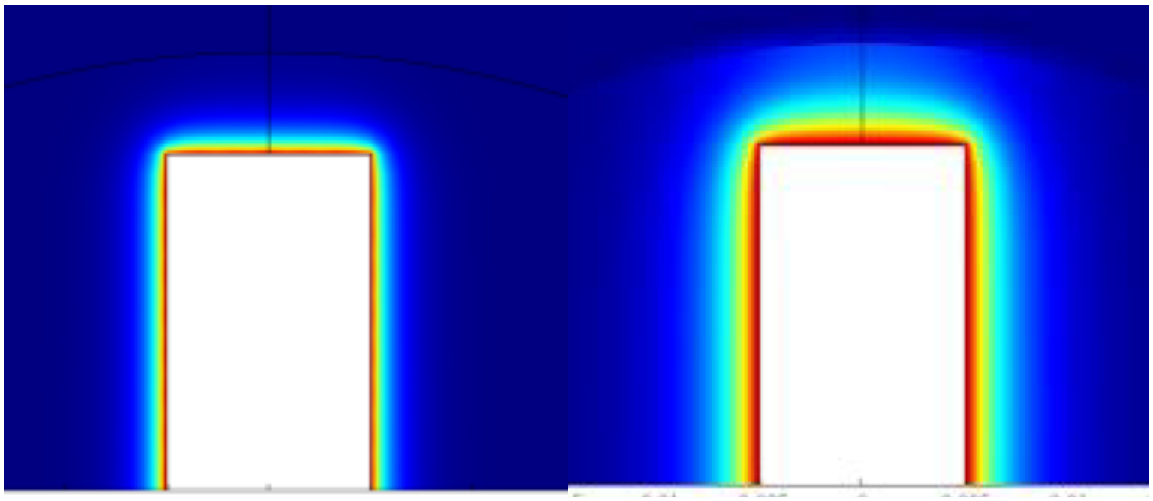

Figure 55 Detail of the micromodel where the grain (white) at 1 nanosecond (left) and 1 microsecond (right) obtained through Comsol, where the colours are isotherms above the boiling temperature of the coolant.

6.3. Best characterization parameter

It is possible to see which parameter will affect the critical temperature the most. As the maximum undeformed chip thickness is proportional to the aggressiveness number, and the interaction time was discovered to be a critical parameter in the phase transformation, aggressiveness, material removal rate and interaction time will be used. The critical temperature will be found at 5µm, where the material will suffer from consecutive tempering and a linear behaviour, and 10HK:

Table 6 Characterization Parameter and the Critical Surface Temperature obtained in the different cases

Case	Interaction time (ms)	Aggressiveness	Material removal rate (mm^2/s)	Critical Surface Temperature (°C)
1 and 2	0.60	98	6.9	473
3 and 4	0.45	74	3.9	469
5 and 6	0.72	82	5.8	455
7 and 8	0.54	62	3.3	452
9 and 10	0.60	117	6.9	473
11 and 12	0.45	88	3.9	469
13 and 14	0.72	98	5.8	455
15 and 16	0.54	74	3.3	452

It is possible to see that both the interaction time and the material removal rate showcase the increase of the critical temperature with a decrease of the interaction time if the depth of cut is maintained (cases 1-5-9-13 being 4.4 and 3-7-11-15 being 2.5). However, a decrease of the depth of cut even if it causes a decrease in the interaction time will decrease the critical temperature doing the damage during grinding more likely. This decrease is due to the important effect that the removal of the damaged material will have as well as increasing the depth at which the point will be during the previous passes and possibly reducing the total amount of passes the material will be subject to. All of this will significantly decrease the effect of repetitive tempering.

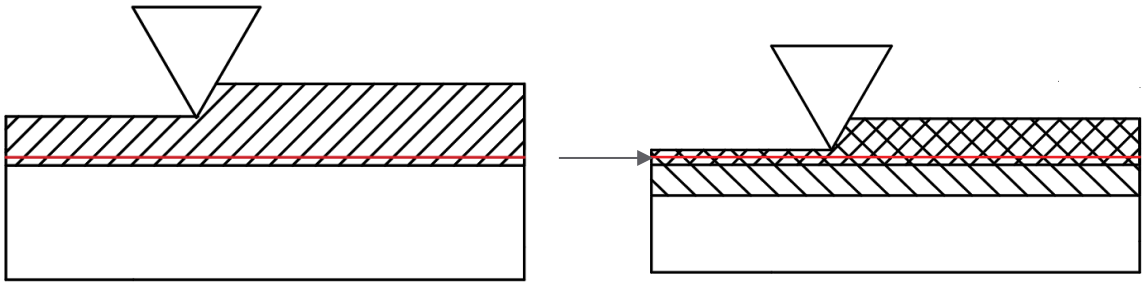

Figure 56 Thermal effect of grinding: HAZ (hatched) not completely removed in one pass leaves a residual in the following passes

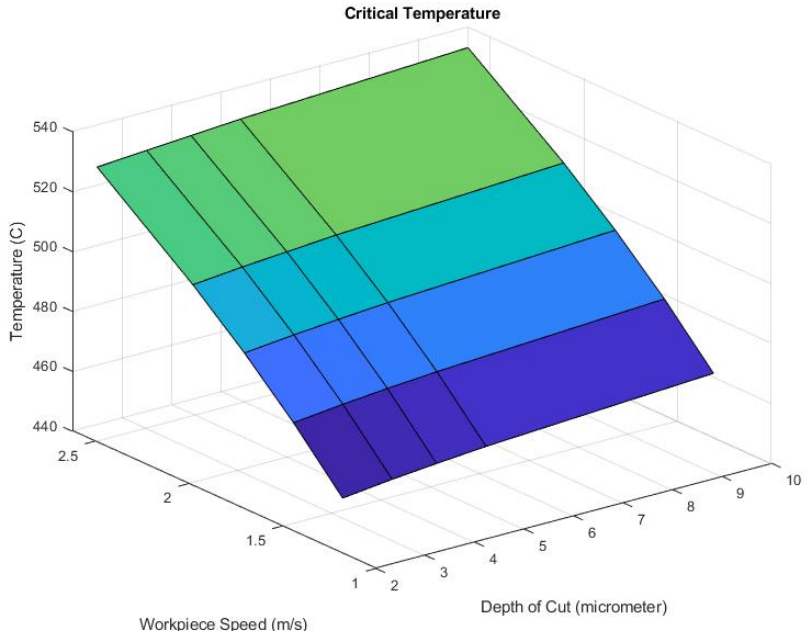

Figure 57 Surface of the critical temperature with the depth of cut and workpiece speed

The effect of the wheel speed is non-important in these calculations, but the lower spindle speed trials took more workpieces to reach the necessary conditions to see burn. This is due to even if lower wheel speeds increase the damage the wheel suffers, an increase of the force exerted on each grain would change the damage mechanism from attritious wear to grain fracture which would cause a degree of self-sharpening on the tool.

Another essential thing to consider would be the size of the HAZ at a given surface temperature. It is important to consider that for a similar critical temperature, a higher heat flux is required for a higher depth of cut, as the contact area increases. The increase in the heat flux will create a larger HAZ even if the critical temperature to start obtaining this damage is higher. Otherwise, the increase seen with the depth of cut is not as substantial as the drop seen with the workpiece speed decrease.

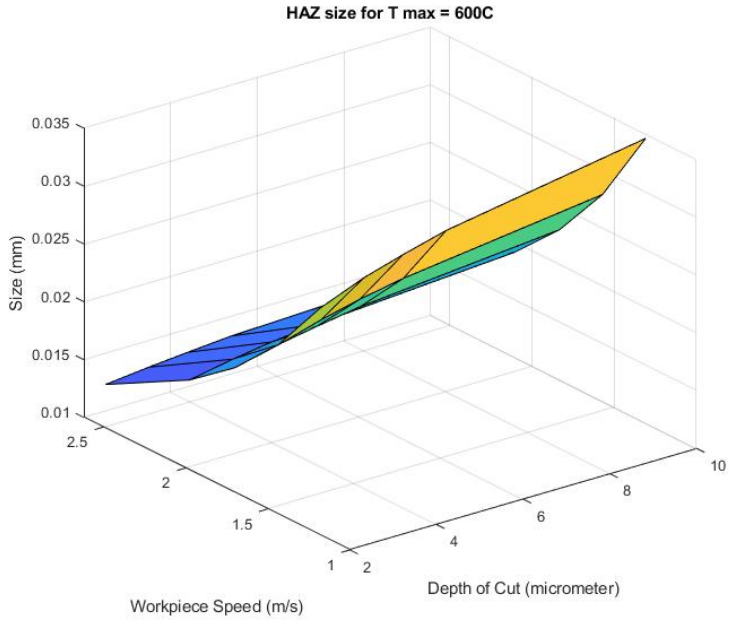

Figure 58 Size of the HAZ for a given constant surface temperature of 600°C

7. Conclusions

Several conclusions can be obtained from the different approaches taken:

The Larson Miller approach, which would create a master tempering curve for the process, has been previously tried without much success. Similarly, during this study, the obtained results could not be fitted using the different temperature profiles nor different time constraints. This is due to the tempering not being isothermal and the repetitive passes that occur during the grinding cycle. However, it can still be used to roughly estimate the initial temperature at which temper burns will occur

The JMAK Method showcases the different steps in the degradation of martensite into other phases, in this case, the cementite transformation being the most crucial part. The obtained results see a good fit for the lower temperature transformations, overestimating the hardness drop when using high temperatures. This overestimation could be due to the assumption of a constant growth with temperature as well as the material parameters requiring additional experiments to verify them for the component. However, the initial shape of the transformation before the linear growth shows promise.

The differential approach as explained by Malkin can show both the over tempering and the rehardening process during grinding and correlates with the behaviour seen during the hardness testing. The methodology of the tempering transformation had been both corroborated with other grinding situations and fitted correctly with the expected hardness results. Importantly, the effect of multiple passes can be taken into consideration in the curve, obtaining a good fit on the outmost layers of the material where this effect is significant. The inclusion of the multi-pass approach makes it the best of all three approaches, as well as an important field of investigation in shallow grinding, where the material removed is much smaller than the HAZ it has created.

On the temperature profiles, as seen in the analytical models they quickly decrease in the first layers of the material. In the models, this was seen as the temperature being half the surface value at 50µm depth, which correlates with the obtained results where, even when rehardening burns are obtained, the affected depth is less than 0.1 mm. In grinding with a much larger depth of cut, most of this affected material will be removed, but in shallow grinding, most of the affected volume will remain. As a significant amount of damaged material is kept between passes, it is necessary to consider not only one tempering process but the total accumulation of damage in the component during grinding. Considering the whole grinding process means that any prediction methodology of hardness that is only based on one single pass will find itself underestimating the drop of the hardness values during shallow grinding. As this effect is of much more significant importance near the surface, where the requirements for hardness are much more important, it is essential to realize what the critical temperature is and compare the heat affected zone size with the depth of cut.

On the topic of critical temperature, temperatures above 450°C are required for burn, increasing massively with the workpiece speed. The depth of cut is quite significant as a larger depth of cut will remove more of the outmost part of the material, which has been damaged the most. The removal of the damaged material dramatically decreases the need for a multi-pass approach reaching a point where most of the damage will be done on the last pass with depths of cut higher than 50µm. For a depth of cut of 5.4µm and a workpiece speed of 2.1 m/s, the critical temperature would be 504°C.

On the topic of the characterization parameters, none of the characterization parameters would correctly depict the effect of the HAZ if there is an effect of the repetitive overtempering. In case of one pass grind, the interaction time will be of great importance, with a greater interaction time giving

us a bigger HAZ, as more amount of the material will have time to transform. However, the effect of the depth of cut is of great importance once the multiple passes are considered, as a higher depth of cut will lower its importance increasing the critical temperature. As the difference between similar workpiece speed is small compared to different speeds, it is a more important aspect than the interaction time. Similarly, as the interaction time plays a significant part in the LM calculations, this shows some of the issues of the temper curve approach.

When looking into the numerical models, both show much of promise, with the micromodel being able to follow the expected results more closely. The BEAST model shows great promise for a 3D model, being able to predict the maximum temperature closely. However, the temperature variation with respect to depth is not as accurate, mainly due to issues with the heat flow and the mesh size, which could be fixed in the future. As the micromodel would be more specific to each application while the Beast model could be more easily expanded into different geometries, it would be interesting to keep working on the Beast program to solve these issues.

8. Future research

Several aspects of this project could be further developed. In the case of measurements, more focus should be put on the first 50µm of the surface. This could be done by, for instance, nanohardness or by analysing the phase composition at different depths. More in-depth analysis under more lab-like conditions such as constant force / specific removal energy would be recommended, as a source of possible error comes from them not being continuously the same. Further analysis of the partition ratio can also be interesting as a small improvement of it could lead to a noticeable decrease of damage in the component, as the temperature in the component will decrease sharply with a decrease on the partition ratio. This decrease in the damage would not be related to the critical temperature, which will remain constant but rather to the decrease of heat going into the workpiece.

An extension of the differential phase transformation approach exists in theory and has been implemented by Malkin. However, not enough information to correctly replicate the results was provided and this part was left behind as most of the interest of this research is in preventing any damage and over tempering occurring before rehardening burns. Still, it could be interesting to be able to map this correctly both to correct some of the results that happen due to that.

More research could be done in the JMA equation, as the material parameters were taken from previous works and may not be accurate enough and the reason why some of the results did not fit with the expected ones. However, as explained in the conclusions, the overreliance on the temperature gradient may become an issue when looking into subsurface part of the component, as both the temperature and exposure time may change.

Different type of shallow grinding operations may benefit from an analysis that estimates the effect of the consecutive tempering and studying them and seeing if they behave similarly to the obtained results would be interesting.

On the model creation part, several improvements on Beast would greatly help in further geometries: local heat sources and point forces. Most of the current grinding models use them extensively to simulate the heat source in the grinding area. Easier creation of the superfine mesh required in the contact surface while not increasing the total number of polygons by, for instance, dividing the body into two parts, the external part that will not be subject to any noticeable temperature from grinding being a black body that will not contain any mesh.

Micromodels are also interesting as the focus of interest is on the first 100µm of the material. This makes the results dependent on the wheel properties, as the force they have been subject to will vary depending on the abrasive conditions. This modelling is also able to utilize fewer resources thanks to the 2D nature and only considering the outmost layers of the component. However, the 2D nature of it will hinder the main future goal of the project: utilizing this as a base for more complex geometries.

9. References

1. **SKF.** Bearing rating life. *SKF.* [Online] SKF, 2 May 2018. http://www.skf.com/uk/products/bearings-units-housings/principles/bearing-selection-process/bearing-size/size-selection-based-on-rating-life/bearing-rating-life/index.html.

2. **Dowling, Norman E-.** *Mechanical Behavior of Materials.* s.l. : Pearson Education M.U.A, 2013.

3. *Grinding of Metals: Theory and Application.* **Malkin, S.** 3, s.l. : Journal of Applied Metalworking, 1984.

4. **SKF.** About Us. *SKF.* [Online] SKF, 2 May 2018. http://www.skf.com/uk/our-company/index.html.

5. —. *Hard Machining Course: Level 3.* s.l. : SKF, 2015.

6. **Staffan Larsson, Mans angard.** *Determination of Phase Transformation Kinetics when Tempering Martenstitc Hardened Low Alloy Steels.* Linköping : Linköpings Universitet, 1995.

7. **S. Malkin, Changsheng Guo.** *Grinding Technology - Theory and Applications of Machining with Abrasives.* s.l. : Industrial Press, 2008.

8. **Rowe, W. Brian.** *Principles of Modern Grinding Theory.* s.l. : William Andrew, 2013.

9. *An Analytical Approach to the DEtermination of Residual Stresses in Surface Grinding.* **A. Mishra, U. R.K. Rao, R. Natarajan.** New Delhi : Inst. Mech. Engrs. (India) and CIRP, 1977, Proceedings, International Conference on Production Engineering.

10. **Ioan D. Marinescu, Mike P. Hitchiner, Eckart Uhlmann, W. Brian Rowe, Ichiro Inasaki.** *Handbook of Machining with Grinding Wheels.* Boca Raton : CRC Press, 2016.

11. **Fritz Klocke, Aaron Kuchle.** *Manufacturing Processes 2: Grinding, Honing, Lapping.* s.l. : Springer, 2009.

12. *The dimensionless aggressiveness number in abrasive processes.* **Jeffrey Badger, Radovan Drazumeric, Roope Roininen, Peter Krajnik.** Texas : North American Manufacturing Research Conference, 2018. NAMRC6 46.

13. *Creep-feed - an effective method to reduce workpiece surface temperatures in high efficiency grinding processes.* **Werner, P.G., Younis, M.A., Sclingensiepen.** s.l. : SME, 1980, Proceedings of the Eighth North American Metalworking Research Conference, pp. 312-319.

14. *The wear of grinding wheels, Part 2 - Fracture wear.* **Malkin, S., Cook, N.H.** s.l. : ASME, November 1971, J. Eng. Ind., pp. 1129-1133.

15. *Thermal Aspects of Grinding, Part 1 - Energy Partition.* **S. Malkin, R. B. Anderson.** 96, 1974, J. of Eng. for Ind., p. 1177.

16. *Energy Partition to the Workpiece for Grinding with Aluminium Oxide and CBN Abrasive Wheels.* **S. Kohli, C. Guo, S. Malkin.** 117, s.l. : ASME, May 1995, Transactions of the ASME, pp. 160-168.

17. *Moving Sources of Heat and the Temperature at Sliding Contacts.* **Jaeger, J. C.** 76, s.l. : Proceedings of the Royal Society of New South Wales, 1942.

18. *Burning Limits for Surface and Cylindrical Grinding of Steels.* **Malkin, S.** s.l. : Annals of the CIRP, 1978.

19. *Analytical and Experimental Investigation of Burnout in Creep-Feed Grinding.* **C. Guo, S. Malkin.** 76, s.l. : Annals of the CIRP, 1994, p. 283.

20. *Thermally Induced damage in grinding.* **M. Maris, R. Swoeys, J. Peters.** 2, s.l. : Annals of the CIRP, 1978, Vol. 27, pp. 571-581.

21. *Effects of Grinding Variables on Surface Structure of Hardenes Steels.* **Takazawa, K.** s.l. : Bull. Japan Soc. Prec. Engg., 1966, Vol. 2.

22. *Analysis of Tempering and Rehardening for Grinding of Hardened Steels.* **S. Malkin, O.B. Fedoseev.** November 1991, Journal for Engineering for Industry, pp. 388-393.

23. *Temperature case studies in grinding including an inclined heat source model.* **Rowe, W. B.** s.l. : Proc. Instn. Mech. Engrs., 2015, Vol. 215.

24. *Cooling characteristics of the cutting grains in grinding.* **T. Ueda, M. Sato, K. Nakayama.** 1995 : CIPR, Vol. 42.

25. **E. Brinksmeier, J. Eckebrecht, A. Wilkens.** Wheel Based Temperature Measurement in Grinding. *Advanced Materials Research.* 2011, Vol. 325.

26. *The measurement of grinding temperatures at high specific material removal rates.* **I.M. Walton, D.J. Stephenson, A. Baldwin.** s.l. : International Journal of Machine Tools and Manufacture, 2006, Vol. 46.

27. **ASM.** *Heat Treating ASM Handbook Vol 4.* s.l. : ASM International, 1991.

28. **David A. Porter, Kenneth E. Easterling, Mohamed Y. Sherif.** *Phase transformations in metal and alloys.* London : Taylor & Francis, 2009.

29. **S. J. NA, Y.S. Yang.** Influence of Heating Rate on the Laser Surface Hardening of a Medium Carbon Steel. *Surface and Coatings Technolog.* 1988, Vol. 34.

30. **KW, Andrews.** *Empirical Formulae for the Calculation of some Transformation Temperatures.* s.l. : JISI, 1965.

31. *Kinetics of Phase Change. I General Theory.* **Avrami, M.** s.l. : The Journal of Chemical Physics, 1939, Vol. 7.

32. **E.J. Mittemeijer, F.C. Van Doorn.** Heat Effects of Precipitation Stages on Tempering of Carbon Martensites. *Metallurgical Transactions A.* May, 1983, Vol. 14A.

33. **ASTM.** *Standard Test Method for Knoop and Vickers Hardness Materials.* West Conshahacken : ASTM International, 2012. E384-11.

34. *Finite element modeling approaches in grinding.* **D.A. Doman, A. Warkentin, R. Bauer.** 2009, International Journal of Machine Tools & Manufacture, pp. 109-116.

35. *An experimental investigation of the grinding process.* **H. Makino, T. Suto, E. Fokushima,.** 17, s.l. : J. Mech. Lab. Japan, 1966.

36. *Controlling the Surface Integrity of Ground Components.* **W. B. Rowe, D. F. McCormack, T. Jin.** December/January 2002, Abrasives Magazine, pp. 24-30.

37. **E.J.Mittemeijer, Liu Cheng, P.J.Van der Schaaf, C.M. Brakman, B.M. Korevaar.** Analysis of Nonisothermal Transformation Kinetics; Tempering of Iron-Carbon and Iron-Nitrogen Martensites. *Metallurgical Transactions A.* April, 1988, Vol. 19A.

38. **Cong Mao, Zhixiong Zhou Kexi Guo, Xuyu Liu.** Numerical Simulation and Experimental Validation of the Temperature Field in Surface Grinding. *Machining Science and Technology.* 2010.

39. **Mokhtar O. Mohamed, Andrew Warkentin, Robert Bauer.** Variable heat flux in numerical simulation of grinding temperatures. *Advanced Manufaturing Technology.* 2012.

40. **A. Micietova, J. Pistora, Z. Durstova, M. Neslusan.** Concept of Damage Monitoring after Grinding for Components of Variable Hardness. *Procedia Materials Science.* 2016.

41. *A Production Engineering Approach to Grinding Temperatures.* **Shaw, M. C.** s.l. : Journal of Materials Processing Technology, 1994, Vol. 44.

Appendix

Larson Miller Data

Table 7 Tempering results for Hardness Vickers with a time of 4 hours

Temperature	1	2	3	4	5	Average
647	253	252	253	250	252	252
470	435	424	443	435	443	436
187	721	715	727	730	724	723.4
230	677	679	674	693	687	682
390	536	544	533	541	536	538.1
596	311	300	299	308	300	303.5
452	454	455	459	458	459	457
243	679	687	682	676	695	683.8
290	641	644	632	639	636	638.4
690	228	230	240	238	233	233.8
340	577	577	598	589	579	584
542	346	344	354	346	344	346.8

Table 8 Tempering results for Hardness Knoop with a time of 4 hours

Temperature	1	2	3	4	5	Average
647	304.4	299	295.1	301.1	294.9	298.9
470	480.4	474.1	485.6	484.7	490.6	483.08
187	803.5	780.5	798.6	819.1	769.5	794.24
230	698.9	705.2	718.6	731.3	705.2	711.84
390	579.9	561.6	552.8	557.2	570.5	564.4
596	324.2	324.2	327.6	325.9	342.7	328.92
452	475.2	485.6	478.5	464.6	461.7	473.1
243	705.2	731.3	758.8	758.7	731	737
290	713.4	716.9	695.6	674.6	705.2	701.14
690	259.1	277.6	257.9	272	272.4	267.
340	640.5	629.7	629.8	629.8	663.2	638.6
542	397.8	385.9	379.1	428.7	405.2	399.44

Settings Table

Setting Number	Cutting Speed (m/s)	Workpiece Speed (m/s)	Depth of cut (µm)	f_{ad}	Q' (mm^2/s)
1	75.39	1.57	4.4	70	6.91
2	75.39	1.57	4.4	35	6.91
3	75.39	1.57	2.5	70	3.93
4	75.39	1.57	2.5	35	3.93
5	75.39	1.31	4.44	70	5.81
6	75.39	1.31	4.44	35	5.81
7	75.39	1.31	2.52	70	3.3
8	75.39	1.31	2.52	35	3.3
9	62.83	1.57	4.4	70	6.91
10	62.83	1.57	4.4	35	6.91
11	62.83	1.57	2.5	70	3.93
12	62.83	1.57	2.5	35	3.93
13	62.83	1.31	4.44	70	5.81
14	62.83	1.31	4.44	35	5.81
15	62.83	1.31	2.52	70	3.3
16	62.83	1.31	2.52	35	3.3
20	75.39	2.09	4.42	70	9.27
21	75.39	2.09	4.42	35	9.27
22	75.39	2.09	2.47	70	5.18
23	75.39	2.09	2.47	35	5.18
28	62.83	2.09	4.42	70	9.27
29	62.83	2.09	4.42	35	9.27
30	62.83	2.09	2.47	70	5.18
31	62.83	2.09	2.47	35	5.18

Results and figures

Case 1D

Line 1(mm)	0.1	0.029	0.043	0.061	0.079	0.096
Hardness 1(HK)	859.8	869.9	878	849.3	868.8	869.1
Line 2	0.01	0.029	0.043	0.061	0.079	0.096
Hardness 2	892.4	861.3	841.2	898.9	858.8	870.8
Line 3	0.011	0.026	0.044	0.062	0.079	0.096
Hardness 3	858.4	843.2	902.1	869.4	878.9	878.4
Line 4	0.01	0.026	0.043	0.061	0.079	0.096
Hardness 4	869.2	882.4	880.8	868.6	859.3	888.4
Line 5	0.01	0.027	0.046	0.061	0.079	0.096
Hardness 5	877.7	884.9	831.6	843.2	868.5	864.8

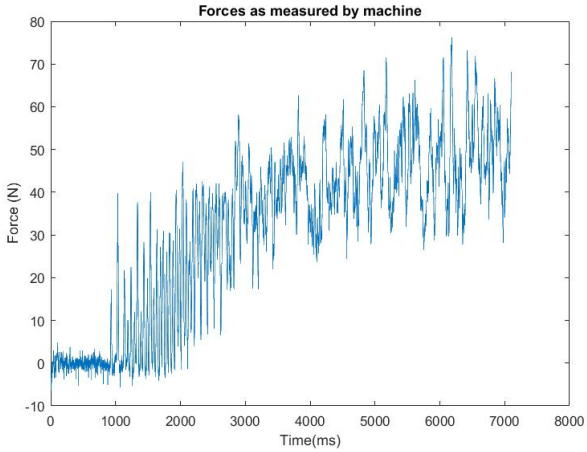

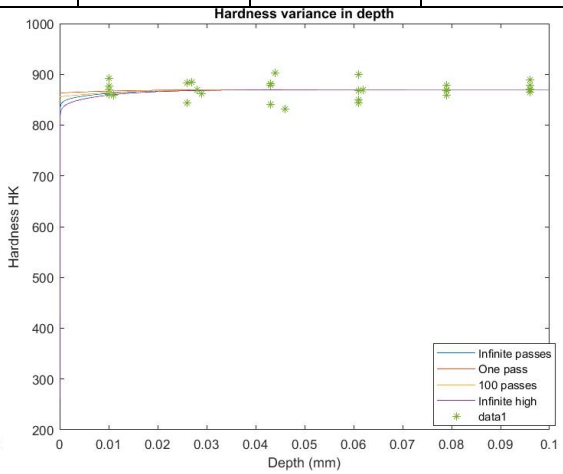

Case 2D

Line 1(mm)	0.01	0.027	0.045	0.062	0.079	0.096
Hardness 1 (HK)	839.3	832.6	871	873.7	855.8	872.6
Line 2 (mm)	0.01	0.027	0.043	0.061	0.079	0.096
Hardness 2 (HK)	757.6	878.3	868.2	870.5	865.7	872.8
Line 3 (mm)	0.007	0.027	0.045	0.06	0.079	0.096
Hardness 3 (HK)	708.9	828.9	827.6	859.6	850.9	868.6
Line 4 (mm)	0.01	0.027	0.046	0.061	0.079	0.096
Hardness 4 (HK)	830.4	873.8	865.4	877.6	870.1	874.3
Line 5 (mm)	0.01	0.027	0.045	0.061	0.079	0.096
Hardness 5 (HK)	832.9	848.8	862.8	869.5	866.9	869.1

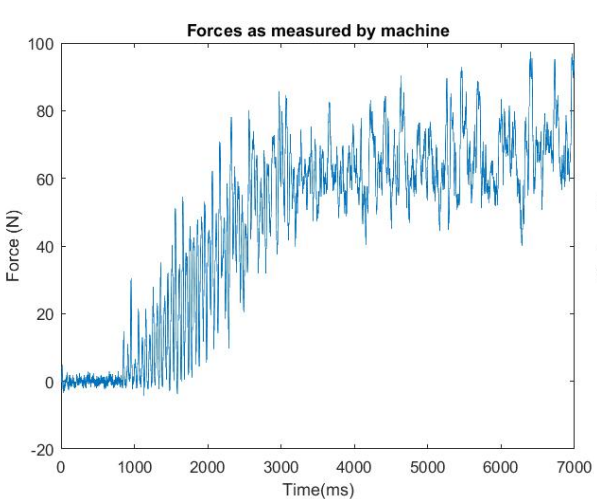

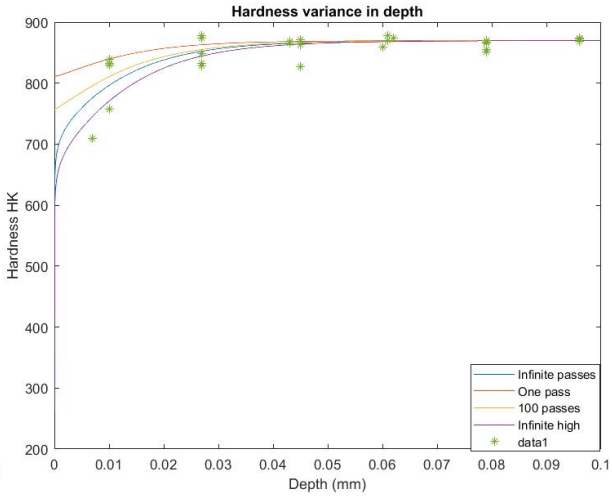

Case 3E

Line 1(mm)	0.012	0.027	0.042	0.062	0.079	0.095
Hardness 1 (HK)	791.7	878.2	883.8	875.8	870.5	878.7
Line 2 (mm)	0.01	0.028	0.043	0.062	0.079	0.096
Hardness 2 (HK)	848.4	868.5	882.6	878.4	873.5	888.4
Line 3 (mm)	0.01	0.026	0.044	0.062	0.079	0.096
Hardness 3 (HK)	834.5	871.4	872.8	878	878.4	878.2
Line 4 (mm)	0.01	0.028	0.043	0.062	0.079	0.096
Hardness 4 (HK)	858.4	868.3	900.6	863.1	931	868.6
Line 5 (mm)	0.01	0.027	0.046	0.062	0.079	0.096
Hardness 5 (HK)	799.8	870.2	871.8	882.3	868.7	888.6

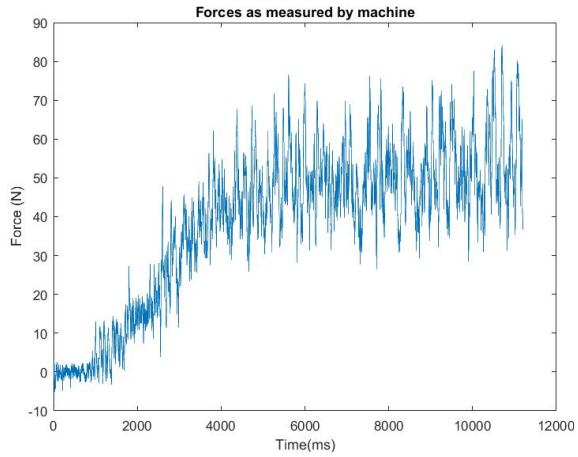

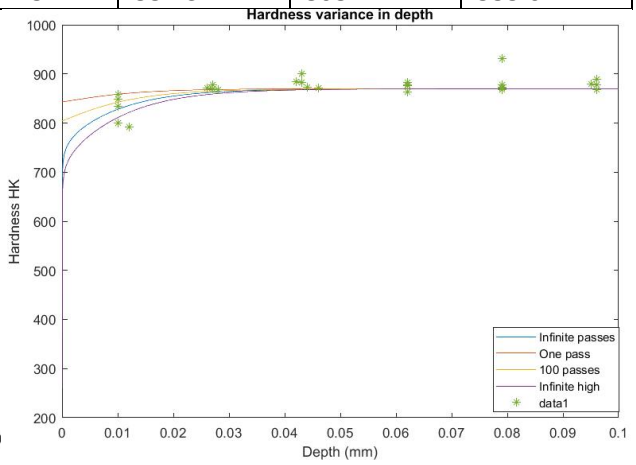

Case 4D

Line 1(mm)	0.01	0.027	0.044	0.06	0.079	0.096
Hardness 1 (HK)	642.1	716.5	839.9	832.4	843.8	843.3
Line 2 (mm)	0.01	0.029	0.043	0.062	0.079	0.096
Hardness 2 (HK)	860.2	814.7	829.9	839	830.5	862.4
Line 3 (mm)	0.01	0.028	0.044	0.061	0.079	0.096
Hardness 3 (HK)	948.5	713.6	844.2	865.5	825.2	875.9
Line 4 (mm)	0.01	0.026	0.044	0.06	0.079	0.096
Hardness 4 (HK)	762.2	799.5	813	844	837.4	859

Line 5 (mm)	0.01	0.028	0.043	0.061	0.079	0.096
Hardness 5 (HK)	742.9	802.5	841.2	871.4	851.1	868.5
Line 6(mm)	0.009	0.026	0.044	0.062	0.079	0.096
Hardness 6 (HK)	883.5	800.6	858	878.4	868.5	874.5
Line 7 (mm)	0.011	0.026	0.044	0.062	0.079	0.096
Hardness 7 (HK)	1000	757.6	846.6	878.4	875.6	878.6
Line 8 (mm)	0.01	0.027	0.043	0.062	0.079	0.096
Hardness 8 (HK)	691.1	771	858.3	888.4	868.9	877.9
Line 9 (mm)	0.01	0.027	0.045	0.062	0.079	0.096
Hardness 9 (HK)	887.7	782.4	852.4	865.5	874.1	875.1
Line 10 (mm)	0.01	0.027	0.046	0.062	0.079	0.096
Hardness 10 (HK)	873.5	772.3	852.4	872.7	874.1	872.8

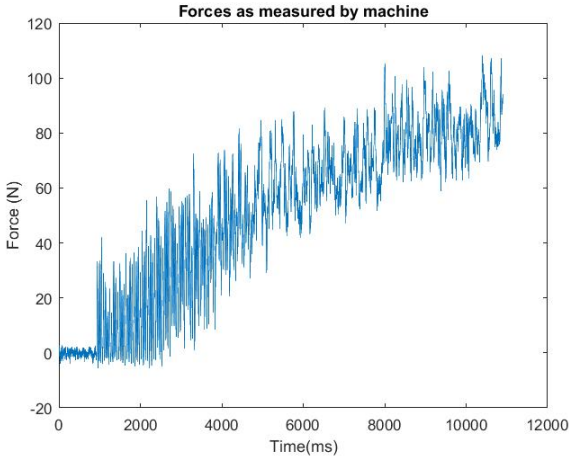

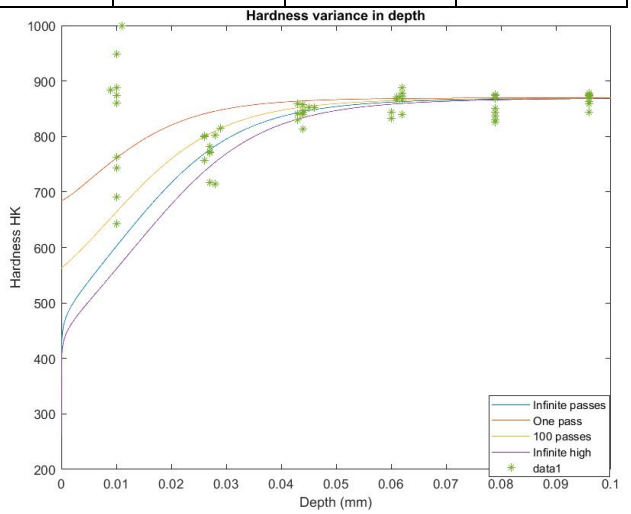

Case 5D

Line 1(mm)	0.01	0.027	0.046	0.061	0.079	0.096
Hardness 1 (HK)	793.8	835.3	855.4	888.3	867.5	867.4
Line 2 (mm)	0.01	0.027	0.045	0.061	0.079	0.096
Hardness 2 (HK)	779	841.7	873.4	872.8	863.3	878.8
Line 3 (mm)	0.007	0.027	0.045	0.06	0.078	0.096
Hardness 3 (HK)	624.7	773	838.4	858.9	864.1	867.2
Line 4 (mm)	0.01	0.027	0.045	0.062	0.079	0.096
Hardness 4 (HK)	732.9	840.4	844.5	863.4	866.5	868.3
Line 5 (mm)	0.01	0.027	0.045	0.063	0.079	0.096
Hardness 5 (HK)	669.1	828	888.4	864.8	867.1	868.2

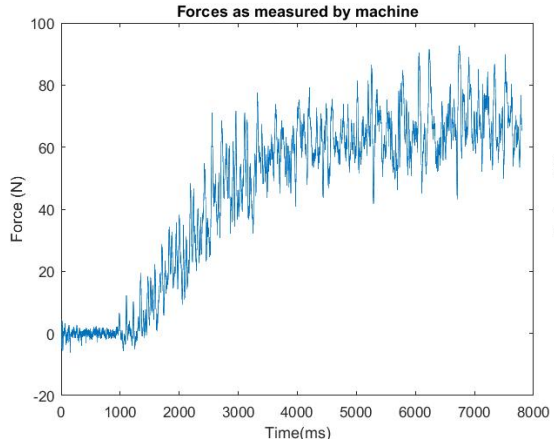

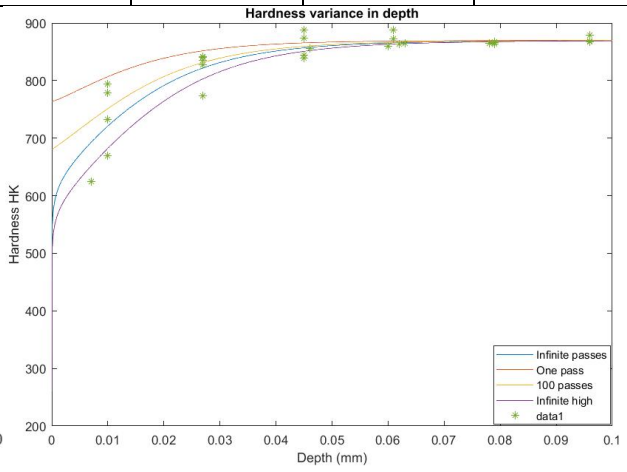

Case 6D

Line 1(mm)	0.011	0.026	0.043	0.062	0.079	0.096
Hardness 1 (HK)	727.1	811.4	771.6	867.7	8588	855.6
Line 2 (mm)	0.01	0.026	0.043	0.061	0.079	0.096
Hardness 2 (HK)	614	830.7	757.4	877.8	853.1	854
Line 3 (mm)	0.011	0.026	0.044	0.061	0.079	0.096
Hardness 3 (HK)	987.9	693	770.4	846	830.5	867.1
Line 4 (mm)	0.01	0.027	0.043	0.061	0.079	0.096
Hardness 4 (HK)	800.5	779	839.4	898.6	830.5	888.4
Line 5 (mm)	0.01	0.026	0.043	0.06	0.079	0.096
Hardness 5 (HK)	979.7	700.6	783	830.7	868.5	898.4

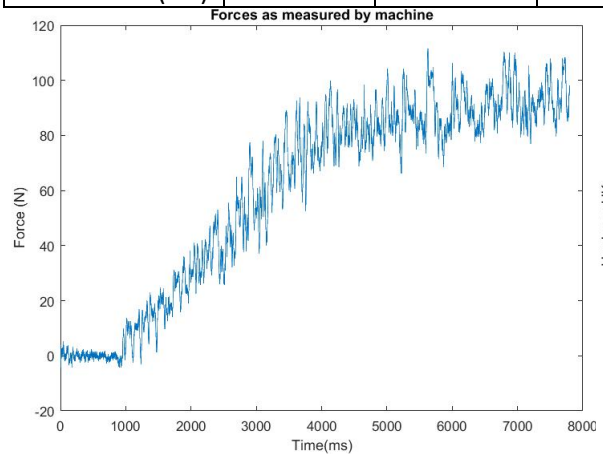

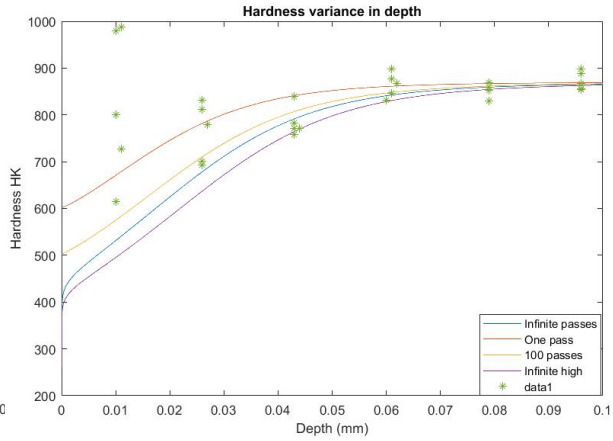

Case 7D

Line 1(mm)	0.01	0.027	0.045	0.062	0.079	0.096
Hardness 1 (HK)	851.3	850.6	888.6	881.1	881	887.6
Line 2 (mm)	0.01	0.028	0.044	0.061	0.079	0.096
Hardness 2 (HK)	860.9	867.5	858.8	878.3	871.2	878.4
Line 3 (mm)	0.01	0.027	0.043	0.061	0.079	0.096
Hardness 3 (HK)	793.9	856.6	878.4	873.2	859.2	864.3
Line 4 (mm)	0.01	0.028	0.044	0.062	0.079	0.096
Hardness 4 (HK)	833.6	866.4	871.9	866.5	889.5	878.5
Line 5 (mm)	0.01	0.028	0.043	0.062	0.079	0.096
Hardness 5 (HK)	849.4	863.4	867.8	868.6	870	908.9

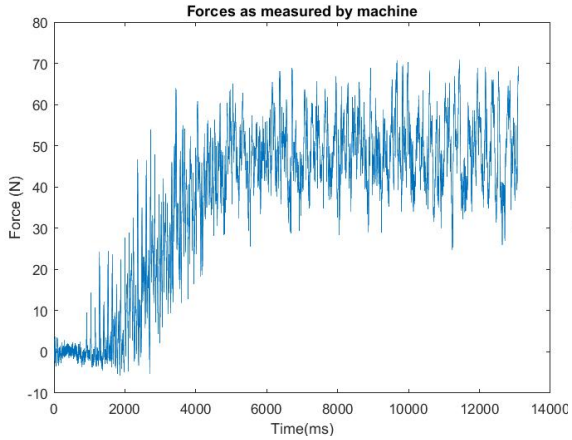

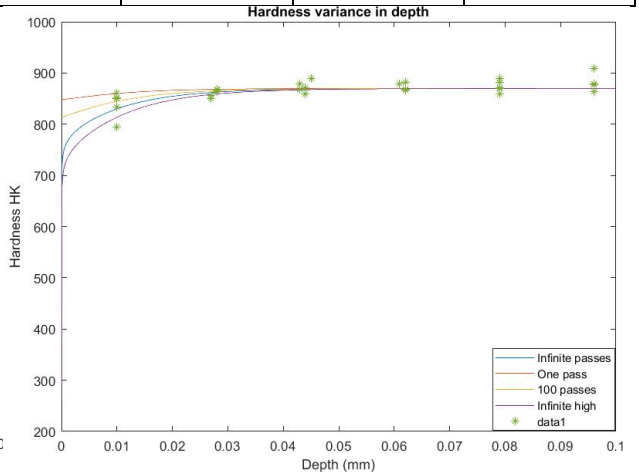

Case 8C

Line 1(mm)	0.01	0.027	0.044	0.06	0.079	0.096
Hardness 1 (HK)	700.6	788.3	832.1	849.2	878.4	858.6
Line 2 (mm)	0.01	0.027	0.044	0.061	0.079	0.096
Hardness 2 (HK)	776.5	747.6	840.9	868.5	848.8	879.4
Line 3 (mm)	0.01	0.027	0.044	0.061	0.079	0.096
Hardness 3 (HK)	882.4	689.1	800.4	877.2	872.9	878.4
Line 4 (mm)	0.01	0.027	0.046	0.06	0.079	0.096
Hardness 4 (HK)	776.5	771.6	880.5	868.9	864.2	859
Line 5 (mm)	0.01	0.029	0.046	0.061	0.079	0.096
Hardness 5 (HK)	756.3	765.1	801.3	858.8	862.8	879.3

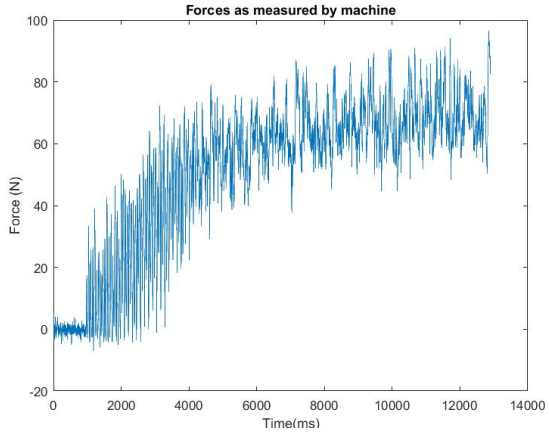

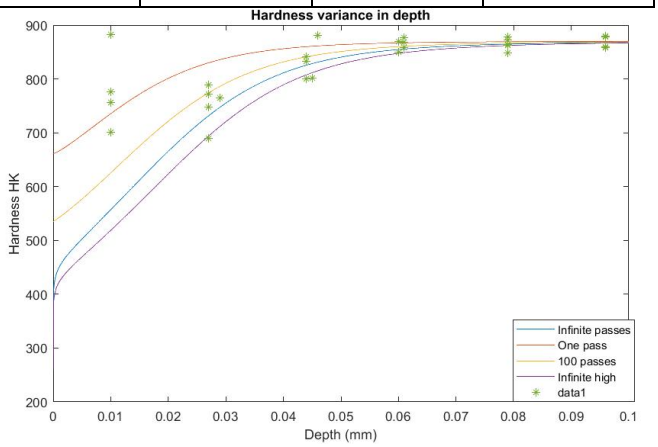

Case 9J

Line 1(mm)	0.011	0.026	0.044	0.062	0.079	0.096
Hardness 1 (HK)	825.1	865.3	870.4	878.5	873.4	849.2
Line 2 (mm)	0.01	0.029	0.044	0.062	0.079	0.096
Hardness 2 (HK)	829.3	855	878.9	878.1	865.2	878.5
Line 3 (mm)	0.009	0.026	0.043	0.062	0.079	0.096
Hardness 3 (HK)	838.8	868.6	843.7	869.1	879.4	878.3
Line 4 (mm)	0.01	0.028	0.043	0.06	0.079	0.096
Hardness 4 (HK)	854.3	878.2	878.3	858.8	862.1	888.4
Line 5 (mm)	0.01	0.027	0.046	0.06	0.079	0.096
Hardness 5 (HK)	848.2	835.6	870.5	888.4	870.2	868.5

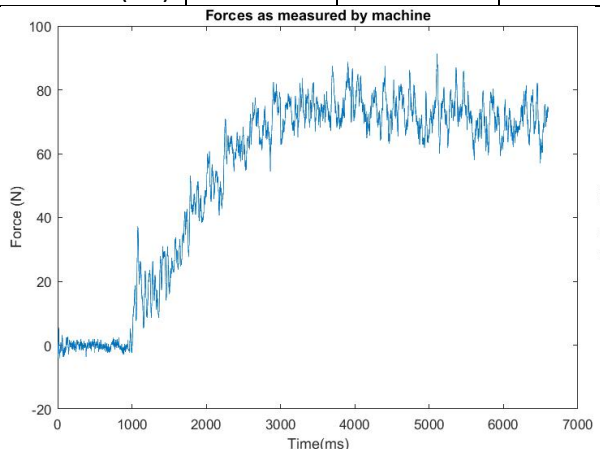

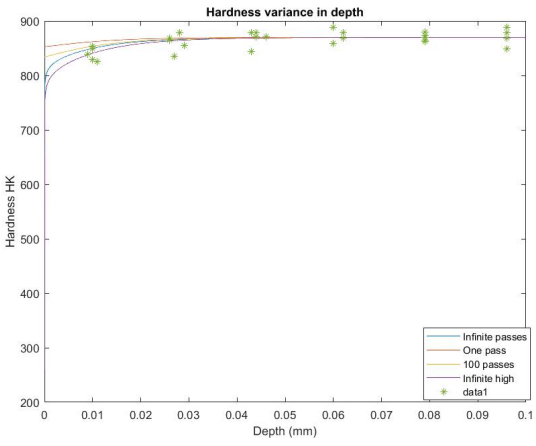

Case 10F

Line 1(mm)	0.01	0.026	0.043	0.062	0.079	0.096
Hardness 1 (HK)	843.9	862.1	858.9	878.2	862.4	862.4

Line 2 (mm)	0.011	0.026	0.044	0.062	0.078	0.096
Hardness 2 (HK)	857.6	861.9	888.8	878.3	870.5	865.6
Line 3 (mm)	0.011	0.026	0.044	0.062	0.079	0.096
Hardness 3 (HK)	834.7	846.8	858.9	868.6	870.3	881.5
Line 4 (mm)	0.011	0.028	0.048	0.068	0.087	0.096
Hardness 4 (HK)	822.4	865.9	888.5	869.6	865.5	860.3
Line 5 (mm)	0.01	0.028	0.044	0.062	0.076	0.096
Hardness 5 (HK)	850.5	854.7	849.3	864.4	859.1	868.5

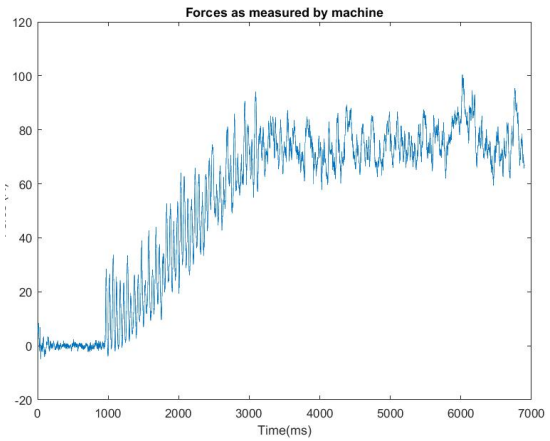

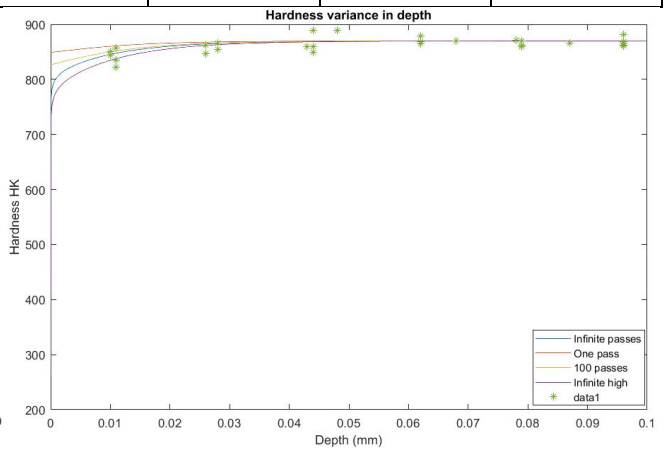

Case 11H

Line 1(mm)	0.01	0.026	0.04	0.062	0.079	0.096
Hardness 1 (HK)	851.3	856.1	871.8	869	864	888.6
Line 2 (mm)	0.011	0.026	0.044	0.062	0.079	0.096
Hardness 2 (HK)	882.4	859.3	866.9	868.9	870.1	849.2
Line 3 (mm)	0.011	0.026	0.043	0.062	0.079	0.096
Hardness 3 (HK)	855.2	869.3	850.8	868.6	868.5	888.4
Line 4 (mm)	0.01	0.029	0.044	0.062	0.079	0.096
Hardness 4 (HK)	869.5	886.7	908.9	868.5	862.6	849.3
Line 5 (mm)	0.01	0.028	0.043	0.062	0.079	0.096
Hardness 5 (HK)	866.7	853	860.8	868.5	875.6	862.2

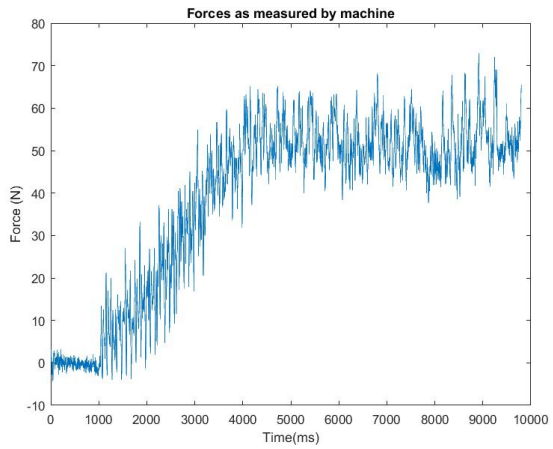

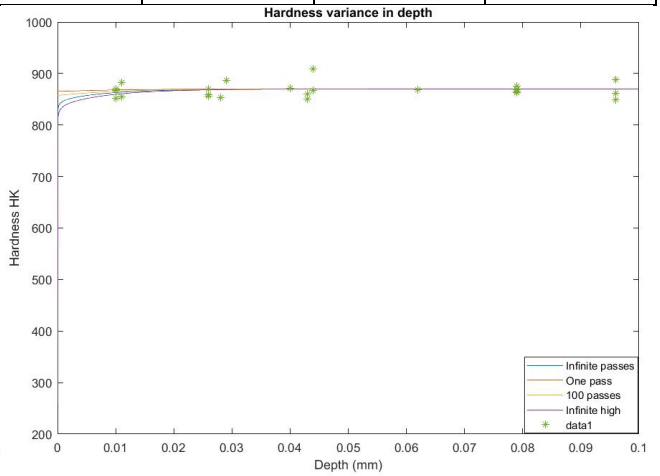

Case 12E

Line 1(mm)	0.01	0.026	0.044	0.061	0.079	0.096
Hardness 1 (HK)	808.5	822	872.4	858.8	871.8	868.7
Line 2 (mm)	0.01	0.029	0.043	0.06	0.079	0.096
Hardness 2 (HK)	801.5	857.8	898.5	888.4	878.3	868.6

Line 3 (mm)	0.01	0.029	0.044	0.062	0.079	0.096
Hardness 3 (HK)	796.8	830.9	888.4	858.9	858.8	868.6
Line 4 (mm)	0.01	0.028	0.044	0.061	0.079	0.096
Hardness 4 (HK)	814.5	849.7	869.1	858.8	888.4	866.1
Line 5 (mm)	0.01	0.028	0.044	0.061	0.079	0.096
Hardness 5 (HK)	797.2	851.1	878.4	860.5	879.1	875.1

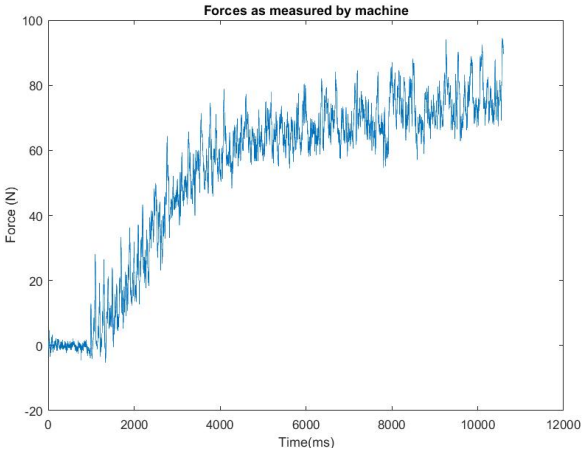

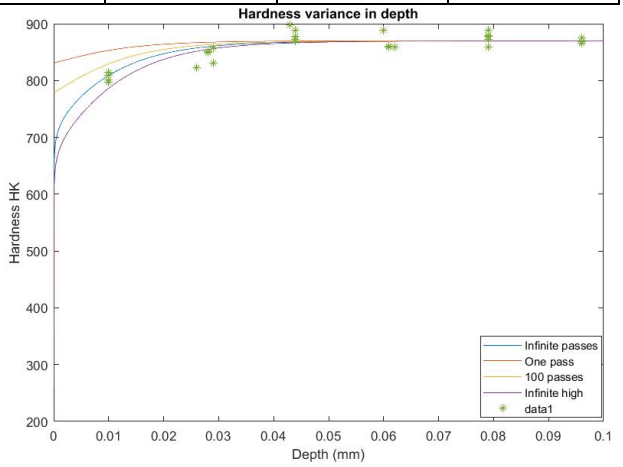

Case 13H

Line 1(mm)	0.01	0.026	0.043	0.061	0.079	0.096
Hardness 1 (HK)	818.4	832.8	860.6	868.6	870.1	853.2
Line 2 (mm)	0.011	0.026	0.044	0.062	0.079	0.096
Hardness 2 (HK)	806	819.9	878.4	876.2	869.3	858.8
Line 3 (mm)	0.01	0.026	0.043	0.062	0.079	0.096
Hardness 3 (HK)	826.2	840.5	858.9	852.7	858.8	860.9
Line 4 (mm)	0.01	0.028	0.043	0.061	0.079	0.096
Hardness 4 (HK)	839	852	866.6	869.6	860.2	888.3
Depth 5 (mm)	0.01	0.028	0.043	0.062	0.079	0.096
Hardness 5 (HK)	759.4	809.1	851.6	861.8	854	864.4

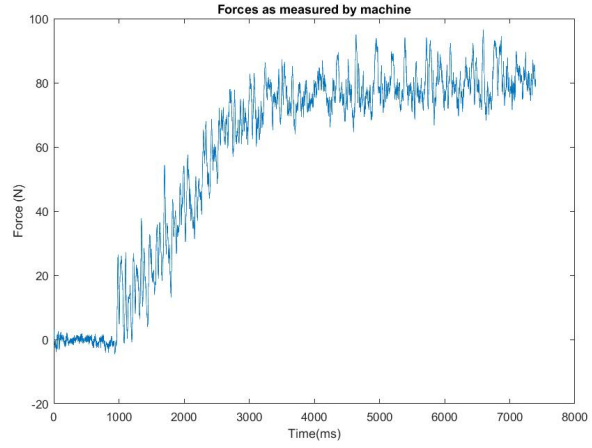

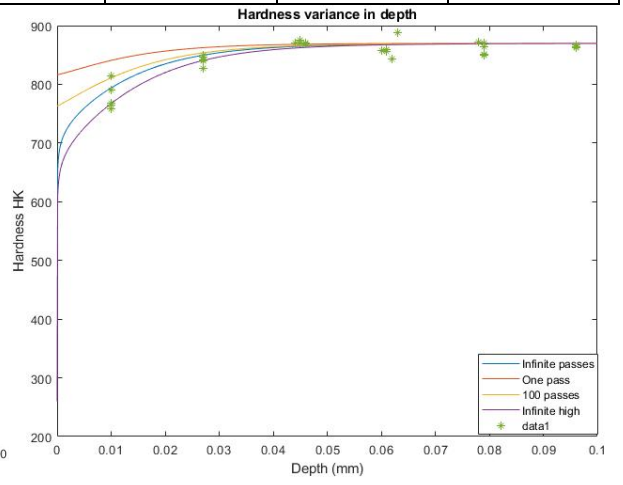

Case 14E

Line 1(mm)	0.01	0.027	0.045	0.061	0.079	0.096
Hardness 1 (HK)	768.5	850.3	875.2	859.2	851.3	862.4
Line 2 (mm)	0.01	0.027	0.046	0.060	0.078	0.096
Hardness 2 (HK)	765.4	847	868.7	857.8	871.4	867.6
Line 3 (mm)	0.01	0.027	0.044	0.062	0.079	0.096
Hardness 3 (HK)	789.5	839.4	870.3	843.9	850.2	864.4

Line 4 (mm)	0.01	0.027	0.046	0.061	0.079	0.096
Hardness 4 (HK)	814.5	827.7	869.6	856.3	869.9	862
Depth 5 (mm)	0.01	0.027	0.045	0.063	0.079	0.096
Hardness 5 (HK)	757.6	841.6	870.9	888.3	863.6	861.9

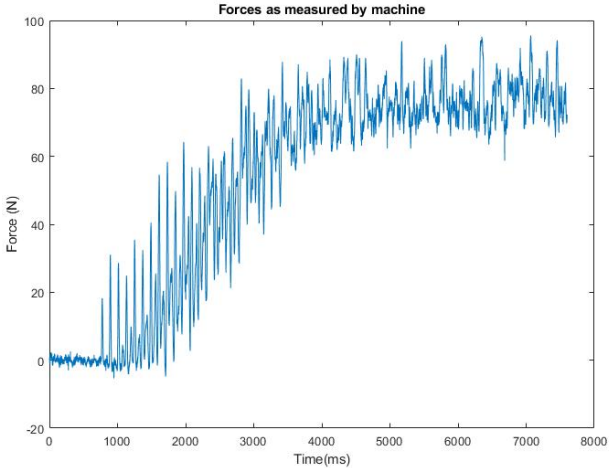

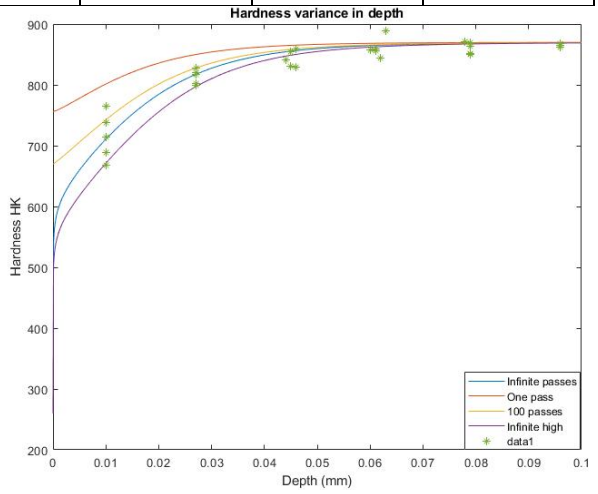

Case 15G

Line 1(mm)	0.01	0.028	0.044	0.062	0.079	0.096
Hardness 1 (HK)	854.6	852.6	865.5	823.4	849.2	858.8
Line 2 (mm)	0.011	0.028	0.043	0.061	0.079	0.096
Hardness 2 (HK)	856.3	841	940.8	876.4	830.5	868.5
Line 3 (mm)	0.006	0.026	0.043	0.062	0.079	0.096
Hardness 3 (HK)	764.1	876.3	875.2	868.6	819.2	844.5
Line 4 (mm)	0.01	0.028	0.043	0.061	0.079	0.096
Hardness 4 (HK)	821.8	838.7	844.7	864.4	830.5	830.5
Line 5 (mm)	0.011	0.026	0.043	0.061	0.079	0.096
Hardness 5 (HK)	822.9	874.7	864.3	868.8	878.4	868.5
Line 6(mm)	0.01	0.027	0.044	0.061	0.079	0.096
Hardness 6 (HK)	808.1	895.2	806.9	860	871.4	865.2
Line 7 (mm)	0.01	0.027	0.045	0.063	0.079	0.096
Hardness 7 (HK)	796.6	851.1	8586	872.8	863.4	863.3
Line 8 (mm)	0.006	0.027	0.043	0.061	0.079	0.096
Hardness 8 (HK)	765.5	846.9	839.2	878.4	870.7	863.7
Line 9 (mm)	0.007	0.027	0.045	0.063	0.079	0.096
Hardness 9 (HK)	779.5	840.3	804.2	858.8	855.2	864.4
Line 10 (mm)	0.006	0.027	0.045	0.062	0.079	0.096
Hardness 10 (HK)	751.5	848.3	835.4	858.8	853.9	856.8

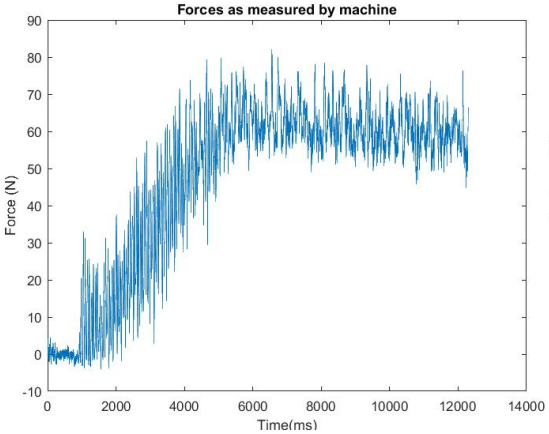

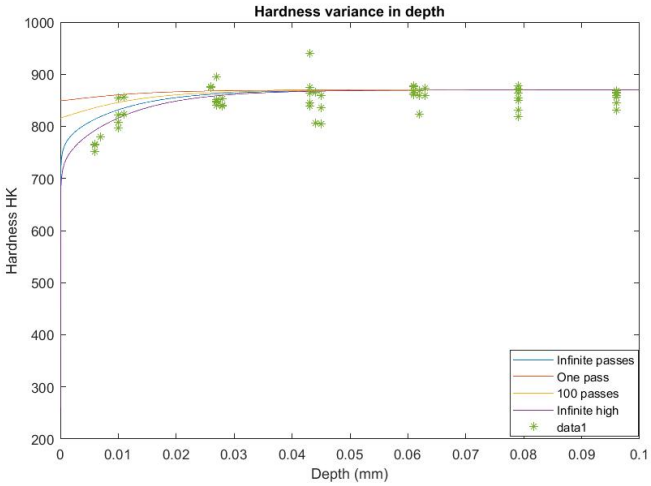

Case 16E

Line 1(mm)	0.01	0.028	0.044	0.062	0.079	0.096
Hardness 1 (HK)	854.6	852.6	865.5	823.4	849.2	858.8
Line 2 (mm)	0.011	0.028	0.043	0.061	0.079	0.096
Hardness 2 (HK)	856.3	841	940.8	876.4	830.5	868.8
Line 3 (mm)	0.006	0.026	0.043	0.062	0.079	0.096
Hardness 3 (HK)	764.1	876.3	875.2	868.6	819.2	844.5
Line 4 (mm)	0.01	0.028	0.043	0.061	0.079	0.096
Hardness 4 (HK)	821.8	838.7	844.7	864.4	830.5	830.5
Line 5 (mm)	0.011	0.026	0.043	0.061	0.079	0.096
Hardness 5 (HK)	822.9	874.7	864.3	868.8	878.4	868.5
Line 6(mm)	0.01	0.027	0.044	0.061	0.079	0.096
Hardness 6 (HK)	808.1	895.2	806.9	860	871.4	865.2
Line 7 (mm)	0.01	0.027	0.045	0.063	0.079	0.096
Hardness 7 (HK)	796.6	851.1	858.6	872.8	863.4	863.3
Line 8 (mm)	0.006	0.027	0.043	0.061	0.079	0.096
Hardness 8 (HK)	765.5	846.9	839.	878.4	870.7	863.7
Line 9 (mm)	0.007	0.027	0.045	0.063	0.079	0.096
Hardness 9 (HK)	779.5	840.3	804.2	858.8	855.2	864.4
Line 10 (mm)	0.006	0.027	0.045	0.062	0.079	0.096
Hardness 10 (HK)	751.5	848.3	835.4	858.8	853.9	856.8